UNIVERSITÀ DEGLI STUDI DI MILANO

Scuola di Dottorato in Fisica, Astrofisica e Fisica Applicata
Dipartimento di Fisica

Corso di Dottorato di Ricerca in Fisica, Astrofisica e Fisica Applicata
Ciclo XXVII

Decoherence, non-Markovianity and quantum estimation in qubit systems subject to classical noise

Settore Scientifico Disciplinare FIS/03

Supervisore: Professor Matteo PARIS

Co-Supervisore: Doctor Paolo BORDONE

Coordinatore: Professor Marco BERSANELLI

Tesi di Dottorato di:
Claudia BENEDETTI

Anno Accademico 2013/2014

Commission of the final examination:

External Referee:
Dr. Elisabetta Paladino

External Members:
Prof. Sabrina Maniscalco
Prof. Chiara Macchiavello

Final examination:

Date 30/01/2015

Università degli Studi di Milano, Dipartimento di Fisica, Milano, Italy

MIUR subjects:

FIS/03

PACS:

03.67.-a
03.65.Yz

"All that is gold does not glitter,
Not all those who wander are lost;
The old that is strong does not wither,
Deep roots are not reached by the frost."
- J.R.R. Tolkien

To Michela

Contents

Introduction

We live in the age of quantum technologies. We talk about quantum computers and quantum computation and we are able to write quantum algorithms that achieve exponential speedup over their classical analogues; quantum communication and quantum cryptography promise absolute secure transmission of messages and faithful transfer of unknown quantum states; not to cite the many ways in which quantum mechanics affects our daily life. The common denominator to all these applications is the concept of quantum information. Since the world is ultimately quantum-mechanical, it is a natural thought imagining to encode information in a quantum system: this idea lies at the heart of quantum information theory. Quantum information theory is the quantum analogue of classical information theory. It was born from the union between quantum physics and computer science. It describes the notions of quantum source and quantum channels and studies how the exploitation of non-classical correlations enables encoding, processing and distribution of information in ways impossible or inefficient in the classical world. Encoding information in a quantum system opened to the possibility of using the concepts of quantum theory in a whole new way and of thinking a different set of rules to describe how the information can be manipulated and accessed. The results are impressive: quantum teleportation, superdense coding, quantum key distribution, just to cite a few.

Quantum entanglement is a key resource in quantum communication and information processing and it embodies quantum correlations that have no classical analogue. To such an extent they are often regarded as synonyms. However, over the last years, the dichotomy entanglement-quantum correlations was challenged and it is nowadays recognized that entanglement does not capture all the possible quantum correlations residing in a quantum system. There exist non-classical correlations that are possibly more fundamental and more general than entanglement. Specifically, it was shown that there exist separable states that still have correlations without classical analogue. Various measures of these correlations were introduced and among them the quantum discord, an entropic measure introduced in 2001 [1,2], has been the center of a lot of studies over the last decade. Under suitable conditions, quantum discord has been proved to be more robust against decoherence than entanglement [3,4].

As a consequence of the recent advances in the design of semiconductors structures, the working of an increasing number of nanodevices is affected by or based on the the quantum nature of their components. Solid-state systems are very promising candidates for the realization of quantum information processing devices, due to the controllability of their quantum state, their scalability and the feasible integration with microelec-

tronic devices. An essential ingredient to exploit the quantumness of a physical system is the preservation of its coherent time evolution and its non-classical correlations. This would be no problem if quantum systems could be regarded as isolated systems. But the standard description of quantum dynamics, in terms of Schrödinger equation and unitary evolution, is an idealization. In fact, the unavoidable interaction with an incontrollable environment usually destroys coherence and quantumness, making their use for quantum technology ineffective. The fragile quantum information encoded in an open quantum system is lost due to the presence of the environment that continuously monitors the system. The result of the interaction with the environment is to replace the unitary evolution with a non-unitary dynamics. For this reason, decoherence may be considered the ultimate obstacle to the practical and efficient realization of the quantum information and communication protocols. Decoherence may be induced by a classical or a quantum bath, i.e. by the interaction with an environment described classically or quantum-mechanically. Although the quantum modeling for the bath is more common, there are situations where this description may be mathematically challenging, for example if the environment is very complex and tracing out the degrees of freedom of the bath can be a difficult task, or even inappropriate, for example because of the approximations introduced to derive a master equation are too strong to hold in real systems. As a matter of fact, the classical description becomes progressively more reliable as far as the environment has many degrees of freedom or when the interaction between a quantum system and a classical fluctuating field is taken into account. Recently, it has also been shown that even certain quantum environments may be described with equivalent classical models. However understanding whether and under which conditions the two descriptions are equivalent is still a debated topic [5–8].

It is well established that quantum correlations are a fundamental resource for the quantum information processing. But recently, another figure of merit as been addressed as resource for quantum technology, i.e. the concept of quantum non- Markovianity. While Markovianity is well defined for classical stochastic process, it does not generalize in a straightforward way to the quantum world. The effort to find a generalization of the concept of non-Markovianity for quantum system led to many different definitions [9–15] but an agreement is still missed. Classically, it is possible to quantify the non-Markovianity of a stochastic process in terms of the Kolmogorov n-point probability distribution. However it has been proved [16, 17] that there are clear differences between the classical and the quantum notions of non-Markovianity. When we talk about 'quantum non-Markovianity' we refer to the non-Markovian character of the dynamical map describing the evolution of the quantum system, according to some measure. From a qualitative approach, systems in which recoherence phenomena occur, such as revivals of quantum correlations, are called non-Markovian open quantum system. For such system, the Born-Markov approximation leading to a master equation of the Lindblad form, does not lead to a correct description of the dynamics of the physical system. Non-Markovianity is the focal point of recent research in understanding if the existence of memory effects enable to accomplish tasks that cannot be achieved with Markovian processes [18–22]. However, to date there is no general theory linking non-Markovian dynamics with an increase in the efficiency of quantum information processing and communication. Efforts have been made to understand if it is possible to connect the presence of non-Markovianity with the efficiency enhancement of quantum protocols. Would that be true, non-Markovianity becomes a key concept in quantum information theory, not a mere label to classify different kinds dynamical maps.

Since the interaction of a quantum systems with the external environment introduces noise, thus degrading the overall performances of any device or protocol exploiting the quantumness of the system, the precise characterization of the noise is a crucial ingredient for the design of high-precision measurements and reliable communication protocols. A suitable description of classical noise is given in terms of stochastic processes [6, 23–26]. The characterization of classical noise is often performed by collecting a series of measurements at different times to estimate its autocorrelation function and its spectral properties [27–29]. This procedure is generally time consuming and may require the control of a complex system. A question thus arises whether more effective techniques may be developed. To this purpose, the use of *quantum probes* to estimate the parameters of classical noise comes into play. The idea is to use a simple quantum system, such as a qubit, coupled to a classical fluctuating field and explore the performances of quantum measurements performed at a single fixed interaction time to extract information about the classical noise. The power and implications of this idea are undeniable: the features of a complex system may be determined by monitoring a small probe, which is usually characterized by few and easily controllable degrees of freedom. The canonical way to attack this problem is by using the tools of quantum estimation theory [30–33]. Indeed, quantum estimation theory allows one to find the best strategy to estimate the value of an unknown parameter, even if it is not accessible by direct measurement. Upon collecting the outcomes from a measurement of a suitably optimized observable, it is possible to build an estimator to infer the value of the unknown parameter with the ultimate precision allowed by quantum mechanics.

A deep understanding of the mechanisms of the decoherence in quantum systems, in order to reduce its detrimental effects, is an essential step toward the development of quantum technologies. The precise characterization of the stochastic process generating the classical noise, possibly using minimal resources, is thus a crucial ingredient for the design of high-precision measurements and reliable communication protocols. Moreover, from an applicative point of view, increasing ability in reservoir engineering techniques paves the way to new methods of decoherence control based on the manipulation and modification of properties of the environment such as its spectrum or its microscopic structure.

This PhD dissertation collects my personal contribution to the study and understanding of the role played by different kinds of classical noise in affecting the dynamics of a quantum system. I consider a qubit system coupled to a stochastic classical field and address the decoherence and non-Markovianity induced by the external noise as well as the spectral characterization of the classical field by quantum-limited measurement on the qubit. In order to maintain the analysis self-contained and to address situations of practical interest, I focus on dephasing dynamics, i.e. I assume that the dephasing effects of the environment are much stronger than relaxation ones. This situation happens when the typical frequencies of the environment are smaller compared to the natural frequency of the quantum system under investigation. In this case, fluctuations can cause a superposition of states to decohere, without inducing transitions between different energy levels.
I thus analyze the dynamics of quantum correlations for two non-interacting qubits initially prepared in a maximally entangled state and interacting with a classical noise. The dynamics of the two qubits is ruled by a stochastic Hamiltonian with time dependent coupling. The ensemble average of the time-evolved states over the noise parameters describes the evolution of the quantum system under the effect of the classical noise. Upon a suitable choice of the stochastic time-dependent terms in the Hamiltonian, I was

able to describe the effects of both independent (separate) and common environments: in the former, each qubit is locally coupled to a random external process, while in the latter both qubits are subject to the effect of a common classical source of noise. Then, I address a simpler single-qubit system, in order to evaluate the non-Markovianity of a dephasing map as a function of the noise nature and parameters. Finally, I analyze how a single-qubit system can be exploited to gain information about a classical noise that affects its dynamics.
Two kinds of noise are taken into account: Gaussian and non-Gaussian noise. Gaussian stochastic processes are fully characterized by their mean and variance. Relevant examples of Gaussian processes are the Ornstein-Uhlenbeck process [34,35] and the fractional Brownian motion [36]. A Gaussian statistics for the noise may be legitimately assumed when the environment surrounding the quantum system is composed by a large number fluctuators. Moreover, the Gaussian approximation is valid even in the presence of non-Gaussian noise, as far as the coupling with the environment is weak. However there are situations where the Gaussian assumption is not a priori justified and the non-Gaussian nature of the noise must be taken into account. Non-Gaussian processes cannot be fully characterized by their second order statistics. Moreover, the knowledge of the spectrum or equivalently the autocorrelation function alone is not sufficient to describe the dynamics and the decoherence phenomena of a quantum system. Among the class of open quantum systems interacting with a non-Gaussian classical environment, a lot of attention has been devoted to qubit-systems subject to random telegraph noise and $1/f^\alpha$ noise. The random telegraph noise is generated by a bistable fluctuator, i.e. some quantity which flips between two values with a switching rate γ. Examples of fluctuators are dynamical defects which randomly switch between two metastable states. This noise affect numerous devices based on semiconductors, superconductors and normal metals [37–44]. It also represents the building block to describe noises with $1/f^\alpha$ spectrum.
$1/f^\alpha$ noise is an ubiquitous noise in nature (see Ref.s [45–48] and references therein). Moreover, in almost all quantum computing nanodevices, fluctuations with $1/f^\alpha$ spectrum of different variables and physical origin have been detected. Actually, this noise represents the main source of decoherence in solid-state quantum system. Despite the huge variety of systems affected by this noise, its origin and the shape of its spectrum have been an unsolved problem for a long time and still many open issues related to this noise remain unsolved. However, $1/f^\alpha$ noise is commonly attributed to fluctuators, specifically a collection of bistable fluctuators whose switching rates γ are distributed according to a specific distribution $p_\alpha(\gamma)$.

This Thesis is organized as follows.

- In Chapter 1 I review the basics concepts and terminology of quantum mechanics that I will use in the later chapters. Then I introduce the concept of non-Markovianity according to two recent measures, and the tools of quantum estimation theory necessary to infer the value of an unknown parameter.

- In Chapter 2 I review the main concepts about stochastic processes and how they are characterized. I introduce the two classes in which stochastic processes may be divided into, that is Gaussian and non-Gaussian processes and introduce some paradigmatic representatives of both classes.

- In Chapter 3 I introduce my contribution to the study of the dynamics of quantum correlations, both entanglement and discord, between two non interacting qubit

subject to a classical noise generated either by a Gaussian or a non-Gaussian process. I study how different kinds of noise affect the decaying of quantum correlations and find that, depending on the nature and the parameters of the noise considered, correlations decay either with a monotonic or a damped oscillating behavior. In this chapter I also introduce a new microscopic model for $1/f^{\alpha}$ noise based on random bistable fluctuators.

- Chapter 4 is devoted to the analysis of non-Markovianity of the dynamical map of a qubit subject to classical noise, in terms of information backflow and channel capacities. I show how the non-Markovian character of the channel depends upon the noise parameters and I also make a connection between the appearance of revivals in the quantum correlations and the presence of an information backflow to the system. Moreover, I show that non-Markovianity leads to an increase in the capacities of quantum channels compared to the corresponding Markovian ones.

- In Chapter 5 I address the complementary problem of decoherence induced by a classical environment on a quantum system, that is to use a quantum system as a probe to characterize the properties of a classical noise, e.g. its spectral properties. By using the tools of quantum estimation theory I show that it is possible to effectively extract information on the noise, by using a single qubit as a probe.

List of Publications

Most of the material presented in this thesis has been published in these papers:

1. P. Bordone, F. Buscemi, C. Benedetti,
   Effect of Markov and Non-Markov Classical Noise on Entanglement Dynamics,
   Fluctuation and Noise Letters, **11**, 1242003 (2012) .

2. C. Benedetti, F. Buscemi, P. Bordone, M. G. A. Paris,
   Effects of classical environmental noise on entanglement and quantum discord,
   Int. J. Quantum Inf. **10**, 1241005 (2012).

3. C. Benedetti, F. Buscemi, P. Bordone, M. G. A. Paris,
   Dynamics of quantum correlations in colored-noise environments,
   Phys. Rev. A **87**, 052328 (2013).

4. C. Benedetti, F. Buscemi, P. Bordone, M. G. A. Paris,
   Time-evolution of entanglement and quantum discord of bipartite systems subject to 1/f noise,
   Proc. 22nd Int. Conf. on Noise and Fluctuations (ICNF), 24-28 June 2013 (Montpellier, France), 2013 © IEEE, doi: 10.1109/ICNF.2013.6578952

5. C. Benedetti, M. G. A. Paris, S. Maniscalco
   Non-Markovianity of colored noisy channels,
   Phys. Rev. A **89**, 012114 (2014).

6. C. Benedetti,F. Buscemi, P. Bordone, M. G. A. Paris
   Quantum probes for the spectral properties of a classical environment,
   Phys. Rev. A **89**, 032114 (2014) .

7. C. Benedetti and M. G. A. Paris,
   Characterization of classical Gaussian processes using quantum probes,
   Phys. Lett. A **378**, 2495 (2014).

8. M. Rossi, C. Benedetti, M. G. A. Paris,
   Engineering decoherence for two-qubit systems interacting with a classical environment,
   Int. J. Quantum Inf. 1560003 (2015)
   DOI: 10.1142/S0219749915600035

Other published material

This is a list of the publications which have not been included in the thesis.

1. C. Benedetti, F. Buscemi, P. Bordone,
   Quantum correlations in continuous-time quantum walks of two indistinguishable particles,
   Phys. Rev. A **85**, 042301 (2012).
   Selected by Virtual Journal of Quantum Information, Vol. 12, Issue 4 (April 2012).

2. C. Benedetti, A. P. Shurupov, M. G. A. Paris, G. Brida, M. Genovese,
   Experimental estimation of quantum discord for a polarization qubit and the use of fidelity to assess quantum correlations,
   Phys. Rev. A **87**, 052136 (2013).

3. C. Benedetti and M. G. A. Paris,
   Effective dephasing for a qubit interacting with a transverse classical field,
   Int. J. Quantum Inf. **12**, 1461004 (2014).

Other material

1. M. Brunelli, C. Benedetti, S. Olivares, A. Ferraro, M. G. A Paris,
   Single- and two-mode quantumness at a beam splitter,
   in preparation.

Acknowledgments

These three years have been quite intense, I have learned a lot of interesting things, met new people, visited beautiful places and somehow changed along the way. And I thank all the people who were with me in this journey, with their help, support and friendship.

First of all, I want to thank Matteo for being an excellent supervisor and for guiding me through the amazing world of quantum physics with patience and kindness. A very big thank you to my irreplaceable co-supervisor Paolo. Impossible not to thank Fabrizio Buscemi, Stefano Olivares and all other members of our groups both in Milan and Modena: it's been a pleasure working with you. A special mention for Antonio Mandarino, who is not only a colleague, but also a very good friend who has shared with me a lot of (dis-)adventures in this journey.
Thanks to two amazing women I had the fortune to meet and work with: Sabrina Maniscalco, who hosted me for six months in beautiful (and cold!) Edinburgh and Roberta Zambrini, who gave me the chance to spend other six months in the amazing (and hot!) Palma de Mallorca. They both taught me a lot, introduced me to new topics and great people in their groups.

Thanks to my family for their support, love and genetic craziness. Thanks to all the people who were there for me in these years, for the laughs, the travels, the phone and skype calls, the gluten free dinners, the lunches at university, the chats and the dances. Thanks to old friends and thanks to new people who just recently jumped into my life making me feel special and loved. And last, but not least, thanks to my guardian angels on Earth, Fede, Sammy, Ilaria e Michi...I love you girls.

CHAPTER 1

Preliminaries and Mathematical tools

This chapter is introductory. I review the key concepts in quantum mechanics, quantum non-Markovianity and quantum estimation theory. This chapter is not intended to be exhaustive about the discussed topics. I just introduce the basic ingredients which constitute the preliminary notions necessary to my research project.

1.1 Introduction to quantum mechanics

Quantum mechanics provides the mathematical and conceptual framework we need for the description of the physical processes we are interested in and the low that they obey. The postulates of quantum mechanics give a connection between the physical world and the mathematical formalism of quantum mechanics [49].

> **Postulate 1**: Associated to any isolated physical system there is a complex vector space with inner product, that is a Hilbert space, known as the state space of the system. The system is completely described by its *state vector* $|\psi\rangle$, which is a unit vector in the system's state space.

The word "state" means the available information about the properties of the system (e.g. energy, spin, etc..) we are interested in. According to the superposition principle any linear superposition of N quantum states is also a quantum state:

$$|\psi\rangle = \sum_{n=1}^{N} a_n |\psi_n\rangle. \tag{1.1}$$

If $|\psi\rangle$ is normalized and the $|\psi_n\rangle$ are orthonormal states, the coefficients a_n must satisfy the constrain

$$\sum_{n=1}^{M} a_n = 1 \tag{1.2}$$

and the quantity $|a_n|^2$ is interpreted as the probability to find the system $|\psi\rangle$ in the state $|\psi_n\rangle$ after a suitable measurement.

The time evolution of a quantum state is prescribed by the second postulate of quantum mechanics.

Postulate 2: The evolution of a closed quantum system is described by a *unitary transformation*. The state $|\psi(t)\rangle$ of the system at time t is related to the state $|\psi(t_0)\rangle$ at time $t_0 < t$ by a unitary operator U

$$|\psi(t)\rangle = U|\psi(t_0)\rangle. \tag{1.3}$$

The time evolution of a ket state is governed by the Schrödinger equation

$$i\hbar\frac{d}{dt}|\psi(t)\rangle = H|\psi(t)\rangle \tag{1.4}$$

where H is the Hamiltonian of the system. Eq. (1.4) is linear and homogeneous and of first order in t. It follows that, given an initial state $|\psi(0)\rangle$, the state at any subsequent time is determined. The formal solution of Eq. (1.4) can be written as

$$|\psi(t)\rangle = U(t,t_0)|\psi(t_0)\rangle \tag{1.5}$$

where we introduced the time-evolution operator $U(t,t_0)$ and t_0 is the initial time. U is a unitary operator which satisfies the following properties:

$$U(t,t) = \mathbb{I} \tag{1.6}$$
$$U(t,t')U(t',t_0) = U(t,t_0) \tag{1.7}$$
$$U^\dagger(t,t_0)U(t,t_0) = U(t,t_0)U^\dagger(t,t_0) = \mathbb{I} \tag{1.8}$$

and it itself satisfies the Schrödinger equation:

$$i\hbar\frac{d}{dt}U(t,t_0) = HU(t,t_0), \tag{1.9}$$

with initial condition $U(t_0,t_0) = \mathbb{I}$. This initial condition, together with Eq. (1.9) allows one to completely define the operator $U(t,t_0)$. In fact, we can rewrite Eq. (1.9) as:

$$U(t,t_0) = \mathbb{I} - \frac{i}{\hbar}\int_{t_0}^{t} H(s)U(s,t_0)ds. \tag{1.10}$$

However the solution (1.10) is only formal. We can rewrite it using an iterative procedure for the integrand:

$$U(t,t_0) = \mathbb{I} - \frac{i}{\hbar}\int_{t_0}^{t} dt_1 H(t_1) + \left(-\frac{i}{\hbar}\right)\int_{t_0}^{t} dt_1 \int_{t_0}^{t_1} dt_2 H(t_1)H(t_2) + \dots \tag{1.11}$$

obtaining a series expansion for $H(t)$. Note that $t_2 \leq t_1$ and the ordering in which the terms $H(t)$ appears is important only in the case the Hamiltonian does not commute at different times. But let us here focus on Hamiltonians which commutes at different times $[H(t_1), H(t_2)] = 0$. It follows that we can rewrite the expression:

$$\int_{t_0}^{t} dt_1 \int_{t_0}^{t_1} dt_2 H(t_1)H(t_2) = \frac{1}{2!}\int_{t_0}^{t} dt_1 \int_{t_0}^{t} dt_2\, H(t_1)H(t_2) \tag{1.12}$$

without the need of using a time-ordering operator. By generalizing the equivalence to an n-dimensional integral, one can write the Dyson series for the time evolution operator:

$$U(t,t_0) = \exp\left[-\frac{i}{\hbar}\int H(s)\, ds\right]. \tag{1.13}$$
$$= \mathbb{I} + \sum_{n=1}^{\infty}\frac{1}{n!}\left(-\frac{i}{\hbar}\right)^n \int_{t_0}^{t} dt_1 \dots \int_{t_0}^{t} dt_n\, H(t_1)\dots H(t_n). \tag{1.14}$$

We recall that Eq. (1.14) gives the explicit expression for the evolution operator $U(t, t_0)$ in the case in which the system Hamiltonian $H(t)$ commute at different times.

The physical properties of a quantum state can be access by measuring some observables, represented by Hermitian operators. Observables are described through Hermitian operators because these operators have real eigenvalues, which are appropriate for representing physical quantities. The third postulate of quantum mechanics provides a means for describing the effects of measurements on quantum systems.

> **Postulate 3**: Quantum measurements are described by a collection $\{M_i\}$ of *measurement operators* acting on the state space of the system being measured. The index i refers to the measurement outcomes that may occur in the experiment. If the state of the quantum system is $|\psi\rangle$ immediately before the measurement then the probability that result i occurs is given by:
>
> $$p(i) = \langle\psi|M_i^\dagger M_i|\psi\rangle \tag{1.15}$$
>
> and the state of the system after the measurement gave result i is
>
> $$|\psi\rangle \longrightarrow \frac{M_i|\psi\rangle}{\sqrt{\langle\psi|M_i^\dagger M_i|\psi\rangle}} \tag{1.16}$$
>
> The measurement operators satisfy the completeness equation
>
> $$\sum_i M_i^\dagger M_i = \mathbb{I}. \tag{1.17}$$

An important class of measurements is known as *projective measurements*. A projective measurement is described by an observable, M, that is a Hermitian operator on the state space of the system being observed. An Hermitian operator M, with the set of eigenvectors $\{|i\rangle\}$ satisfies the eigenvalue equation $M|i\rangle = m_i|i\rangle$ and admits a spectral decomposition:

$$M = \sum_i m_i|i\rangle\langle i| = \sum_i m_i P_i \tag{1.18}$$

where we introduced the projectors P_i onto the eigenspace of M with eigenvalue m_i. The projector operator satisfies the completeness relation $\sum_i P_i = \mathbb{I}$ and the orthogonality condition $P_i P_k = \delta_{ik} P_k$. The possible outcomes of the measurement correspond to the eigenvalues m_i of the observable.

Projective measurements are a special case of Postulate 3, and this can easily be seen by supposing that the measurement operators M in (1.15) and (1.16) in addition to satisfy the completeness relation, also satisfy the conditions that they are Hermitian and $M_i M_j = \delta_{ij} M_i$. With these additional restrictions, Postulate 3 reduces to a projective measurement and the average value of the observable M is written as:

$$\langle M\rangle = \sum_i m_i p_i = \sum_i m_i \langle\psi|P_i|\psi\rangle = \langle\psi|M|\psi\rangle \tag{1.19}$$

Every time we are given a set of orthogonal projectors P_i satisfying the completeness relation and the $P_i P_k = \delta_{ik} P_k$, we know that the corresponding observable is $M = \sum_i m_i P_i$. Moreover, the phrase "measure in a basis $|i\rangle$, where $|i\rangle$ forms an orthonormal basis", means to perform the projective measurement with projectors $P_i = |i\rangle\langle i|$.

1.1.1 The qubit

The bit is the fundamental concept in classical computation and information theory. Quantum computation and information processing are built upon the quantum analogue of the bit, the quantum bit or *qubit*. A qubit is a two-level quantum system, like the two spin states of a spin-$\frac{1}{2}$ particle, the vertical and horizontal polarization states of a single photon or the ground and excited states of an atom. The difference between bits and qubits is that a qubit can be in other states than $|0\rangle$ or $|1\rangle$. In fact, it can be in any superposition of these two states. Its most general state can be written as:

$$|\psi\rangle = \alpha|0\rangle + \beta|1\rangle \tag{1.20}$$

with $|\alpha|^2 + |\beta|^2 = 1$. Put in another way, the qubit is a vector in a two-dimensional complex vector space. We shall usually identify the state $|0\rangle$ with the vector $(1, 0)$ and similarly $|1\rangle$ with $(0, 1)$. Upon introducing the spherical polar coordinates $0 \leq \theta \leq \pi$ and $0 \leq \phi \leq 2\pi$, this state can be equivalently written as:

$$|\psi\rangle = \cos\frac{\theta}{2}|0\rangle + \sin\frac{\theta}{2}e^{i\phi}|1\rangle. \tag{1.21}$$

The parameters θ and ϕ define a point on a unit three-dimensional sphere, called the Bloch sphere. This is a sphere of unit radius, with each point on its surface corresponding to different pure states. Opposite points on the surface represent a pair of mutually orthogonal states. The north and the south poles correspond to the states $|0\rangle$ and $|1\rangle$ respectively.

1.1.2 Density matrix

In the more general case, the state of a physical system is not fully known and some information about it is missing. It is only known that the system is in the normalized state $|\psi_i\rangle$ with probability p_i. In this case the system is in a statistical ensemble and the mean value of an observable M is given by:

$$\langle M\rangle = \sum_i p_i \langle\psi_i|M|\psi_i\rangle. \tag{1.22}$$

It is convenient to introduce the density operator, or density matrix, in order to mathematically describe the statistical ensemble. The density matrix is defined as:

$$\rho = \sum_i p_i\, |\psi_i\rangle\langle\psi_i|. \tag{1.23}$$

The states $|\psi_i\rangle$ in Eq. (1.23) do not need to be orthogonal, however it is always possible to write the density operator in diagonal form:

$$\rho = \sum_i \rho_i |\rho_i\rangle\langle\rho_i| \tag{1.24}$$

with ρ_i the non-negative real eigenvalues of the density matrix and $|\rho_i\rangle$ the corresponding eigenvectors. The density matrix is represented by a complex matrix which satisfies the following three properties:

1. ρ is Hermitian:
   In fact, upon expanding a any pure state $|\psi_i\rangle$ over an orthonormal basis $\{j\}$, that is $|\psi_i\rangle = \sum_n a_n^{(i)}|n\rangle$, it is possible to write the density matrix and its elements as

$$\rho = \sum_i p_i|\psi_i\rangle\langle\psi_i| = \sum_i p_i \sum_{l,m} a_l^{(i)} a_m^{(i)*}|l\rangle\langle m| \tag{1.25}$$

$$\rho_{jk} = \langle j|\rho|k\rangle = \sum_i p_i a_j^{(i)} a_k^{(i)*} \tag{1.26}$$

   From this last equality is easy to check that the density matrix is Hermitian, since

$$\rho_{jk}^* = \sum_i a_j^{(i)*} a_k^{(i)} = \rho_{kj} \tag{1.27}$$

2. ρ has a unit trace:

$$\mathrm{Tr}[\rho] = \sum_k \rho_{kk} \overset{\text{Eq. (1.26)}}{=} \sum_{k,i} p_i a_k^{(i)} a_k^{(i)*} = \sum_i p_i \sum_k |a_k^{(i)}|^2 = 1 \tag{1.28}$$

   where we used the condition (1.2).

3. ρ is a non-negative operator:
   An operator ρ is non-negative if, for any vector $|\varphi\rangle$ in the Hilbert space, the condition $\langle\varphi|\rho|\varphi\rangle \geq 0$ holds. For density matrices we have

$$\langle\varphi|\rho|\varphi\rangle = \sum_i p_i \langle\varphi|\psi_i\rangle\langle\psi_i|\varphi\rangle = \sum_i p_i |\langle\varphi|\psi_i\rangle|^2 \geq 0 \tag{1.29}$$

If one of the probabilities p_i is unity, that is if $p_i = \delta_{ki}$, then the density operator (1.23) reduces to the simple form $\rho = |\psi_k\rangle\langle\psi_k|$. In this case, that is when the state vector is known, ρ is referred to as pure density operator or pure state. In the case of a pure state $\mathrm{Tr}[\rho^2] = 1$ while for mixed states $\mathrm{Tr}[\rho^2] < 1$. This can be easily shown by diagonalizing the density matrix as in Eq. (1.24) with eigenvalues $\rho_i \geq 0$. Once the density matrix is diagonalized it is very easy to compute ρ^2 as:

$$\rho^2 = \sum_i \rho_i^2 |\rho_i\rangle\langle\rho_i|. \tag{1.30}$$

The trace is calculated as $\mathrm{Tr}[\rho^2] = \sum_i \rho_i^2$. But since $\sum_i \rho_i = 1$ and $\rho_i \geq 0$, it follows that $0 \leq \rho_i \leq 1$, therefore $\mathrm{Tr}[\rho^2] \leq 1$ and it is equal to one if and only if $\rho_i = 1$ for only one value $\bar{i}$ and zero otherwise. This corresponds exactly to a pure state described by density matrix $\rho = |\bar{i}\rangle\langle\bar{i}|$.

From Eq. (1.22), we can rewrite the average value of an operator M as:

$$\begin{aligned}
\langle M\rangle &= \sum_j p_j \langle\psi_j|M \sum_i |i\rangle\langle i|\psi_j\rangle = \sum_i \sum_j \langle i|\psi_j\rangle p_j \langle\psi_j|M|i\rangle \\
&= \sum_i \langle i| \sum_j p_j |\psi_j\rangle\langle\psi_j|M|i\rangle = \sum_i \langle i|\rho M|i\rangle \\
&= \mathrm{Tr}\left[\rho\, M\right].
\end{aligned} \tag{1.31}$$

where we have used the equality $\mathbb{I} = \sum_i |i\rangle\langle i|$ and Eq. (1.23). Notice that, in Eq. (1.31), the trace in independent of the basis $\{i\}$ used to calculate the average value of M.
The diagonal elements of a density matrix have an important physical meaning. From Eq. (1.26) we can write the diagonal terms as:

$$\rho_{ii} = \sum_k p_k |a_i^{(k)}|^2 = \text{Tr}[\rho P_i] \tag{1.32}$$

where $P_i = |i\rangle\langle i|$ is the projector operator introduced in (1.18). The diagonal elements thus represent the probability that the system is left in the state $|i\rangle$ after measuring the observable whose eigenstates are $\{|i\rangle\}$. For this reason the diagonal elements of the density matrix are called the population of $\{|i\rangle\}$. The off-diagonal terms ρ_{jk}, instead, represent the quantum interference between the states $|j\rangle$ and $|k\rangle$. We can see from Eq. (1.26) that ρ_{jk} is a weighted sum of interference terms $a_j^{(i)} a_k^{*(i)}$. If $\rho_{ij} \neq 0$ then a quantum-coherence effect between the states is present. For this reason the off-diagonal elements of the density matrix are called coherences. It is important to highlight that the distinction between diagonal and off-diagonal terms depends on the choice of the basis $\{|i\rangle\}$.

Using the density matrix approach, we can reformulate the postulates of quantum mechanics, as follows.
Postulate 1: Associated to any isolated physical system there is a Hilbert space known as the *state space* of the system. The system is completely described by its *density operator*, which is a Hermitian positive operator ρ with trace one, acting on the state space of the system. If a quantum system is in the state ρ_i with probability p_i, then the density operator for the system is $\sum_i p_i \rho_i$.
Postulate 2: Eq. (1.5), written for state vectors, may be rewritten in terms of the density matrix describing a quantum system. In particular, the time evolution of a closed quantum system is described again by the unitary transformation (1.14) through the relation:

$$\rho(t) = U(t, t_0)\rho(t_0)U^\dagger(t, t_0). \tag{1.33}$$

Postulate 3: Quantum measurements are described by a collection of measurement operators $\{M_i\}$, that act on the state space of the system being measured. The index i refers to the outcome that may occur in the experiment. The probability that the result i occurs is given by:

$$p_i = \text{Tr}[M_i \rho M_i^\dagger] = \text{Tr}[M_i^\dagger M_i \rho], \tag{1.34}$$

and the measurement maps the initial state ρ into a statistical ensemble of states $\{p_i, \rho_i^{'}\}$ where

$$\rho_i^{'} = \frac{M_i \rho M_i^\dagger}{\text{Tr}[M_i \rho M_i^\dagger]}. \tag{1.35}$$

The reformulation of the postulates of quantum mechanics in terms of density operators is mathematically equivalent to the description in terms of state vectors. However the density operator approach permits to describe systems whose state is not completely known and subsystems of a composite system.

In section 1.1.1 we introduced the concept of quantum bit and the mathematical representation for pure states of a single qubit through the Bloch sphere Eq. (1.21). This

description has an important generalization to mixed states. In fact, the density matrix for an arbitrary mixed state qubit may be written as:

$$\rho = \frac{\mathbb{I} + \vec{r} \cdot \vec{\sigma}}{2}, \tag{1.36}$$

where $\vec{\sigma} = \{\sigma_x, \sigma_y, \sigma_z\}$ is the vector of Pauli matrices defines as:

$$\sigma_x = \begin{pmatrix} 0 & 1 \\ 1 & 0 \end{pmatrix} \qquad \sigma_y = \begin{pmatrix} 0 & -i \\ i & 0 \end{pmatrix} \qquad \sigma_z = \begin{pmatrix} 1 & 0 \\ 0 & -1 \end{pmatrix}. \tag{1.37}$$

The Pauli matrices have determinant $\det(\sigma_j) = -1$, zero trace $\mathrm{Tr}[\sigma_j] = 0$ and satisfy the condition $\sigma_j^2 = \mathbb{I}$ for $j = x, y, z$. The vector $\vec{r} = \{r_x, r_y, r_z\}$ is called the Bloch vector and is a real three-dimensional vector satisfying the condition $||\vec{r}|| \leq 1$. For pure states this condition becomes $||\vec{r}|| = 1$. The expression (1.36) is obtained by expanding the general qubit density matrix $\rho = |\psi\rangle\langle\psi|$, obtained from Eq. (1.21) over the basis $\{\mathbb{I}, \sigma_x, \sigma_y, \sigma_z\}$ as $\rho = r_0\mathbb{I} + c_x\sigma_x + c_y\sigma_y + c_z\sigma_z$. Since the condition $\mathrm{Tr}[\rho] = 1$ must hold for all density matrices, it immediately follows that $r_0 = \frac{1}{2}$. The expansion coefficient are computed as $c_i = \frac{1}{2}r_i$ for $i = x, y, z$ and the relations between the parameters θ and ϕ and the Bloch vector components are:

$$r_x = \cos\phi \, \sin\theta \qquad r_y = \sin\phi \, \sin\theta \qquad r_x = \cos\theta \tag{1.38}$$

1.1.3 Composite systems and the reduced density matrix

The Hilbert space of a composite physical system composed by n subsystems is the tensor product of the vector spaces of the subsystems $\mathcal{H} = \mathcal{H}_1 \otimes \mathcal{H}_2 \otimes \ldots \mathcal{H}_n$.
The density operator approach is very useful when describing a quantum system whose state is not fully known and to describe a subsystem of a composite larger system. The equation (1.23) describes the state of the global system.
Suppose we have a bipartite system ρ, that is two physical systems A and B (which we call Alice and Bob, as they are ususally referred to in the quantum information community) whose joint state is described by the density matrix ρ. There are plenty of situations in which we might be interested in describing the state of only one subsystem. The mathematical tool that allows one to address only a subsystem of a composite system is called *reduced density matrix*. The reduced density matrix of a bipartite system is defined as:

$$\rho_A \equiv \mathrm{Tr}_B\left[\rho\right] \tag{1.39}$$
$$\rho_B \equiv \mathrm{Tr}_A\left[\rho\right], \tag{1.40}$$

where $\mathrm{Tr}_{A(B)}$ is the partial trace operator over system $A(B)$. The most general expression of a density matrix ρ for a bipartite system may be written as:

$$\rho = \sum_{lnmp} \rho_{ln,mp} |ln\rangle\langle mp|, \tag{1.41}$$

where we introduced the notation $|jk\rangle = |j\rangle_A \otimes |k\rangle_B$ to describe the sets of orthonormal basis for subsystems A and B respectively. The partial trace is then defined by:

$$\begin{aligned}\rho_A &= \mathrm{Tr}_B \left[\sum_{lmnp} \rho_{ln,mp} |ln\rangle\langle mp| \right] = \sum_k {}_B\langle k| \sum_{lmnp} \rho_{ln,mp} |ln\rangle\langle mp|k\rangle_B \\ &= \sum_k \sum_{lm} \rho_{lk;mk} |l\rangle\langle m|. \\ (\rho_A)_{lm} &= \sum_k \rho_{lk;mk} \end{aligned} \tag{1.42}$$

and equivalently for ρ_B, where we used the orthogonality relations ${}_B\langle k|n\rangle_B = \delta_{kn}$ and ${}_B\langle p|k\rangle_B = \delta_{pk}$
The reason why the reduced density operator describes the state of a subsystem is justified by the fact that it provides the correct statistics for the measurements made on the subsystem. To understand this, let us assume that we wish to compute the mean value of an operator O_1 acting only on subsystem 1 of a bipartite system. We require that the same operator acting on the entire Hilbert space can be written as $\tilde{O} = O_1 \otimes \mathbb{I}_2$, with $\mathbb{I}_2$ the identity operator in $\mathcal{H}_2$. Thus, we can write:

$$\begin{aligned}\langle \tilde{O} \rangle &= \mathrm{Tr}[\rho \tilde{O}] = \sum_{jk} \langle jk|\rho \tilde{O}|jk\rangle \\ &= \sum_{jk} \langle jk| \left(\sum_{\substack{lm \\ np}} \rho_{ln,mp} |ln\rangle\langle mp| \right) (O_1 \otimes \mathbb{I}_2) |jk\rangle \\ &= \sum_{jk} \sum_m \rho_{jk,mk} \langle m|O_1|j\rangle = \sum_{jm} \langle j|\rho_A|m\rangle\langle m|O_1|j\rangle \\ &= \sum_j \langle j|\rho_A O_1|j\rangle = \mathrm{Tr}[\rho_A O_1] \end{aligned} \tag{1.43}$$

where we used Eq.s (1.41) and (1.42).

1.1.4 Open quantum systems

Although all closed quantum systems are described by unitary evolutions, more general state changes are possible for open quantum systems. In fact, quantum systems are never isolated from their environments, and the theory of closed quantum systems fails to describe many features of quantum dynamics.

In the context of open quantum system, the open system S, described by density matrix ρ, is coupled to another quantum system B, described by ρ_B, called the environment. Thus S can be regarded as a subsystem of the global system $S + B$, consisting of open system plus environment. The Hilbert space of the total system is the tensor product of the two subsystems spaces $\mathcal{H} = \mathcal{H}_S \otimes \mathcal{H}_B$. The interaction with the environment creates system-environment correlations that prevent the state of S to be described in terms of unitary evolution.

In the case of an open quantum system, in fact, the dynamics is described by quantum

maps $\mathcal{E}(\rho)$. Given an input state ρ, the output state of the system ρ' is thus given by:

$$\rho' = \frac{\mathcal{E}(\rho)}{\mathrm{Tr}[\mathcal{E}]}. \tag{1.44}$$

The dynamical map $\mathcal{E}$ is called a *quantum operation*, i.e. a linear, trace-decreasing map that preserve positivity and satisfies the additional property of complete positivity. Complete positivity means that if we introduce an extra system ρ_B of arbitrary dimensionality to the principal system ρ, such that the global state is described by the density matrix ρ_T, then it must be true that $(\mathbb{I} \otimes \mathcal{E})(\rho_T)$ is positive for any positive operator ρ_T of the combined system. The trace in denominator in Eq. (1.44) is included in order to preserve the trace condition $\mathrm{Tr}(\rho) = 1$. A class of operations that is of particular interest is the *trace-preserving* operations, for which the condition $\mathrm{Tr}[\mathcal{E}(\rho)] = 1$ holds and Eq. (1.44) may be rewritten as:

$$\rho' = \mathcal{E}(\rho). \tag{1.45}$$

Physically, trace-preserving operations arise in situations where the system is coupled to some environment that is not under observation and the effect of the evolution is averaged over all possible outcomes of the interaction with the environment. In the following we will focus on trace-preserving operations.

We stated that, in general, the final state of the system $\mathcal{E}(\rho)$ may not be related by a unitary operator to the initial state ρ. However the composite system, assumed to start from an initial product state $\rho \otimes \rho_B$, will evolve according to a unitary transformation U. The dynamics of the system alone is given by the partial trace of the total system over the environment degrees of freedom:

$$\mathcal{E}(\rho) = \mathrm{Tr}_B \left[U(\rho \otimes \rho_B) U^\dagger \right] \tag{1.46}$$

This equation tells us that any completely positive trace-preserving (CPTP) quantum operation can always be mocked up as a unitary evolution on a larger system.
$\mathcal{E}$ in Eq. (1.46) can be rewritten using an equivalent and very elegant form, known as the operator-sum representation. Let us call $\{|\omega_i\rangle\}$ the orthonormal basis for the state space of the environment, and $\rho_B = |\omega_0\rangle\langle\omega_0|$ its initial state. Eq. (1.46) can thus be rewritten as:

$$\begin{aligned} \mathcal{E}(\rho) &= \sum_i \langle\omega_i| U \big(\rho \otimes |\omega_0\rangle\langle\omega_0|\big) U^\dagger |\omega_i\rangle \\ &= \sum_i K_i \rho K_i^\dagger. \end{aligned} \tag{1.47}$$

where the $K_i = \langle\omega_i|U|\omega_0\rangle$ are operators acting on the state space of the principal system alone. The operators K_i must satisfy the completeness condition $\sum_i K_i^\dagger K_i = \mathbb{I}$ and they completely specify the quantum operation. Eq. (1.47) is also known as the Kraus decomposition [50]. Once we know the expression for the Kraus operators K_i, it is possible to describe the dynamics of the principal system ρ without having to explicitly consider properties of the environment. Two examples of quantum operations are the unitary transformations U (1.33) and the measurements M (1.35), for which $\mathcal{E}(\rho) = U\rho U^\dagger$ and $\mathcal{E}_i(\rho) = M_i \rho M_i^\dagger$ respectively.

A quantum channel $\mathcal{E}_t$ is a completely positive trace preserving map, which connects an input state ρ_0 at time t_0 with the final state ρ at time t: $\rho = \mathcal{E}_{t,t_0}(\rho_0)$. It can be mathematically described using equivalently Eq. (1.46) or Eq. (1.47).
The possibility of reliably sending a message through a channel is a fundamental problem in quantum communication. The typical scenario of a communication procedure sees a sender, Alice, transmitting unknown quantum states through the channel to the receiver Bob. Unfortunately, the channel is usually subject to noise, quantum or classical, which prevent a transmission of the message with a very high fidelity to the original states. More details about quantum channels will be given in Sec. (1.3.2) Here we just want to introduce a very important channel, that will be addressed in later chapters to describe the dynamics of the systems we are interested in, that is the dephasing channel. The dephasing, or phase damping, channel is an ideal model of noise that capture the the important feature of quantum open system of losing quantum information without the loss of energy. Physically, it describe situations where the quantum system interacts with an external environment whose frequencies are much smaller that the system characteristic frequency.
The Kraus decomposition for the dephasing channel in the case of a qubit system may be written as $\rho = p\rho_0 + (1-p)\sigma_z\rho_0\sigma_z$, where ρ_0 is the initial state of the system before entering the dephasing channel, ρ is the output state and the quantities p and $(1-p)$ represent the probability that the operation to be applied on the physical system is the identity and σ_z respectively. That is, with probability p the system will be left in its initial state ρ_0 and with probability $(1-p)$ will be subject to a σ_z operation. By letting the probability depending on time and introducing the *dephasing coefficient* $\Lambda(t) = 2p(t) - 1$, we can write the dephasing map as

$$\rho(t) = \frac{1+\Lambda(t)}{2}\rho_0 + \frac{1-\Lambda(t)}{2}\,\sigma_z\rho_0\sigma_z. \tag{1.48}$$

The effect of a dephasing channel is to leave the populations unchanged and multiplying the off-diagonal elements by the dephasing coefficient Λ. In fact, by writing the initial density matrix as $\rho_0 = \sum_{j,k=0}^{1}\rho_{jk}|j\rangle\langle k|$, Eq. (1.48) can be explicitly written as

$$\rho(t) = \begin{pmatrix} \rho_{00} & \Lambda(t)\rho_{01} \\ \Lambda(t)\rho_{10} & \rho_{11} \end{pmatrix} \tag{1.49}$$

Since the off-diagonal elements have no classical analogue, the effect of the dephasing channel is to introduce quantum decoherence, altering the quantum phase between the components of the quantum state. If the dephasing function is a decaying function with time, for example $\Lambda(t) = e^{-\lambda t}$, we will call the corresponding map 'phase damping'.
The importance of dephasing channel relies in the fact it provides a useful model to describe many physical situation and, since it induces a decay of quantum coherences, it plays a central role in the transition from quantum to classical world.

1.1.5 Classical and quantum information theory

The classical theory of information was developed by Shannon in 1948, in the context of sending information over a channel, such as a telephone wire. The first requirement for a measure of information is that the amount of information in an event X must depend upon its probability p. This is a very natural requirement. Suppose, in fact, that the possible outcomes of the event X are $\{x_i\}$ and the probability of an event, say x_0 to occur is one $p(x_0) = 1$. Then learning the value of X by measuring it bring us no information. If

x_0 is close but not equal to unity, then learning that $X = x_0$ gives us some information but still not much. In fact in this case finding that $X = x_0$ simply confirm something that we would have already guessed. However, if X takes an unlikely value, we would be surprised about it and we could say that we have acquired a large amount of information.
The second requirement for a measure of information is that it should be a continuous function of the probability p. This means that if the probability of an event slight changes, the information contained in that event changes only by a small amount.
A third constrain is that the information measure is an additive quantity. If we call S_E the measure of information, then we require that $S_E(p_x, p_y) = S_E(p_x) + S_E(p_y)$. The reason behind this requirement is explained by considering two independent events X and Y that happen with probabilities p_x and p_y such that $p(x_i, y_i) = p_x(x_i)p_y(y_i)$. If we know that $X = x_i$ and we learn that $Y = y_i$, then we expect we are adding something to our knowledge by providing additional information. The fact that the product of probabilities becomes a sum for S_E suggest that the measure of information is a logarithm.
Shannon proved that there is a unique measure which satisfies the previous requirements. It is called the *Shannon entropy* and it is the quantity which quantifies the ignorance about the random variable X or otherwise stated the information gain that is obtained after learning the value of X. It is defined as follows: If the random variable X can take the value x with probability $p(X = x) = p(x)$, then the Shannon entropy of the random variable X is

$$S_E(X) = -\sum_x p(x) \log_2 p(x) \tag{1.50}$$

where the minus sign is put in order for S_E to be a positive quantity. The logarithm in basis 2 means that the information is counted in 'bits'. When the random variable X describes a binary system, that is it can only assume the two values 0, with probability p and 1 with probability $(1 - p)$, then the associated Shannon information is

$$S_E(X) = -p \log_2 p - (1 - p) \log_2(1 - p). \tag{1.51}$$

This quantity has a maximum of 1 bit for $p = 1/2$, that is when the outcomes 0 and 1 are equally likely to be found after a measure, and it takes value zero for $p = 0$ and $p = 1$, meaning that there is no gain of information if we know from the start the value of the random variable X.
The Shannon entropy $S_E(X)$ is a fundamental quantity in classical information theory. Shannon showed that a classical source of letters taken from an alphabet $\{x_i\}$ with probabilities p_i can be compressed so that on average each use of the source can be represented using $S_E(p_i)$ bits of information. This theorem is known as the noiseless channel coding theorem [51]. Moreover, Shannon also proved that data distributed according to X^n, i.e. n copies of X, can be transmitted with an arbitrarily small probability of error as n becomes large by sending $nS_E(X)$ bits. This is called noiseless data compression.
Other relevant measures of information can be defined starting from the definition of the Shannon entropy. These measures capture the relationship between two random variables X and Y. I will here briefly recall only the ones that will be useful for further discussions.
The *joint entropy* measures the combined information in two random variables:

$$S_E(X, Y) = -\sum_{x,y} p(x, y) \log_2 p(x, y) \tag{1.52}$$

where $p(x, y)$ is the joint probability distribution of the two random variable. This quantity tells us about the total uncertainty about the pair (X, Y). If X and Y are independent, then the additive property of the Shannon entropy shows that $S_E(X, Y) = S_E(X) + S_E(Y)$. In fact, for independent variables we have:

$$S_E(X,Y) = -\sum_{x,y} p(x)p(y)\log[p(x)p(y)] = \\ = -\sum_y p_y \sum_x p_x \log p_x - \sum_x p_x \sum_y p_y \log p_y = S_E(X) + S_E(Y). \tag{1.53}$$

This equality does not hold when X and Y are not independent.
The *conditional entropy* measures the information contained in one random variable given that the outcome of the other random variable is known. It is defined as:

$$S_E(X|Y) = -\sum_{x,y} p(x,y)\log[p(x|y)] \tag{1.54}$$

where $p(x|y) = \frac{p(x,y)}{p(y)}$ is the conditional entropy. If X and Y are completely independent then $H(X|Y) = H(X)$, since the conditional probability is $p(x|y) = \frac{p(x)p(y)}{p(y)} = p(x)$. This is due to the fact that acquiring information from Y does not increase the knowledge about X. The conditional and the joint entropies are related. In fact, it is possible to describe the joint distribution of X and Y by measuring first X and then measuring Y given that Y is already known. This leads to the relationship:

$$S_E(X,Y) = S_E(X) + S_E(Y|X). \tag{1.55}$$

Eq. (1.55) can easily be proven by applying the definition of $p(x|y)$.
The *mutual information* is the difference between the information gained from learning the value of X and Y separately and as a joint distribution:

$$S_E(X:Y) = S_E(X) + S_E(Y) - S_E(X,Y) \tag{1.56}$$

The mutual information is used to describe the situation in which two events share information about one other. Having mutual information means that the two events are no longer independent and it is possible, by looking just at one of them, to extract information about the other. The quantity $S_E(X) + S_E(Y)$ represents the uncertainty on the variables X and Y treated separately and $S_E(X, Y)$ is the joint entropy . It is usually used as a measure of correlations between two events.
$S_E(X : Y)$ is symmetric, i.e. $S_E(X : Y) = S_E(Y : X)$. If variables X and Y are independent, the expression for the mutual information is zero, meaning that there is no difference between measuring the two variables independently or as a joint distribution.

In the quantum scenario, the information is stored in the quantum state of a system, described by the density operator ρ which evolves according to the laws of quantum mechanics. The classical probability distributions are replaced with with density matrices, and the summations with trace operations. The unit of quantum information is the qubit, introduced in Sec. 1.1.1. A qubit can be physically implemented, for example, by a spin of an electron or nucleus, or in the polarization of a photon.

If we want to generalize the measures of information previously introduced to the quantum world, we find that quantum information can be quantified in the same way

as classical information using Shannon's requirements. The measure, which we will call S, should be a continuous function of the probabilities of the outcomes of measurements made on a quantum system and it should be additive, that is, if ρ_1 and ρ_2 are uncorrelated systems, then $S(\rho_1 \otimes \rho_2) = S(\rho_1) + S(\rho_2)$. S is called the von Neumann entropy. If we diagonalize the density matrix $\rho = \sum_i \rho_i |\rho_i\rangle\langle\rho_i|$, with ρ_i its eigenvalues, then the von Neumann entropy is defined as:

$$S(\rho) = -\text{Tr}[\rho \log_2 \rho] \tag{1.57}$$

and can be reformulated as:

$$S(\rho) = -\sum_i \rho_i \log_2(\rho_i). \tag{1.58}$$

The von Neumann entropy quantifies the mixedness of a state. If a state is pure, its entropy is zero, while a maximally mixed state has the largest possible amount of entropy, which is $\log_2 D$, if D is the dimension of the system. For qubit system, the maximum of the von Neumann entropy is $\log_2 2 = 1$. From this last expression, we can deduce that the von Neumann entropy is the Shannon entropy for the probability distribution $\{\rho_i\}$, i.e. the Shannon entropy of a random variable X which takes values i with probability ρ_i. This confirms the fact that a density matrix in its diagonal basis can be seen as a classical probability distribution. Analogously to Shannon entropy, it can be proved that the von Neumann entropy is the expected rate of compression of a string of quantum states [52].
By analogy with the Shannon entropies, it is possible to define quantum joint and conditional entropies and the quantum mutual information. The *quantum joint entropy* of two quantum states ρ_A and ρ_B is the von Neumann entropy of their joint density operator, $S(\rho_{AB})$.
The *quantum conditional entropy* is the information gained from ρ_{AB} when ρ_B is known:

$$S(\rho_A|\rho_B) = S(\rho_{AB}) - S(\rho_B) \tag{1.59}$$

The *quantum mutual information* measures the correlations between two quantum systems ρ_A and ρ_B. The generalization to the quantum world of the mutual information (1.56) can be written as:

$$S(\rho_A : \rho_B) = S(\rho_A) + S(\rho_B) - S(\rho_A, \rho_B). \tag{1.60}$$

Quantum mutual information is a very important quantity, since its quantum generalizations lead to the definition of quantum discord. We will give more details about this in Sec. (1.2.2).

1.2 Quantum correlations

One of the best signature of non-classicality in a quantum system is the existence of correlations that do not have a classical counterpart. Entanglement and discord describe the quantum correlations contained in a system, coming either from non-separability or the impossibility of local discrimination. Quantum correlations are a fundamental resource for quantum technology, e.g. the processing of quantum information and for the effective implementation of quantum enhanced protocols.

Entanglement is the most prominent form of quantum correlations, but in many cases disentangled states exhibit non-classical behavior too. The paradigm entanglement-separability has been, for decades, the standard approach to address the quantification of quantum correlations in a physical system. In fact, separable states were thought to carry only classical correlations, while the presence of correlations other than classical were associated solely to the presence of entanglement. However, since the work of Knill and Laflamme [53] on the deterministic quantum computation with one qubit, many works appeared trying to investigate the role of entanglement as a prerequisite for obtaining quantum speedups of information processing tasks [54–56]. Several other measures of quantum correlations have been investigated in the literature [1, 2, 57–59], and among them quantum discord has received a lot of attention. In the past decade it has been recognized that separable mixed states may represent a quantum resource if they show non-zero quantum discord [4, 60–62].
In the next section we will briefly introduce the concepts of entanglement and quantum discord, and we will review their main properties.

1.2.1 Entanglement

Entangled states have been known almost from the very beginning of quantum mechanics, and already in 1935 Schrödinger was defining them as "the most characteristic trait of quantum mechanics". Entanglement is a key element in quantum information processing and quantum communications. Examples of its applications include quantum teleportation, fast quantum algorithms and quantum error-correction [63–66].

For decades entanglement was studied in works related to the foundations of quantum mechanics, such as non-locality and the violations of Bell's inequalities [67–71]. However, in the last decade, entanglement begun to be seen as a powerful resource. For example, the efficient working of a quantum computer or the speed-up of certain quantum algorithms compared to the classical counterparts, relies on the presence of entanglement. For an exhaustive review on entanglement, we address the reader to the Ref.s [72–74].
Entanglement describes quantum correlations that can appear in a quantum system. In this context, we define classical correlations those correlations that can be generated by local operations and classical communication (LOCC). If, by observing a quantum system, we find correlations that cannot be reproduced by LOCC, then we label them as entanglement.
Mathematically, a quantum state is called entangled if it is not separable, i.e. if it cannot be written as a convex combination of tensor product states:

$$\rho_{\text{sep}} = \sum_k p_k \, \rho_k^A \otimes \rho_k^B \tag{1.61}$$

$$\rho_{\text{ent}} \neq \sum_k p_k \, \rho_k^A \otimes \rho_k^B \, . \tag{1.62}$$

Separable states can be produced locally using only a LOCC-scheme. This means that Alice and Bob can solely communicate in a classical way and perform quantum operations only on their subsystem. Any combination of this sequence is allowed but nothing more general. Because of the way in which they are produced, separable states cannot be entangled.
Another important property of entanglement is that it does not increase under LOCC

transformations. This immediately follows from the fact that LOCC can only create separable states. Moreover, entanglement does not change under local unitary operations. This is due to the fact that local unitaries can be inverted and, by the non-increase of entanglement under LOCC, two states connected by local unitaries have an equal amount of entanglement.
Another feature about entanglement is that there are maximally entangled states, i.e. states that are more entangled than all other states living in the same Hilbert space. If we focus on bipartite systems of qubits, these states are called Bell states. There are four Bell states:

$$|\Phi^{\pm}\rangle = \frac{1}{\sqrt{2}}\left(|00\rangle \pm |11\rangle\right) \tag{1.63}$$

$$|\Psi^{\pm}\rangle = \frac{1}{\sqrt{2}}\left(|01\rangle \pm |10\rangle\right). \tag{1.64}$$

These states are very important for the quantum information processing and communications and will be addressed in the later chapters.
As a result of the interaction with a noisy environment, entanglement may decay as a function of time. This decay of entanglement may display different qualitative behaviors. For example, entanglement may be degraded exponentially in time, reaching a zero value asymptotically, or it can decay to zero in a finite time. In this case we talk about *entanglement sudden death* (ESD) [75]. However, in certain cases it is possible to see rebirth of entanglement, i.e. entanglement can decay to zero and then display revivals, with an oscillating dynamics.

Given the definition of entanglement and separability, it is natural to ask whether a given quantum state is entangled or not. Answering this question is a fundamental but not trivial task.

There are many criteria for bipartite entanglement in mixed states. Since it is beyond the scope of this work to discuss all of them, here I will focus on PPT criterion, which will be useful for later discussion.
PPT criterion is based on the concept of *partial transpose* operation. By expanding the density matrix of a composite system ρ in a chosen product basis

$$\rho = \sum_{i,j}\sum_{k,l} \rho_{ij,kl}|i\rangle\langle j| \otimes |k\rangle\langle l|, \tag{1.65}$$

one defines the partial transposition as the transposition operation with respect one subsystem:

$$\rho^{T_A} = \sum_{i,j}\sum_{k,l} \rho_{ji,kl}|i\rangle\langle j| \otimes |k\rangle\langle l| \tag{1.66}$$

where the superscript T_A refers to the fact that the transposition is done by respect Alice indexes. While the partial transpose depends on the basis in which the operation is performed, its spectrum is basis-independent. A density matrix has a positive partial transpose (PPT) if its partial transposition has no negative eigenvalues.
The PPT criterion (also called Peres-Horodecki criterion) [76] states that:

If ρ is a bipartite separable state, then ρ is PPT.

The proof follows directly from the definition of separable state (1.61). In fact, by applying the partial transposition operation, we obtain $\rho^{T_A} = \sum_k p_k \left(\rho_k^A\right)^T \otimes \rho_k^B$. But

$(\rho_k^A)^T = (\rho_k^A)^*$ are non-negative matrices with unitary trace, so they are legitimate density matrices. If follows that none of the eigenvalues of ρ^{T_A} is negative.
This criterion provides a very powerful tool to detect entanglement. Given a density matrix, it is sufficient to compute the partial transpose and its eigenvalues. If at least one of them is negative, then the state is entangled. The PPT criterion was proved to be a necessary and sufficient condition for separability in 2×2 and 2×3 systems [77,78]
Many efforts have been devoted through years to find physically motivated quantitative measures of entanglement, especially for mixed states of a bipartite systems. Examples include the concurrence [79,80], the entanglement of formation [81,82]. the distillable entanglement [81] and the relative entropy of entanglement [83]. However in our work we address the *negativity* as a measure for entanglement.

Negativity

The negativity measure of entanglement is based on the trace norm of the partial transpose ρ^{T_A} of a bipartite mixed state ρ. It measures the degree to which ρ^{T_A} fails to be positive. In this sense the negativity measure of entanglement can be regarded as a quantitative version of Peres' criterion for separability. The negativity was first introduced by Vidal and Werner in 2002 [84] who defined it as:

$$N(\rho) \equiv \frac{||\rho^{T_A}||_1 - 1}{2}. \tag{1.67}$$

This measure vanishes for separable states. The trace norm of a generic operator O is

$$||O||_1 = \mathrm{Tr}\sqrt{O^\dagger O}, \tag{1.68}$$

and it is equal to the sum of the absolute values of the eigenvalues of O, when O is Hermitian. For example, in the case of density matrices $||\rho||_1 = \mathrm{Tr}[\rho] = 1$. In the case of partial transposed matrices, the trace is still $\mathrm{Tr}[\rho^{T_A}] = 1$ but now the eigenvalues may take both negative and positive values. It follows that Eq. (1.67) can be rewritten in terms of the sum of the negative eigenvalues of the partial transposed matrix. In fact, upon diagonalizing the transposed density matrix as $\rho^{T_A} = \sum_k \lambda_k |k\rangle\langle k|$ with $\sum \lambda_k = 1$ but $\sum |\lambda_k|$ may be different from 1, we can write

$$\mathrm{Tr}\sqrt{[\rho^{T_A\dagger}\rho^{T_A}]} = \sum_k |\lambda_k| \tag{1.69}$$

$$||\rho^{T_A}||_1 - 1 = \sum_k |\lambda_k| - \sum_k \lambda_k. \tag{1.70}$$

We can thus renormalized the negativity as

$$N(\rho) = 2\sum_k |\lambda_k^-| \tag{1.71}$$

$$= \sum_k |\lambda_k| - 1 \tag{1.72}$$

where λ_k^- are the negative eigenvalues of the partial transposed density matrix and the factor 2 was added in order for the negativity to be bound between 0 for separable states and 1 for maximally entangled states.

1.2.2 Quantum discord

The state ρ of a bipartite quantum system usually contains both classical and quantum characteristics, in particular, it may have both classical as well as quantum correlations. It is important, in quantum information theory, to be able to distinguish between these two kinds of correlations. For a long time it was believed that entanglement described the whole of quantum correlations and the dichotomy entanglement-separability was the milestone to address this problem. However, entanglement is a special kind of quantum correlations, but not the only kind. Indeed, there exist separable states that have quantum correlations, even if they have zero entanglement.

One of the lesson we learn from quantum mechanics is that the measurement process disturbs the state of a physical system, in contrast to what happen in the classical scenario. It follows that it is possible to claim that the disturbance induced by a measurement on a state is a good evidence of its quantumness. In particular we focus on bipartite systems in which a local measurement is performed on one subsystem. The disturbance induced by the measurement on the system changes indeed the global state, creating correlations that do not have a classical analogue.

Quantum discord arises from the generalization to the quantum world of the classical mutual information. As anticipated in Sec. 1.1.5, the classical mutual information measures the correlations between two random variables X and Y and its quantum generalization was given in Eq. (1.60).
The classical mutual information can also be viewed as the difference between the information gained from learning the value of X and the information gained from learning X when Y is already known:

$$J(X:Y) \equiv S_E(X) - S_E(X|Y), \tag{1.73}$$

where we used the conditional entropy $S_E(X|Y)$ of Eq. (1.54), which measures our uncertainty, on average, about the value of X, given that we know the value of Y. If X and Y are independent, their mutual information in zero while if they are completely correlated, the mutual information is equal to the information contained in X. Eq. (1.56) and (1.73) are equivalent expressions for the classical mutual information.
The generalization of Eq. (1.73) to the quantum case is not trivial. This is due to the presence of the conditional entropy $S(\rho_A|\rho_B)$, which requires to specify the the state of A given the state of B. The ambiguity arises from the fact that in quantum theory a measurement on a subsystem changes the state of the whole system. Let us focus on projective measurements. According to Eq. (1.35), the state of subsystem A after the output corresponding to measurement operator P_j^B on subsystem B has been detected, is given by:

$$\rho_{A|P_j^B} = \frac{\left(\mathbb{I}_A \otimes P_j^B\right) \rho \, \left(\mathbb{I}_A \otimes P_j^B\right)}{\mathrm{Tr}[\mathbb{I}_A \otimes P_j^B \rho]} \tag{1.74}$$

with probability $p_j = \mathrm{Tr}[\mathbb{I}_A \otimes P_j^B \rho]$. Here $\mathbb{I}_A$ is the identity operator acting on subsystem A. The entropies $S(\rho_A|\rho_B)$ may thus be written $S(\rho_{A|P_j^B})$ and they tell us about the missing information about party A. When we weight them by probabilities p_j, we obtain the conditional entropy of A given the complete measurement $\{P_j^B\}$:

$$S\left(\rho_{A|\{P_j^B\}}\right) = \sum_j p_j S(\rho_{A|P_j^B}). \tag{1.75}$$

Eq. (1.73) can thus be generalized to the quantum case as:

$$J(A:B)_{P_j^B} = S(\rho_A) - S(\rho_{A|\{P_j^B\}}). \tag{1.76}$$

Eq. (1.76) represents the information gained about the subsystem A as a result of the measurement $\{P_j^B\}$ on subsystem B. The quantity

$$C(\rho) = \sup_{\{P_j^B\}} J(A:B) \tag{1.77}$$

is interpreted as a measure of classical correlations. See Refs. [1, 2, 85] for further explanations. Maximizing this quantity over all possible measurements $\{P_j^B\}$ on subsystem B corresponds to finding the measurement that disturbs least the quantum state and allows one to extract the most information about A.

We now have two quantum analogs of the classical mutual information: the direct generalization I, which represents the total correlations, and the measurement-induced quantum mutual information J, which represents the classical correlations in a quantum system. The difference between the two quantum versions of the mutual information is called *quantum discord*:

$$\begin{aligned} Q^B(\rho) &= I(\rho) - J(\rho) \\ &= S(\rho_A) - S(\rho) + S\left(\rho_{A|\{P_j^B\}}\right). \end{aligned} \tag{1.78}$$

and it is interpreted as a measure of quantum correlations. It can be shown that the quantum discord is always non-negative. It is moreover worth notice that quantum discord is non-symmetric under the exchange $A \leftrightarrow B$, because the conditional entropy involves a measurement on one subsystem to infer the the state of the other. Analogously to Eq. (1.78), it is possible to define the discord in the case the measurement is performed on subsystem A as:

$$Q^A(\rho) = S(\rho_B) - S(\rho) + S\left(\rho_B|\{P_j^A\}\right). \tag{1.79}$$

Quantum discord is distinct from entanglement for mixed states. In the case of pure states, however, quantum discord reduces to the von Neumann entropy of the reduced density matrix

It is easy to verify that not only entangled, but almost all separable, states have a non-zero quantum discord, that is they are affected by the measurement process. This is an evidence of quantum properties. In order to better understand which states can be classified as purely classical, i.e. they do not have quantum correlations, we introduce the separable 'classical-quantum' (CQ) states [86] as:

$$\rho_{CQ} = \sum_k p_k |\alpha_k\rangle\langle\alpha_k| \otimes \rho_k^B \tag{1.80}$$

$$\rho_{QC} = \sum_k p_k \rho_k^A \otimes |\beta_k\rangle\langle\beta_k| \tag{1.81}$$

where the sets $\{\alpha_k\}$ and $\{\beta_k\}$ represents orthogonal basis in the A and B subsystem respectively, and ρ_k^A and ρ_k^B are quantum states. It is trivial to prove that if we apply a

projective measurement $\{P_i\}$ on the basis $\{\alpha_k\}$, we obtain $Q^A(\rho_{CQ}) = 0$ and the state $\rho_{CQ}^{\{P_i\}} = \rho_{CQ}$ is left unperturbed. In fact:

$$\begin{aligned}\rho_{CQ}^{\{P_i\}} &= \sum_i (P_i \otimes \mathbb{I})\rho_{CQ}(P_i \otimes \mathbb{I}) = \sum_{ik} p_k |\alpha_i\rangle\langle\alpha_i|\alpha_k\rangle\langle\alpha_k|\alpha_i\rangle\langle\alpha_i| \otimes \rho_k^B \\ &= \sum_k p_k |\alpha_k\rangle\langle\alpha_k| \otimes \rho_k^B = \rho_{CQ}\end{aligned} \tag{1.82}$$

On the contrary, a projective measurement on subsystem A of a QC state, changes the state of the system:

$$\rho_{QC}^{\{P_i\}} = \sum_i (P_i \otimes \mathbb{I})\rho_{QC}(P_i \otimes \mathbb{I}) = \sum_{ik} p_k |\alpha_i\rangle\langle\alpha_i|\rho_k^A|\alpha_i\rangle\langle\alpha_i| \otimes |\beta_k\rangle\langle\beta_k| \neq \rho_{QC}. \tag{1.83}$$

CQ states are not disturbed by the measurement on subsystem A. A subset of CQ states which display a zero-discord are written as:

$$\rho_{CC} = \sum_k p_k |\alpha_k\rangle\langle\alpha_k| \otimes |\beta_k\rangle\langle\beta_k| \tag{1.84}$$

where $\{\alpha_k\}$ and $\{\beta_k\}$ are again two orthonormal sets and all the uncertainty about the physical state is given by the probability distribution $\{p_k\}$. These states are called classical-classical states and display only classical correlations. One could consider CC states to correspond simply to the embedding into the quantum formalism of a classical joint probability distribution $\{p_k\}$.

Computing the quantum discord (1.78) for a generic quantum state is not an easy task because it involves an optimization procedure. However, for a certain family of of two-qubit states, called X-states, an analytical solution was found by Luo in Ref. [87]. X-states are characterized by the density matrix

$$\rho = \frac{1}{4}\left(\mathbb{I}_A \otimes \mathbb{I}_B + \sum_{j=x,y,z} a_i \sigma_j^A \otimes \sigma_j^B\right) \tag{1.85}$$

where a_j are real coefficients and σ_j are the Pauli matrices. The quantum discord for such states has an analytical expression:

$$\begin{aligned}Q(\rho) =& \frac{1}{4}[(1-a_x-a_y-a_z)\log_2(1-a_x-a_y-a_z) \\ &+ (1-a_x+a_y+a_z)\log_2(1-a_x+a_y+a_z) \\ &+ (1+a_x-a_y+a_z)\log_2(1+a_x-a_y+a_z) \\ &+ (1+a_x+a_y-a_z)\log_2(1+a_x+a_y-a_z)] \\ &- \frac{1-a}{2}\log_2(1-a) - \frac{1+a}{2}\log_2(1+a)]\end{aligned} \tag{1.86}$$

where $a = \max(|a_x|, |a_y|, |a_z|)$.
In the most general case of an arbitrary two-qubit state, it was shown in Ref. [88] that an analytical expression for the discord cannot be obtained, since the optimization problem for the conditional entropy requires the solution to a pair of transcendental equations in

the parameters of the state.
For the sake of completeness, we mention here a class of two-qubit states that belong to the X-states and that we will consider in the following discussions. It is the class of Bell-states mixtures, or Bell-diagonal states, i.e. combinations of the four Bell states (1.63) and (1.64):

$$\rho = c_1|\Phi^+\rangle\langle\Phi^+| + c_2|\Phi^-\rangle\langle\Phi^-| + c_3|\Psi^+\rangle\langle\Psi^+| + c_4|\Psi^-\rangle\langle\Psi^-| \tag{1.87}$$

where the coefficients $0 < c_i < 1$ satisfy the relation $\sum_i c_i = 1$. The relations between the a_i coefficients in Eq. (1.85) and the c_i coefficients in Eq. (1.87) are given by:

$$\begin{aligned} a_x &= c_1 - c_2 + c_3 - c_4 \\ a_y &= -c_1 + c_2 + c_3 - c_4 \\ a_z &= c_1 + c_2 - c_3 - c_4. \end{aligned} \tag{1.88}$$

Generally, quantum discord is more robust than entanglement, in the sense that it decays to zero at a slower rate with respect to entanglement. Actually, under certain conditions, not only quantum discord is degraded in slow way, but it can be completely unaffected by decoherence, while entanglement decays. This phenomenon is called *frozen* quantum discord [89].

1.3 Quantum non-Markovianity

Quantum systems inevitably interact with their environment. As a result, they are not isolated and the theory of closed quantum systems fails to correctly describe many essential features of their dynamics. It is therefore necessary to include the effects of the environment in the description of the dynamics of the quantum system. The effect of the environment on the dynamics of an open quantum system is to replace the unitary evolution with non-unitary dynamics. Dynamical maps are conventionally classified into two categories: Markovian maps, which describe memoryless dynamics and non-Markovian maps, whose evolution is characterized by memory effects. In many practical situations, Markovian dynamics is only an approximation of the more realistic and more complicated non-Markovian dynamics and a Markovian description fails to account to for the phenomena appearing because of memory effects.
In classical theory of stochastic processes, a Markov process is defined by the Markov condition, which is a condition for the hierarchy of the n-point probability distribution function pertaining to the process, as will be discussed in the next chapter (for a definition of Markovian stochastic processes, see Chap. 2). However this hierarchy does not exist in quantum mechanics. It follows that while Markovianity is well defined for classical stochastic processes, its quantum extension remains elusive and subtle and is the subject of an ongoing debate in the quantum information community. The definition of non-Markovianity and the quantification of quantum memory effects in the dynamics of open quantum systems have received a lot of interest in recent years. Historically, quantum Markovianity has been associated to the property of divisibility of the dynamical map describing the system evolution. A dynamical map $\mathcal{E}_t$ has the property of divisibility if it can be written as the composition of two CPTP maps:

$$\mathcal{E}_t = \mathcal{E}_{t,t'}\,\mathcal{E}_{t'}, \qquad \forall\, t' \leq t. \tag{1.89}$$

It follows that non divisibility occurs if there exist times t' at which $\mathcal{E}_{t,t'}$ is not CPTP.
Several measures for quantum non-Markovianity have been proposed in the past years,

which are based on different mathematical and physical concepts. Examples include measures based on the distinguishability of quantum states, as measured by the trace distance [90] or fidelity [91], semigroup properties [15], divisibility of the dynamical maps [13], Fisher [14] or mutual quantum information [11] and the channel capacities [9]. A common characteristic to many of these measures is that they are based on the non-monotonic behavior of certain quantities appearing when the divisibility property is violated. Among the different measures of non-Markovianity, we focus our attention on two of them, because of their interpretation of non-Markovianty from a quantum information theory perspective, by linking the concept of non-Markovianity to the flow of information and exchange of entropy between the system and the environment. These measures, called BLP and BCM measures, are based on the non-monotonic time evolution of the distinguishability of states and of the quantum capacity respectively.

1.3.1 BLP measure of non-Markovianity

This measure was introduced by Breuer, Laine and Piilo (BLP) in Ref. [90]. They used the concept of information flow between the system and the environment and distinguishability between quantum states to define non-Markovianity.
BLP measure is based on the idea that a Markovian dynamics tends to reduce the distinguishability between any two initial states, while non-Markovianity is associated with a partial regrowth, for at least one interval of time, in distinguishability. Loss of state distinguishability is interpreted as an irreversible flow of information from the system to the environment. An increase in distinguishability, on the contrary, reflects a partial, and often temporary, reversed flow of information back to the system. Memory effects thus emerge through information backflow. The distinguishability between any two states ρ_1 and ρ_2 can be quantified using the trace distance:

$$D(t;\rho_1,\rho_1) = \frac{1}{2}||\rho_1(t) - \rho_2(t)||_1 \tag{1.90}$$

where $||.||$ is the trace norm defined in Eq. (1.68). The trace distance is well defined and finite for all pairs of quantum states and provides a metric on the space of physical states. D is equal to zero if and only if $\rho_1(t) = \rho_2(t)$ and is equal to 1 for orthogonal states. Moreover D is symmetric in the inputs and satisfies the triangular inequality $D(\rho_1,\rho_2) \leq D(\rho_1,\rho_3) + D(\rho_3,\rho_2)$.

It can be proved that the trace distance is preserved under unitary transformations U:

$$D(t;U\rho_1U^\dagger, U\rho_2U^\dagger) = D(t;\rho_1,\rho_2). \tag{1.91}$$

More generally, called $\mathcal{E}$ a complete positive and trace-preserving (CPTP) maps, $\mathcal{E}$ is a contraction of the trace distance $D(\mathcal{E}\rho_1,\mathcal{E}\rho_2) \leq D(\rho_1,\rho_2)$.
The trace distance between any two quantum states is related to the probability of distinguishing the two states [92]. Imagine Alice prepares a quantum system in the state ρ_1 with probability $1/2$ and in the state ρ_2 with probability $1/2$. Then she gives the system to Bob, who performs a measurement to distinguish the two states. The maximal probability that Bob can identify the state is:

$$P_{\max} = \frac{1}{2}\left[1 + D(\rho_1,\rho_2)\right]. \tag{1.92}$$

For example, if ρ_1 and ρ_2 are orthogonal, the trace distance $D(\rho_1,\rho_2) = 1$, the probability $p_{\max} = 1$, which means that Bob is able to distinguish the states with certainty. In this

sense, the trace distance can be interpreted as a measure of distinguishability between quantum states. The dynamical change of the distinguishability between quantum states can be interpreted in terms of a flow of information between the system and the environment. When a quantum process reduces the distinguishability between quantum states, information is leaking from the system. Correspondingly, an increase of distinguishability means that there is a backflow of information into the system. The invariance under unitary transformations indicates that information is preserved under the dynamics of closed systems, while the contraction property guarantees that the maximal amount of information that the system can recover is the same amount that earlier flowed out of it. BLP introduce an "information flux" σ as the rate of change of the trace distance by means of

$$\sigma(t, \rho_{12}(0)) = \frac{d}{dt} D(\rho_1(t), \rho_2(t)) \tag{1.93}$$

where $\rho_{12}(0)$ is the initial joint density matrix of the two states, and the initial time is $t_0 = 0$. For non-Markovian processes, the information must flow back to the system for some intervals of time and thus σ must be positive for such intervals. The BLP measure of non-Markovianity quantifies the total increase of distinguishability over the whole time evolution, that is the total amount of information backflow:

$$N_{\text{BLP}} = \max_{\rho_{12}(0)} \int_{\sigma>0} dt\, \sigma(t, \rho_{12}(0)). \tag{1.94}$$

The time integration is over all time intervals in which $\sigma > 0$ and the maximum is taken over all pairs of initial states. Negative σ means information loss from the system to the environment, while positive σ indicates a reversed flow of information. The integration over all positive fluxes accumulates the information that returns to the system . Whenever $N_{\text{BLP}} > 0$ the dynamics is non-Markovian.

It is possible to show that all divisible maps, i.e. maps having the property $\mathcal{E}_t = \mathcal{E}_{t,s}\mathcal{E}_s$ with $t > s > t_0$, are Markovian according to this measure, but the converse is not true in general [12]. Notice that the notation $\mathcal{E}_{t,s}$ indicates a quantum channel that describe the evolution of a density matrix from an initial time s to a final time t. Using Eq. (1.93), the measure of non-Markovianity can be rewritten as:

$$N_{\text{BLP}} = \max_{\rho_{12}(0)} \sum_n \left[D\left(\rho_1(t_n^{\max}), \rho_2(t_n^{\max})\right) - D\left(\rho_1(t_n^{\min}), \rho_2(t_n^{\min})\right) \right], \tag{1.95}$$

where $t_n^{\max}$ and $t_n^{\min}$ correspond to the time points of the local maximum and minimum of the trace distance $D(\rho_1(t), \rho_2(t))$ respectively. In order to calculate the non-Markovianity according to this measure one should sum up the total contributions of all intervals $\{t_n^{\max}, t_n^{\min}\}$ and finally perform the maximization over all pairs of initial states. Generally, the optimization over all pairs of initial states is not an easy task and it makes the measure difficult to compute, although it has been shown that the two states maximizing the measure are orthogonal to each other [93]. Moreover, for some simple dynamical maps the maximizing pair has been found [94–96]. In particular for the case of a dephasing channel, the trace distance calculated for the two optimal initial states is given by:

$$D(t) = |\Lambda(t)|, \tag{1.96}$$

which is the absolute value of the dephasing coefficient appearing in Eq. (1.49).
In the following, we use the name *optimal trace distance* for the expression (1.96), that is

the trace distance computed for the optimal pair. Thus the study of non-Markovianity can be reduced to the analysis of the optimal trace distance (1.96). Once its expression is known it is possible to write the information flux σ and then numerically compute the non-Markovianity as the integral of σ over the time intervals in which it is positive.

1.3.2 BCM measure of non-Markovianity

The second measure that we use, introduced by Bylicka, Chruściński and Maniscalco, is based on the concept of quantum capacities.
We introduced the concept of quantum channels in Sec. (1.1.4). In the typical scenario of quantum information processing and communication, Alice and Bob are at opposite ends of a quantum channel. Alice sends informations (classical or quantum) through the channel and Bob receives it. The maximum amount of information that can be reliably transmitted along a noisy channel is known as the *channel capacity*. The quantum capacity bounds the rate at which quantum information can be reliably transmitted through the channel $\mathcal{E}_t$.
In the case of degradable channels [97], such as the dephasing channel, the single-use quantum capacity may be written as

$$C_Q(\mathcal{E}_t) = \sup_{\rho} I_c(\rho, \mathcal{E}_t) \tag{1.97}$$

where I_c represents the coherent information [98]:

$$I_c(\rho, \mathcal{E}_t) = S\big(\mathcal{E}_t(\rho)\big) - S_{\text{ex}}(\rho, \mathcal{E}_t), \tag{1.98}$$

with $S(\rho)$ the von Neumann entropy defined in Eq. (1.57) and $S_{\text{ex}}(\rho, \mathcal{E}_t)$ is the entropy exchange [98, 99]. The superior in Eq. (1.97) should be taken over all possible states of the considered system. It is worth stressing that, contrarily to the trace distance, the coherent information describes how the entropy of both the system and the environment change. Hence, this quantity is more apt to capture the concept of information flow between the system and the environment. More explicitly, coherent information is, in fact, quantifying the flow of information between system and environment, while the trace distance is quantifying only the loss of information that we have on the system without any indication on whether this information is acquired by another agent (and may come back).
Strictly speaking, Eq. (1.97) describes the quantum capacity only for memoryless degradable channels [100–102] and thus it seems unsuitable to to address quantum channels arising from the interaction with a classical environment exhibiting long-lasting time correlations. However, in the following chapters, we will be interested in the effects of memory *during the propagation* of the information carriers, rather than the memory effects among subsequent uses of the channel. For this reason expression (1.97) will fit nicely for our purposes.
A central result in quantum information theory is the data processing inequality [98] which says that processing quantum information reduces the amount of correlations between input and output. For a divisible channel $\mathcal{E}_t = \mathcal{E}_{t,s}\mathcal{E}_s$ with $s \leq t$, this inequality may be written as $I(\rho, \mathcal{E}_t) \leq I(\rho, \mathcal{E}_s)$. As a consequence of the quantum data-processing inequality, the quantum capacity is a monotonically decreasing function of time for divisible quantum channels. Divisibility, however is a property of Markovian dynamical

maps. The BCM measure is therefore based on the non-monotonic behavior of $C_Q(\mathcal{E}_t)$:

$$N_{\text{BCM}} = \int_{\frac{dC_Q(\mathcal{E}_t)}{dt}>0} \frac{dC_Q(\mathcal{E}_t)}{dt} dt \tag{1.99}$$

$$= \sum_n \left[C_Q\left(\rho_1(t_n^{\max}), \rho_2(t_n^{\max})\right) - C_Q\left(\rho_1(t_n^{\min}), \rho_2(t_n^{\min})\right)\right] \tag{1.100}$$

Non-Markovianity corresponds to $N_{\text{BCM}} > 0$. Even if this measure does not explicitly involve a maximization procedure, an optimization procedure is required in the computation of the quantum capacity (1.97). In the case of a dephasing channel, however, the analytical expression for C_Q is known [30]:

$$C_Q(t) = 1 - S_E\left(\frac{1-\Lambda(t)}{2}\right) \tag{1.101}$$

where $\Lambda(t)$ is the dephasing coefficient in Eq. (1.48) and S_E the Shannon binary entropy (1.51). The operational interpretation of quantum capacity allows one to use N_{BCM} to assess if and how non-Markovianity can be seen as a resource for quantum communication and information processing.

1.4 Quantum estimation theory

Several quantities of interest in quantum information theory do not correspond to quantum observables and cannot be assessed directly by measurement. Examples are the purity of a quantum state, a quantum phase or quantum correlations. The canonical way to address this problem is to use the tools of local quantum estimation theory (QET). In this section we review only the main tools of local QET that will be useful in the following chapters. For a more exhaustive discussion on the topic, see Ref.s [103–105].
The aim of an estimation procedure is to find the best strategy to infer the value of an unknown parameter with the highest possible precision. This is done by performing indirect measurements on the quantum system, i.e. inferring the value of the parameter by processing the set of outputs from the measurement of a different observable, or a set of variables.

The usual scenario in quantum estimation theory is to consider a family of quantum states ρ_λ depending on an unknown parameter λ, usually corresponding to non-observable quantity. The goal of any estimation procedure is to infer the value of the parameter λ by measuring some observable quantity on the system ρ_λ. To this aim, repeated measurements are performed on the system and then the overall sample of outcomes $(x_1, x_2 \ldots, x_M)$ is processed in order to obtain an estimator for the unknown parameter. An estimator $\hat{\lambda} = \hat{\lambda}(x_1, x_2 \ldots x_M)$ is a function of the outcomes $\{x_i\}$. We denote by $V(\hat{\lambda})$ the corresponding mean square error (MSE):

$$V(\hat{\lambda}) = \mathbb{E}\left[\left(\hat{\lambda} - \lambda\right)^2\right] \tag{1.102}$$

where $\mathbb{E}[X]$ denotes the expected value (or mean or first moment) of the random variable X. An estimator is said to be *unbiased* if $\mathbb{E}\left[\hat{\lambda}\right] = \lambda$, that is if the expected value of the estimator is equal to the true value of the parameter. For unbiased estimators, the

MSE is equal to the variance $\sigma^2(\hat{\lambda}) = \mathbb{E}\left[\left(\hat{\lambda} - \mathbb{E}\left[\hat{\lambda}\right]\right)^2\right]$. The concept of the variance of a stochastic process will be introduced in Chapter. 2.
Given a sample of experimental data, there will be an infinite number of functions of the sample that might be proposed as estimators of the unknown parameter. Therefore, we need a figure of merit to quantify the precision of an estimator, in order to find the best estimate of the parameter. This quantity is the variance. The smaller is the variance $\sigma^2(\hat{\lambda})$ associated to the estimator, the more precise is the estimator, because it will tend to have values that are concentrated more closely around the true value of the parameter. However, the accuracy of an estimation procedure can never be infinite. This is due to the Cramér-Rao (CR) inequality, which provides a lower bound to the precision of any unbiased estimator for the parameter λ:

$$V(\bar{\lambda}) \geq \frac{1}{M\, F(\lambda)} \tag{1.103}$$

where M is the number of measurements and $F(\lambda)$ is the Fisher information (FI):

$$F(\lambda) = \int dx\, p(x|\lambda)\ \left[\partial_\lambda \log p(x|\lambda)\right]^2, \tag{1.104}$$

where $p(x|\lambda)$ is the conditional probability of obtaining the outcome x when the true value of the parameter is λ. The proof of the CR inequality and the conditions that must be satisfied for the theorem to hold can be found in Ref. [105].
In the case of a qubit, we may for instance consider the population measurement in a given basis $\{j\}$. The density operator of the system can thus be written as $\rho{=}\sum_{jk=0,1} \rho_{jk}|j\rangle\langle k|$. In such a case the Fisher is given by:

$$F(\lambda) = \frac{(\partial_\lambda \rho_{00})^2}{\rho_{00}} + \frac{(\partial_\lambda \rho_{11})^2}{\rho_{11}} \tag{1.105}$$

where ρ_{ii} are the two diagonal elements of the density matrix in the population basis.

In order to compute the ultimate bound to precision as posed by quantum mechanics, the FI must be maximized over all possible measurements. Given a quantum system, the conditional probability of obtaining outcome x_i knowing that the parameter has the value λ, may be written as according to Eq. (1.34) $p(x_i|\lambda) = \mathrm{Tr}[\rho_\lambda E_i]$, where E_i is a quantum measurement $E_i = M_i^\dagger M_i$. The maximization over all the possible measurements can be achieved upon introducing the Symmetric Logarithmic Derivative L_λ as the operator which satisfies the relation:

$$\frac{L_\lambda \rho_\lambda + \rho_\lambda L_\lambda}{2} = \partial_\lambda \rho_\lambda. \tag{1.106}$$

We address the reader to Ref. [33] for the mathematical details in the optimization procedure. After the maximization one obtains the ultimate bound to the precision of any estimator, as expressed by the quantum Cramér-Rao (QCR) bound:

$$V(\lambda) \geq \frac{1}{M\, G(\lambda)}. \tag{1.107}$$

Here $G(\lambda) = \mathrm{Tr}[\rho_\lambda L_\lambda^2]$ is the so-called quantum Fisher information (QFI), i.e. the superior of $F(\lambda)$ over the quantum measurements. In the case of a qubit, the expression of the

QFI can be found after diagonalizing the density matrix according to Eq. (1.24) $\rho_\lambda = \sum_{n=1}^{2} \rho_n |\rho_n\rangle\langle\rho_n|$:

$$G(\lambda) = \sum_{n=1}^{2} \frac{(\partial_\lambda \rho_n)^2}{\rho_n} + 2 \sum_{n \neq m} \frac{(\rho_n - \rho_m)^2}{\rho_n + \rho_m} |\langle \rho_m | \partial_\lambda \rho_n \rangle|^2. \tag{1.108}$$

The first term in Eq. (1.108) is the classical FI of the distribution $\{\rho_n\}$, while the second term has a quantum nature and vanishes when the eigenvectors of ρ_λ do not depend upon the parameter λ. When the condition $F(\lambda) = G(\lambda)$ is fulfilled, the measurement is said to be *optimal*. Once a measurement has been chosen, and performed, one has to process the data, i.e. chose an estimator. Often in the process of making an estimate, we must choose among several unbiased estimators for a given parameter. Estimators for which the CR bound is saturated, with the equality condition satisfied in Eq. (1.103), are said to be *efficient*.

A suitable figure of merit to assess the overall estimability of a parameter is given by the single-measurement quantum signal-to-noise ratio (QSNR):

$$R = \lambda^2 \, G(\lambda) \tag{1.109}$$

which accounts for the fact that large values of the parameter are generally easier to estimate, while small values need more precise estimators. A given parameter is said to be easily estimable if the corresponding R is large. On the contrary, if R is small the estimation of λ is an inherently inefficient procedure, whatever strategy is employed to infer its value.

Once a measurement has been chosen, possibly the optimal one, one has to find an estimator, i.e. a procedure to process data in order to infer the value of the parameter of interest. An example of an estimator which is asymptotically efficient, i.e. saturates the QCR bound in the limit of large samples, is the maximum likelihood (ML) estimator. Consider M independent measurements of the random variable X, with probability distribution $p(x|\lambda)$. The joint probability function of an experimental sample of size M, $\{x_i\}_{i=1}^{M}$, is given by the product $\prod p(x_i, \lambda)$ and it is usually referred to as the *likelihood* function $\mathcal{L}(\lambda)$:

$$\mathcal{L}(\lambda) = \mathcal{L}(\lambda | x_1, x_2 \ldots, x_M) = \prod_{i=1}^{M} p(x_i|\lambda). \tag{1.110}$$

The likelihood function says how "likely" it is to obtain the experimental sample $\{x_i\}$ for any given value of the parameter λ. The ML estimator for the parameter λ is the value yielding the largest likelihood of the observed values, that is the value that maximizes the quantity in Eq. (1.110):

$$\hat{\lambda}_{\text{ML}} = \arg\max L(\lambda). \tag{1.111}$$

$\hat{\lambda}_{\text{ML}}$ is known to be asymptotically efficient [105] and it saturates the CR bound for a large number of measurements $M \gg 1$. On the other hand, in practical situations one is usually interested in checking whether this regime is achieved for values of M within the experimental capabilities.

We showed in Sec. 1.1.5 that the conditional probability is related to the joint probability by the relation $p(x, y) = p(x|y)p(y)$. But since the joint probability is symmetric for

an exchange $x \leftrightarrow y$, i.e. $p(x,y) = p(y,x)$ we my write:

$$p(x|y) = \frac{p(y|x)p(x)}{p(y)}. \tag{1.112}$$

Eq. (1.112) is know as the Bayes' rule. Suppose we collect a sample of experimental data $\Omega = \{x_i\}_{i=1}^{M}$ obtained from M repeated measurements of the random variable $X(\lambda)$ which depends upon the unknown and unaccessible real parameter λ. If we call $p(\Omega|\lambda)$ the conditional probability distribution of obtaining the experimental sample Ω when the true value of the parameter is λ, we can rewrite Bayes' rule as:

$$p(\lambda|\Omega) = \frac{p(\Omega|\lambda)p(\lambda)}{\int_\Lambda p(\Omega|\lambda')p(\lambda')d\lambda'} \tag{1.113}$$

where $p(\lambda)$ is the *a priori* probability distribution, $p(\lambda|\Omega)$ is called the *a posteriori* probability distribution and it is built using the collected data $\Omega = \{x_i\}$ and Λ is the set of possible values for the parameter λ. Thus, before observing the data, our guess about λ is expressed in terms of the prior distribution, whereas once the data are observed, this priori distribution is updated to yield the posterior distribution. The Bayesian estimator is defined as the mean of the posterior distribution $p(\lambda|\Omega)$:

$$\hat{\lambda}_B = \int_\Lambda \lambda p(\lambda|\Omega)d\lambda. \tag{1.114}$$

The precision of the Bayesian estimator is quantified through its variance:

$$\mathrm{Var}[\hat{\lambda}_B] = \int_\Lambda \left[\lambda - \hat{\lambda}_B\right]^2 p(\lambda|\Omega)d\lambda. \tag{1.115}$$

In the Bayesian approach, the unknown parameter is treated like a random variable, with an associated probability distribution conditioned by the experimental data. As the maximum likelihood estimator, the Bayes estimator is asymptotically efficient, saturating the Cramér-Rao bound.

1.5 Summary

- The formalism of density matrices allows us to describe the state of a quantum system, its temporal evolution and the effects of quantum measurements on such state.
- Quantum correlations, i.e. correlations with no classical analogue such as entanglement and quantum discord, are a resource for quantum information technologies. Entangled states cannot be generated using a LOCC scheme and are mathematically defined as non-separable states. However, quantum discord describes a more general kind of quantum correlations, that can be found also in separable state. Discord quantifies correlations arising from the "sensitivity" to local measurements, i.e. the fact that measuring one subsystem of a global quantum system perturbs the state of the other part.
- While a classical definition of non-Markovianity for stochastic processes is well known, its generalization to the quantum world is not straightforward. According to BLP measure, a non-Markovian dynamics is associated with a regrowth

in distinguishability between quantum states and this regrowth is interpreted as an information backflow to the system. BCM measure, instead, associates non-Markovianity with a non-monotonic behavior of the quantum capacity.

- Quantum estimation theory allows one to find the optimal setting to efficiently estimate the value of an unknown parameter. The ultimate bound to the precision of the variance associated with an estimator is bounded from below according to the quantum Cramér-Rao theorem and it is proportional to the inverse of the quantum Fisher information.

CHAPTER 2

Stochastic processes and classical noise

In this chapter I review the main concepts related to the theory of stochastic processes and classical noise [47, 106–108]. Since the topics is quite large, I present here only the notions that are necessary to the comprehension of my work.

We can define a random phenomenon as an empirical phenomenon that obeys probabilistic, rather than deterministic, laws. Examples are the motion of a particle in Brownian motions or the fluctuating current in an electric circuit due to thermal noise or the growth of a population such as a bacterial colony. Without the need to introduce formal definitions, for our purposes it will be sufficient to state that, from a mathematical point of view, a *random variable* X is an object defined by a set of possible values $\{x_i\}$ and a probability distribution over this set $p(X = x_i) = p(x_i)$. The set may be discrete or continuous. The probability distribution $p(x)$ is non-negative and normalized. The set of states and the probability distribution fully characterize the random variable. However there are other fundamental quantities that are often used.
Let us consider a random variable X whose set of possible values $\{x\}$ is a continuous set. The average, or expected value or expectation, of X is defined as:

$$\mathbb{E}[X] = \int x\, p(x)\, dx \tag{2.1}$$

and the variance:

$$\sigma^2 = \mathbb{E}\left[(X - \mathbb{E}[X])^2\right] = \mathbb{E}\left[X^2\right] - \mathbb{E}[X]^2 . \tag{2.2}$$

If the possible values $\{x_i\}$ of the random variable X are discrete, the integral in Eq. (2.1) is substituted by a sum: $\mathbb{E}[X] = \sum_i x_i p(x_i)$.
The quantity $\mathbb{E}[X^m]$ is called the *m-th moment* of X. It follows that the average is the first order moment and the variance is the difference between the second moment and square of the first one. The characteristic function of a stochastic variable X is defined by:

$$\phi_X(u) = \mathbb{E}\left[e^{iuX}\right] . \tag{2.3}$$

In the case of a Gaussian random variable, i.e. a random variable following a Gaussian distribution $p(x) = \frac{1}{\sqrt{2\pi\sigma^2}} \exp\left[-\frac{(x-\mu)^2}{2\sigma_2}\right]$ with average μ and variance σ^2, the characteristic function can be rewritten as:

$$\phi_X^G(u) = e^{i\mu u - \frac{1}{2}\sigma^2 u^2} . \tag{2.4}$$

The characteristic function completely determines the behaviour and the properties of the probability distribution of the random variable X. In fact, from Eq. (2.3), we can alternatively write it as the Fourier Transform of the probability distribution $p(x)$:

$$\phi_X(u) = \int e^{iux} p(x) dx, \tag{2.5}$$

A *stochastic process* is described as a collection of $\{X(t), t \in T\}$ of random variables indexed by a parameter t varying in an index set T. It should be pointed out that a stochastic process $\{X(t), t \in T\}$ is in reality a function of two arguments $\{X(t,s), t \in T, s \in S\}$. For a fixed value of t, $X(t,\cdot)$ is a function on the probability space S, i.e. $X(t,\cdot)$ is a random variable. On the other hand, if s is fixed in S, then $X(\cdot,s)$ is a function of time that represent a possible observation of the stochastic process $\{X(t), t \in T\}$. The function $X(\cdot,s)$ is called *realization* of the process.

A very important function for stochastic processes is the autocorrelation function $C(t_1,t_2)$, defined as:

$$C(t_1,t_2) = \mathbb{E}\left[X(t_1)X(t_2)\right]. \tag{2.6}$$

where t_1 and t_2 are two instants of time.
A process is called *stationary* when its moments are not affected by a shift in time, i.e. when

$$\mathbb{E}\left[X(t_1+\tau)X(t_2+\tau)\dots X(t_n+\tau)\right] = \mathbb{E}\left[X(t_1)X(t_2)\dots X(t_n)\right] \tag{2.7}$$

for all n and τ. In particular, $\mathbb{E}[X]$ is independent of time. Moreover, the autocorrelation function of a stationary process depends only on time differences $|t_1 - t_2|$, such that $C(t_1,t_2) = C(|t_1 - t_2|)$. Often there exist a constant τ_c such that the autocorrelation function is zero o negligible for $|t_1 - t_2| < \tau_c$; one then calls τ_c the *autocorrelation time*.
The Fourier transform of the autocorrelation function is the power spectral density, as stated by the Wiener-Khinchin theorem [109, 110]:

$$S(\omega) = \int_{-\infty}^{\infty} C(\tau) e^{-i\omega\tau} d\tau. \tag{2.8}$$

Any function of a stochastic process $f_X(t) = f[X(t)]$ is a stochastic process itself. For a fixed random variable X, different realizations of the stochastic process exist. The average of $f_X(t)$ is obtained as the ensemble average over all the possible realizations of the stochastic process:

$$f(t) = \mathbb{E}\left[f_X(t)\right] = \int f_x(t) p(x) dx. \tag{2.9}$$

Another important quantity is the *noise phase*, defined as:

$$\varphi(t) = \int_{t_0}^{t} X(s) ds. \tag{2.10}$$

The noise phase is still a random variable, distributed according to a probability density $p(\varphi)$ which depends upon the specific stochastic process $\{X(t)\}$. The characteristic function of the random variable $\varphi(t)$ is given by:

$$\mathbb{E}\left[e^{i\varphi(t)}\right] = \mathbb{E}\left[e^{i\int_{t_0}^{t} X(s)\,dx}\right] \tag{2.11}$$

and it plays a fundamental role in computing the dynamics of a quantum system subject to classical noise, as we will show in later chapters.
A relevant class of stochastic processes are Markovian processes. A stochastic process is called Markovian if the conditional probabilities satisfy the property that for any set of n successive times one has

$$p(x_n, t_n|x_1, t_1; \ldots; x_{n-1}, t_{n-1}) = p(x_n, t_n|x_{n-1}, t_{n-1}) \tag{2.12}$$

where $t_1 < t_2 < \cdots < t_n$. Eq. (2.12) shows that the probability for X to take the value x_n at time t_n given the values x_i at previous times t_i only depends upon the last assumed value and not on previous ones. In this sense, it is said that Markovian processes do not display memory effects: predictions for the future of the process are based solely on its present state, without the need of knowing the process's full history. The Markov condition (2.12) implies that the conditional transition probability obeys the Chapman-Kolmogorov equation [106]:

$$p(x, t|y, s) = \sum_z p(x, t|z, \tau)p(z, \tau|y, s). \tag{2.13}$$

A Markov process is therefore uniquely characterized by its conditional transition probability and the initial distribution. If a stochastic process does not have the Markov property, then it is said to be non-Markovian.

As we already said, physical systems are never isolated from their environment. Interaction with an external bath introduces noise on the dynamics of the system itself, causing phenomena of decoherence and loss of quantumness. If the environment is described using a classical model, the classical noise may be modeled as a stochastic process, i.e. a function of time that does not have a deterministic behavior. In this sense, in the following, we will often use the expression "noise induced by a random process".

When a stochastic process can be fully characterized using only its second order statistics, i.e. the average and the variance, it is said to be *Gaussian*. All the information about the Gaussian process is thus contained in the autocorrelation function, or equivalently, in the power spectrum. On the other side, a stochastic process is called *non-Gaussian* if it cannot be fully characterized by the mean and variance. As a consequence, the mere knowledge of the spectrum is not sufficient to describe the process and, as we will show in the next chapters, the very structure of the environment plays a very important role. In the following section we review some paradigmatic examples of Gaussian and non-Gaussian processes that will be later referred to in our work.

2.1 Gaussian stochastic processes

A stochastic process $\{X(t), t \in T\}$ is said to be a Gaussian process if for any integer n and any subset $\{t_1, t_2 \ldots, t_n\}$ the n random variables $X_1 \ldots X_n$ are jointly normally distributed, in the sense that their joint characteristic function is given, for any real numbers $u_1, u_2, \ldots, u_n$, by

$$\begin{aligned}&\phi_{X(t_1),X(t_2)\ldots,X(t_n)}(u_1, u_2 \ldots, u_n) = \\ &\mathbb{E}\left[\exp\left(i\sum_{j=1}^{n} u_j X(t_j)\right)\right] = \exp\left[i\sum_j u_j\mu_j - \frac{1}{2}\sum_{j,k}^{n} u_j u_k\, K(t_j, t_k)\right]\end{aligned} \tag{2.14}$$

where $\mu_j = \mathbb{E}[X(t_j)]$ and we introduced the covariance kernel:

$$K(t_j, t_k) = \mathbb{E}[X(t_j)X(t_k)] - \mathbb{E}[X(t_j)]\,\mathbb{E}[X(t_k)]\,. \tag{2.15}$$

Eq. (2.14) is written in the case of a Gaussian process discrete in time, with times t taking only discrete values t_k. Its generalization to a continuous time Gaussian process, where the value of variable t can vary continuously in the set T, is given by:

$$\mathbb{E}\left[\exp\left(i\int_{t_0}^{t} u(s)X(s)ds\right)\right] = \exp\left[i\int_{t_0}^{t} u(s)\mu(s)ds - \frac{1}{2}\int_{t_0}^{t}\int_{t_0}^{t} u(t)u(s')\,K(s,s')\,ds\,ds'\right] \tag{2.16}$$

where we substituted the discrete subset of T, $\{t_1, t_2 \ldots, t_n\}$, with the continuous time interval $[t_0, t]$. As we see from Eq.s (2.14) and (2.16), the Gaussian process is fully characterized by its mean and its autocorrelation function.

From Eq. (2.16), it is immediate to write the explicit expression of the expectation $\mathbb{E}\left[e^{iu\varphi(t)}\right]$ with u a constant function and $\varphi(t)$ defined in Eq. (2.11). In fact, for Gaussian process, this quantity is given by:

$$\mathbb{E}\left[e^{iu\varphi(t)}\right] = \exp\left[i\,u\int_{t_0}^{t}\mu(s)ds - \frac{1}{2}u^2\beta(t)\right] \tag{2.17}$$

where we introduced the β-function as:

$$\beta(t) = \int_{t_0}^{t}\int_{t_0}^{t} K(s,s')\,ds\,ds' \tag{2.18}$$

which depends on the specific form of the autocorrelation kernel K.
From a comparison between Eq. (2.17) and Eq. (2.4), one immediately sees that the characteristic function of $\varphi(t)$ is that of a normal distributed variable. It follows that φ is a random variable with a Gaussian distribution characterized by mean $\int_{t_0}^{t}\mu(s)ds$ and variance $\beta(t)$.

2.1.1 Examples of Gaussian processes

In this section we review the main notions about the Ornstein-Uhlenbeck (OU) process and fractional Brownian (fB) process, that will be employed in later chapters.

The best known example of stationary Gaussian process is the Ornstein-Uhlenbeck process. The OU process is a stationary Markovian Gaussian process which describes the stochastic behavior of the velocity of a Brownian particle. A stochastic process is said to be an *Ornstein-Uhlenbeck process* [111] with zero mean if it is a Gaussian process satisfying:

$$\mu_{OU}(t) = 0 \tag{2.19}$$

$$C_{OU}(|t - t_0|) = \frac{\Gamma\gamma}{2}e^{-\gamma|t-t_0|}. \tag{2.20}$$

Here Γ is the damping rate and γ is the inverse of the autocorrelation time τ_c and plays the role of a memory parameter. In the limit of zero autocorrelation time, i.e. when

$\gamma \to \infty$, the autocorrelation function is a Dirac delta. It follows that in this limit the Ornstein-Uhlenbeck process becomes a Gaussian white noise with a flat power spectrum.
The OU process is a stationary Markovian Gaussian process which describes the stochastic behavior of the velocity of a Brownian particle. From Eq. (2.18), we can easily compute the β function for the OU process as:

$$\beta_{OU}(\gamma, \Gamma, t) = \frac{\Gamma}{\gamma}\left(\gamma t + e^{-\gamma t} - 1\right). \tag{2.21}$$

The power spectrum of the Ornstein-Uhlenbeck process is the Fourier transform of the autocorrelation function (2.20) and it is given by:

$$S_{OU}(\omega) = \frac{\gamma^2 \Gamma}{\sqrt{2\pi}(\gamma^2 + \omega^2)}. \tag{2.22}$$

The power spectrum of the OU process is a Lorentzian.

The *fractional Brownian process*, also called fraction Brownian motion (fBm), describes anomalous diffusion. It is a stochastic non-stationary process with zero average $\mathbb{E}\left[X(t)\right] = 0$ and characterized by the autocorrelation function:

$$C_{fB}(t, t_0) = \frac{1}{2}\left(|t|^{2H} + |t_0|^{2H} - |t - s|^{2H}\right) \tag{2.23}$$

where $\Gamma(x)$ is the Euler Gamma function and H is a real parameter $H \in [0, 1]$ called the Hurst parameter [112]. The Hurst parameter is directly linked to the fractal dimension of the trajectories of the particles exposed to the fractional noise. Because of the non-stationarity of this process, the power spectrum as defined in Eq. (2.8) does not exist and a generalized spectrum should be introduced. In Ref. [113] it was shown that the generalized noise spectrum has a power-low dependence $S(\omega) \propto |\omega|^{-2H-1}$.
Moreover, the fractional Brownian motion is a self similar Gaussian process, that is $B_H(at) = |a|^H B_H t$.

When $H = 1/2$, the autocorrelation function can be written as $\min(t, t_0)$ meaning that the fB process reduces to the Wiener process (i.e. Brownian motion). From Eq. (2.18) we may compute the β function for the fB process as:

$$\beta_{fB}(t) = \frac{t^{2H+2}}{2H+2}. \tag{2.24}$$

Finally, we introduce also noise generated by stationary Gaussian processes with zero average and a Gaussian (G) and a power-law (PL) autocorrelation function:

$$C_G(t - t_0) = \frac{\Gamma\gamma}{\sqrt{\pi}} e^{-\gamma^2 (t - t_0)^2} \tag{2.25}$$

$$C_{PL}(t - t_0, \alpha) = \frac{\alpha - 1}{2} \frac{\gamma\Gamma}{(\gamma|t - t_0| + 1)^\alpha} \tag{2.26}$$

where again γ is a noise parameter, Γ is the damping rate and we assume $\alpha > 2$. From

these autocorrelations functions, it is easy to compute the respective β-functions:

$$\beta_G(t) = \frac{\Gamma}{\gamma}\left[\gamma t\,\mathrm{Erf}(\gamma t) + \frac{e^{-(\gamma t)^2}-1}{\sqrt{\pi}}\right] \tag{2.27}$$

$$\beta_{PL}(t) = \frac{\Gamma}{\gamma}\left[\frac{(1+\gamma t)^{2-\alpha}+\gamma t(\alpha-2)-1}{\alpha-2}\right]. \tag{2.28}$$

In the limit where $\gamma \to \infty$, the β function for the three stationary processes OU, G and PL tends to the quantity Γt.

As we will see in the following chapter the β function is related with the decay of decoherences in the density matrix of a single- and two-qubit system subject to Gaussian noise.

As a final remark, notice that for Gaussian processes with zero average $\mathbb{E}[X(t)] = 0\ \forall t$, the covariance kernel (2.15) coincides with the autocorrelation function (2.6).

2.2 Non-Gaussian stochastic processes

From the knowledge of the mean and the covariance function of a stochastic process, one cannot in general determine its probability law. In particular, Eq.s (2.14) and (2.16) do not hold for a non-Gaussian process and the average and variance are not sufficient to characterize the process, but all the higher order momenta are required. Moreover, the knowledge of only the noise spectrum is not sufficient, since noise sources with identical power spectra can have different decohering effects. It follows that it is necessary to specify the model for the noise source in more detail, providing more information about the stochastic process generating the noise [114].

Non-Gaussian noise cannot be mimicked by any Gaussian model, such as a bath of harmonic oscillators. The microscopic structure of the environment plays a central role in determining the dynamics of the quantum system subject to the noise. A key concept that lies at the very heart of the noise models we will present in the following is that of bistable *fluctuators*. A bistable fluctuator, often referred to also as two-level fluctuator (TLF), is a quantity which switches randomly between two values with a certain switching rate. More details will be given in Sec. (2.2.1). The effect of a single fluctuator is to produce the random telegraph noise (RTN), while a proper collection of TLFs gives rise to $1/f^\alpha$ noise.

In the following we review two paradigmatic examples of non-Gaussian noises, generated by non-Gaussian processes, i.e. the random telegraph noise and the $1/f^\alpha$ noise.

2.2.1 The random telegraph noise

The random telegraph noise describes a discrete stochastic process $\{B(t), t \in [0,\infty]\}$, where the random variable B can only take two possible values, for example $B(t) = \pm 1$. Jumps between the two states ± 1 occur at a switching rate γ such that the average number of flips in a time interval $[0,t]$ is γt. The probability that the fluctuator switch n times after the t follows a Poisson distribution:

$$p_n(t) = \frac{(\gamma t)^n}{n!}e^{-\gamma t}. \tag{2.29}$$

The autocorrelation function of the random variable $B(t)$ is an exponential decaying function:

$$C_{\mathrm{RTN}}(t-t_0) = e^{-2\gamma|t-t_0|} \tag{2.30}$$

and γ is the autocorrelation coefficient. The spectrum of the RTN is a Lorentzian function and it is calculated following Eq. (2.8) as the Fourier transform of the autocorrelation function:

$$S_{\mathrm{RTN}}(\omega) = \frac{4\gamma}{(2\gamma)^2 + \omega^2}. \tag{2.31}$$

We write the noise phase as

$$\varphi^*(t) = \nu\varphi(t) = \nu \int_{t_0}^{t} B(s)ds. \tag{2.32}$$

In this way $\varphi^*(t)$ is a stochastic variable which can take values in the interval $[-\nu(t - t_0), \nu(t - t_0)]$. In the case of RTN, the probability distribution of the noise phase $\varphi^*(t)$ cannot be described by a simple Gaussian distribution function and its characteristic function cannot be calculated as easily as in Eq. (2.17). The analytical expressions for the probability distribution $p(\varphi^*, t)$ and, consequently the characteristic function $\mathbb{E}\left[e^{i\nu\varphi(t)}\right]$ was found [114, 115] and they read:

$$\begin{aligned} p(\varphi^*, t) = {} & \frac{1}{2}e^{-\gamma t}\left[\delta(\varphi + \nu t) + \delta(\varphi - \nu t)\right] + \frac{\gamma}{2\nu}e^{-\gamma t}[\Theta(\varphi + \nu t) - \Theta(\varphi - \nu t)] \\ & \times \left[\frac{I_1\left(\gamma t\sqrt{1 - (\varphi/(\nu t))^2}\right)}{\sqrt{1 - (\varphi/(\nu t))^2}} + I_0\left(\gamma t\sqrt{1 - (\varphi/(\nu t))^2}\right)\right] \end{aligned} \tag{2.33}$$

$$\mathbb{E}\left[e^{i\nu\varphi(t)}\right] = \frac{1}{2}e^{-\gamma t}\left[\left(1 + \frac{\gamma}{2\delta}\right)e^{\delta t} + \left(1 - \frac{\gamma}{2\delta}\right)e^{-\delta t}\right] \tag{2.34}$$

where $I_n(x)$ is the modified Bessel function, $\delta(x)$ is the Dirac delta, $\Theta(x)$ is the Heaviside step function and $\delta = \sqrt{\gamma^2 - \nu^2}$. The proof of Eq.s (2.33) and (2.34) can be found in [114, 115]. Here we just highlight the main ingredients to obtain them. First, by writing the noise phase as a discrete sum with time step τ:

$$\varphi^*(t) = \nu\tau \sum_{n=1}^{N} B(t_n), \qquad B(t_n) = B(n\tau) \tag{2.35}$$

the integration over time can be thought as a one-dimensional random walk process, where at each step the random walker moves a step $\nu\tau$ on the "left" or on the "right" direction. Since γ is the switching rate, we call $\alpha = 1 - \gamma\tau$ the probability for a step in the same direction as the previous one and $\beta = \gamma\tau$ the probability of for a step to be in the opposite direction. We call m the number of steps from the origin and $P_n(m)$ the probability to be in position m at time step n. The probability can then be written as the sum of two contributions: $A_n(m)$ is the probability to reach position m coming from the left and $B_n(m)$ the probability coming from the right: $p_n(m) = A_n(m) + B_n(m)$. It follows that:

$$A_{n+1}(m) = \alpha A_n(m - 1) + \beta B_n(m - 1) \tag{2.36}$$

$$B_{n+1}(m) = \beta A_n(m + 1) + \alpha B_n(m + 1). \tag{2.37}$$

Next step is to rewrite these equations in the continuum limit, with $N \to \infty$, $\tau \to 0$ and $N\tau$ a fixed time. In particular, $A_n(m)$ and $B_n(m)$ are substitute by the quantities

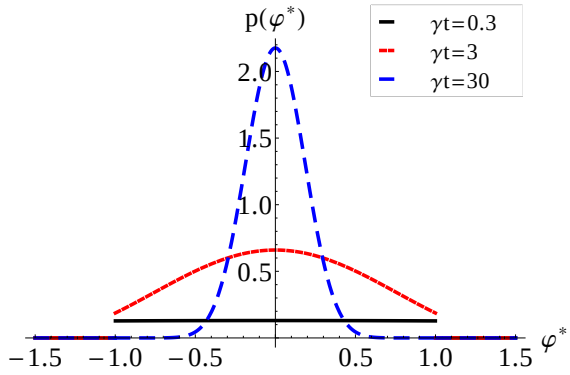

Figure 2.1: Probability distribution function $p(\varphi^*, t)$ as a function of the phase φ^* for $\nu t = 1$. Different lines are for different values γt. For large values of γt the probability distribution approaches a Gaussian distribution

$a(\varphi^*, t) \equiv a(m\nu\tau, n\tau)$ and $b(\varphi^*, t) \equiv b(m\nu\tau, n\tau)$. By expanding to first order in τ the functions a and b, one obtains the telegraph equation:

$$\partial_t^2 p + 2\gamma \partial_t p = \left(\frac{\nu}{2}\right)^2 \partial_\varphi^2 p \tag{2.38}$$

where we introduced the continuous probability $p = a + b$. The solution to the telegraph equation, imposing initial conditions $p(\varphi^*, 0) = \delta(\varphi)$ and $\dot{p}(\varphi^*, 0) = 0$, is given by Eq. (2.33). The characteristic function (2.17) is then obtained as the average $\mathbb{E}\left[e^{i\nu\varphi}\right] = \int e^{i\varphi^*(t)} p(\varphi^*, t) d\varphi^*$.
From Eq. (2.17), we can identify two regimes for the dynamics of the characteristic function $\mathbb{E}\left[e^{i\nu\varphi}\right]$. In fact, when $\gamma > \nu$, i.e. in the weak coupling regime, the function δ is a real quantity and the characteristic function is a monotonic decaying function of time. On the other hand, in the strong coupling regime where $\gamma < \nu$, the characteristic function is a damped oscillating function of time. The explicit expression in the two regimes is given by:

$$\mathbb{E}\left[e^{i\nu\varphi(t)}\right] = \begin{cases} e^{-\gamma t}\left[\cosh(\delta t) + \frac{\gamma}{\delta}\sinh(\delta t)\right] & \delta = \sqrt{\gamma^2 - \nu^2} \quad \gamma > \nu \\ e^{-\gamma t}\left[\cos(\delta t) + \frac{\gamma}{\delta}\sin(\delta t)\right] & \delta = \sqrt{\nu^2 - \gamma^2} \quad \gamma < \nu \end{cases} \tag{2.39}$$

The first regime is usually referred to as fast or Markovian regime, while the second is called slow or non-Markovian regime [116].
The probability distribution $p(\varphi^*, t)$ in Eq. (2.33) is a function of φ^* for fixed values of γt. For small γt, the probability distribution has a large peak centered in $\varphi^* = 0$, which is cut by the δ-function at $\varphi^* = \nu t$. For larger switching rates $\gamma t \gg 1$, the peaks approaches a Gaussian distribution. This behavior is shown in Fig. 2.1. In fact, using the asymptotic behavior of the Bessel function, we can approximate $I_n(x) \to \frac{1}{\sqrt{2\pi x}} e^x$. Moreover, for $\varphi^* \ll \nu t$, one can also expand the square root $\sqrt{1 - (\varphi^*/\nu t)^2}$. It follows that the central peak is thus described by a normal distribution with variance $\mathbb{E}\left[\varphi^{*2}\right] = \nu^2 t/\gamma$. In the weak coupling limit, the Gaussian part of $p(\varphi^*, t)$ will dominate in the average $\mathbb{E}\left[e^{i\varphi^*}\right]$ and the Gaussian approximation is valid. On the contrary, for strong couplings, the average is dominated by the δ-functions and thus the behavior is strongly non-Gaussian, even for $\gamma t > 1$.

2.2.2 The $1/f^\alpha$ noise

The $1/f^\alpha$ noise was first observed in 1925 by Johnson while studying the current fluctuations of electronic emission in a thermoionic tube [117]. Since then, the $1/f^\alpha$ noise has been the focus of many studies. Up to the present, $1/f^\alpha$ noise has been measured on semiconductors, semimetals, normal metals, superconductors, tunnel junctions, etc [118–123].

The exponent α appearing in the spectrum is a positive number. In many practical situations, α is very close to unity. However here we consider a more generic spectrum, allowing a broader range $\alpha \in [0.5, 2.5]$ for the possible values of α . The closeness of α to one justifies the fact that often the term $1/f$ noise is used to address the whole family of noises with power-law spectra of the type $1/f^\alpha$. These kinds of noises are usually referred to as *colored* spectra. The color of the noise depends upon the value of the parameter α. The cases with $\alpha = 1$ and $\alpha = 2$ are often called pink and brown noise respectively. The expression 'color of the noise' is a methaphor to suggest that white noise, in analog with white light, comes from an environment which contains all different frequencies with a flat power spectrum, whereas other colors of noise can be obtained by selecting specific frequency ranges.

The principal property of $1/f$ noise is that its spectral density $S(f)$ increases with decreasing frequency $f = \frac{\omega}{2\pi}$, down to the lowest frequencies that can be measured:

$$S_{1/f}(\omega) \propto \frac{1}{\omega}. \tag{2.40}$$

It is scale invariant, meaning that for a fixed frequency ratio ω_2/ω_1 the integrated noise power is constant. The integrated power id defined as $S_P(\omega_1, \omega_2) = \frac{1}{2\pi}\int_{\omega_1}^{\omega_2} S(\omega)d\omega$ and in the case of $1/f$ noise it has the expression:

$$S_P(\omega_1, \omega_2) \propto \ln\left(\frac{\omega_1}{\omega_2}\right). \tag{2.41}$$

It thus depends only on the ratio between the frequencies ω_1 and ω_2 and not their specific values.
$1/f^\alpha$ fluctuations follow a non-Markovian statistics. In fact, even if the noise arises from a sum of Markovian contributions, the overall effect is essentially non-Markovian, with long autocorrelation times.

The importance of $1/f^\alpha$ noise relies in the fact that it is an ubiquitous noise in nature. In fact, it is found in very different physical systems (insulators, semiconductors, normal metals, superconductors, etc..). However it poses many problems. One of the first question that $1/f$ noise arises is whether the spectral density decreases infinitely with decreasing frequency or a minimum nonzero frequency exists. In fact, the $1/f^\alpha$ noise is not integrable on the whole frequency range: $\int_{-\infty}^{\infty} S(f)df = \infty$, due to its divergence at low frequencies. To fix this problem, it was hypothesized that the noise has a cutoff, such that it manifests only in a frequency range $f_1 < f < f_2$. Experimentalists have tried to find the lower bound f_1 [124], but no cutoff frequency has ever been observed.

The very nature of this kind of noise is still a debated and open question: indeed there is not a universally recognized explanation about the sources and microscopic mechanisms behind $1/f$ noise. Completely different systems display very similar spectra, with

this characteristic behavior. However it is not clear whether this noise is indeed universal, i.e. it is an inherent property of all systems, or not.

The amount of studies about the $1/f^\alpha$ noise problem is huge. For a review see Ref.s [45, 46, 48] and references therein. The interest in studying $1/f^\alpha$ noise stems from the fact that this problem is very general. Indeed, $1/f^\alpha$ noise is a serious interference that limits the proper working of electronic devices at low frequencies. Moreover, the progressive reduction of the systems size led to observation of $1/f^\alpha$ spectra in various mesoscopic systems and in nanodevices. Although a universal mechanism leading to $1/f^\alpha$ noise does not seem to exist, but rather a variety of origins depending on the physical system involved, the scientific community now largely agrees on the fact that flickering noise results from a superposition of fluctuators having switching rated distributed according to a specific probability law. The fluctuators mimic, for example, the dynamic defects in a material.

The $1/f^\alpha$ noise is thus obtained from a collection of N bistable fluctuators, each characterized by a switching rate γ_j and a Lorentzian power spectrum as in Eq. (2.31). Before justifying this statement, let us first show how is it possible, from a mathematical point of view, to obtain a function proportional to $1/\omega$.

Mathematically a $1/\omega$ function is obtained integrating a Lorentzian function, with parameter γ, multiplied by a weight function proportional to γ^{-1}:

$$\int_{\gamma_1}^{\gamma_2} d\gamma \, \frac{4\gamma}{(2\gamma)^2+\omega^2} \, \frac{1}{\gamma} = \frac{2}{\omega} \left[\tan^{-1}\left(\frac{2\gamma_2}{\omega}\right) - \tan^{-1}\left(\frac{2\gamma_1}{\omega}\right) \right]. \tag{2.42}$$

When the two extremes of integration satisfy the conditions $0 < \gamma_1 \ll \omega \ll \gamma_2$ and , then the $\tan^{-1}\left(\frac{2\gamma_2}{\omega}\right)$ tends to $\pi/2$ and $\tan^{-1}\left(\frac{2\gamma_1}{\omega}\right)$ to 0, giving rise to the spectrum:

$$S_{1/f}(\omega) \propto \frac{\pi}{\omega}. \tag{2.43}$$

It follows that the probability distribution p_α of the switching rates in the case $\alpha = 1$ is proportional to the inverse of the switching rate $p_1(\gamma) \propto \gamma^{-1}$. The same line of reasoning can be followed for a generic value of the coefficient α. In particular, one can show that if the Lorentzian function is multiplied by a weight function proportional to $1/\gamma^\alpha$, the result is the desired $1/f^\alpha$ spectrum:

$$\int_{\gamma_1}^{\gamma_2} \frac{4\gamma}{(2\gamma)^2+\omega^2} \, \frac{1}{\gamma^\alpha} = \frac{{}_2F_1\left(1, \frac{\alpha}{2}, \frac{2+\alpha}{2}, -\frac{\omega^2}{4\gamma_1^2}\right)}{\gamma_1^\alpha \alpha} - \frac{{}_2F_1\left(1, \frac{\alpha}{2}, \frac{2+\alpha}{2}, -\frac{\omega^2}{4\gamma_2^2}\right)}{\gamma_2^\alpha \alpha} \tag{2.44}$$

where ${}_2F_1$ is the hypergeometric function. By expanding to first order Eq. (2.44) around $\gamma_1 = 0$ and $\gamma_2 = \infty$ one obtains:

$$S_{1/f^\alpha}(\omega) \propto \frac{2^\alpha \Gamma\left(1-\frac{\alpha}{2}\right) \Gamma\left(\frac{2+\alpha}{2}\right)}{\alpha \, \omega^\alpha} \tag{2.45}$$

where we introduced the Euler Γ function. It is clear from previous equations that, in order to reproduce a $1/f^\alpha$ spectrum, the probability distribution should be proportional to $\gamma^{-\alpha}$. Since $p_\alpha(\gamma)$ should be normalized to unity $\int_{\gamma_1}^{\gamma_2} p_\alpha(\gamma) d\gamma = 1$, the probability distribution reads:

$$p_\alpha(\gamma) = \begin{cases} \frac{1}{\gamma}\left[\frac{1}{\ln(\gamma_2/\gamma_1)}\right] & \alpha = 1 \\ \\ \frac{\alpha-1}{\gamma^\alpha}\left[\frac{(\gamma_1\gamma_2)^{\alpha-1}}{\gamma_2^{\alpha-1}-\gamma_1^{\alpha-1}}\right] & \alpha \neq 1 \end{cases} \tag{2.46}$$

As shown in Eq.s (2.42) and (2.44), we assume that the characteristic behavior $1/f \propto 1/\omega$ is found only in a region of the spectrum satisfying the condition $\gamma_1 < \omega < \gamma_2$.
We can rewrite Eq.s (2.42) and (2.44) in a more general way as

$$S_{1/f^\alpha}(\omega) = \int_{\gamma_1}^{\gamma_2} S_{\mathrm{RTN}}(\omega, \gamma) p_\alpha(\gamma) d\gamma \tag{2.47}$$

where $p_\alpha(\gamma)$ is given by Eq. (2.46), S_{RTN} is the random telegraph noise spectrum (2.31) and we explicitly wrote its dependency on the switching rate γ.
We already stated that $1/f^\alpha$ noise may be obtained from a collection of N bistable fluctuators, each characterized by a switching rate γ_j and a Lorentzian power spectrum. In order to justify this statement, assume that each bistable fluctuator is thus a source of random telegraph noise and that the switching rates are picked from the distribution (2.46). In formula:

$$B(t) = \sum_{j=1}^{N} B_j(t), \qquad B_j(t) = \pm 1, \qquad S_j(f, \gamma_j) = \frac{4\gamma_j}{(2\gamma_j)^2 + 4\pi^2 f^2}. \tag{2.48}$$

The spectrum of N sources of RTN may be calculated as:

$$S_{1/f^\alpha}(\omega) = \sum_{j=1}^{N} S_j(\omega, \gamma_j) = \sum_{j=1}^{N} \frac{4\gamma_j}{(2\gamma_j)^2 + 4\pi^2 f^2} \propto \frac{1}{f^\alpha} \tag{2.49}$$

where the last proportionality is true only if the γ_j are distributed according to Eq. (2.46). Eq. (2.49) may be viewed as the Monte Carlo sampling of the integral $N \int_{\gamma_1}^{\gamma_2} S_{\mathrm{RTN}}(\omega, \gamma) p_\alpha(\gamma) d\gamma$, which is, but for a constant, the one in Eq. (2.47). Therefore, in order to obtain the $1/f^\alpha$ spectrum, it is necessary (i) to consider a sufficiently large number of fluctuators and (ii) that the selected γ_j are a representative sample of the distribution $p_\alpha(\gamma)$ in the range $[\gamma_1, \gamma_2]$. This means that the minimum number of fluctuators one can sum up depends on the range of integration. In fact, a large number of fluctuators is required to sample the distribution of the switching rates over a large range, while few fluctuators are sufficient in the case of a narrow range.

Summarizing, a stochastic process with $1/f^\alpha$ spectrum can be reproduced considering a collection of a large number N of bistable fluctuators. To each fluctuator corresponds a specific switching rate selected from the probability distribution $p_\alpha(\gamma)$ (2.46). However, the expression in Eq. (2.47), can also be interpreted as the power spectrum arising from a bistable fluctuator with an unknown switching rate γ, distributed according to $p_\alpha(\gamma)$. This different microscopic model will be introduced in Sec. 3.2.3. What we want to highlight here is the fact that, because of the non-Gaussian nature of the stochastic process, a given spectrum can arise from environments with different microscopic structures. Diversified noise modelings may lead to different dynamics for the quantum system affected by the noise and, depending on the "engineering " of the environment, the quantum properties may be preserved or degraded in time.

2.3 Summary

- A collection of random variables $\{X(t), t \in T\}$ parametrized by a discrete o continuous index t describe a stochastic process. Stochastic processes provide a useful tool to describe classical fluctuations in physical system.

- Stochastic processes can be divided into two classes: Gaussian processes, which can be fully characterized by their mean and variance, and non-Gaussian processes, that require higher order statistics for their complete description.
- Examples of Gaussian processes are the Ornstein-Uhlenbeck process, which describes the stochastic behavior of the velocity of a Brownian particle, and fractional Brownian motion, that describes anomalous diffusion.
- Random telegraph noise is a non-Gaussian noise arising from a bistable fluctuator that flips between two states with a certain switching rate. Depending on the ratio between the switching rate and the coupling constant, two regimes arise: fast or Markovian RTN and slow or non-Markovian RTN.
- $1/f^{\alpha}$ noise is an ubiquitous noise in nature and affects almost all superconductor and semiconductors nanodevices and it constitutes the main source of decoherence in solid state qubits. It arises from a collection of bistable fluctuators distributed according to a proper distribution function.

CHAPTER 3

Dynamics of quantum correlations

In this chapter I analyze the dynamics of quantum correlations, both entanglement and quantum discord, between two qubits subject to classical noise. In particular, I consider two non-interacting qubit initially prepared in a maximally entangled state or in a Bell mixture, subject to a noisy classical environment which induces dephasing (see Sec. 1.1.4). It is worth remembering that dephasing channels lead to non-dissipative dynamics and are suitable to portray situations where the typical frequencies of the environment are smaller compared to the natural frequency of the qubit ω_0.
The interaction between the qubits and the environment can be either local or global, i.e. both the case of independent environments acting locally on each qubit and the case of a common environment affecting the two qubits are considered. The classical noise is introduced as a stochastic process affecting the energy splitting of the qubits. If we set $\hbar = 1$, the initial time $t_0 = 0$ and adopt the spin notation, the two-qubit Hamiltonian is given by:

$$H(t) = H_A(t) \otimes \mathbb{I}_B + \mathbb{I}_A \otimes H_B(t), \tag{3.1}$$

where $\mathbb{I}_{A(B)}$ is the identity matrix for subspace $A(B)$, $H_{\mathrm{A(B)}}$ is the single qubit Hamiltonian which contains a stochastic term giving rise to noise:

$$H_{\mathrm{A(B)}}(t) = \omega_0 \sigma_z + \nu\, B_{\mathrm{A(B)}}(t)\sigma_z \tag{3.2}$$

with ω_0 the energy splitting of the qubit, ν is the coupling constant between the system and the environment and σ_z is the Pauli matrix. The time-dependent coefficient $B(t)$ describes a stochastic process affecting the coherent dynamics of the quantum system. For the moment, we do not specify the nature of the stochastic process and keep the discussion as general as possible.
As known from Eq. (1.33), the global system evolves according to a unitary evolution operator U. Since the two qubits are non-interacting, the evolution operator for the global system is the tensor product of the two subsystem operators $U(t) = U_A(t) \otimes U_B(t)$. The Hamiltonian (3.2) commutes at different times, thus the single-qubit time evolution operator can be written as in Eq. (1.13) $U_{\mathrm{A(B)}}(t) = e^{-i\int_0^t H_{\mathrm{A(B)}}(s)ds}$ and it is given by:

$$U_{\mathrm{A(B)}}(t) = e^{-i\left[\omega_0 t + \nu\varphi_{\mathrm{A(B)}}(t)\right]\sigma_z} = \begin{pmatrix} e^{-i[\omega_0 t + \nu\varphi(t)]} & 0 \\ 0 & e^{i[\omega_0 t + \nu\varphi(t)]} \end{pmatrix}, \tag{3.3}$$

where we used the noise phase (2.10)

$$\varphi_{\mathrm{A(B)}}(t) = \int_0^t B_{\mathrm{A(B)}}(s)\, ds. \tag{3.4}$$

The global evolution operator $U(t) = U_A(t) \otimes U_B(t)$ is thus a diagonal matrix with elements:

$$\begin{array}{ll} U_{11}(t) = e^{i\{2\omega_0 t + \nu[\varphi_A(t)+\varphi_B(t)]} & U_{44}(t) = U_{11}^{\dagger}(t) \\ U_{22}(t) = e^{i\nu[\varphi_A(t)+\varphi_B(t)]} & U_{33}(t) = U_{22}^{\dagger}(t) \end{array} . \tag{3.5}$$

From the global evolution operator, one computes the evolved density matrix of the global system as $\rho_G(t) = U(t)\rho_0 U^{\dagger}(t)$. As the initial state of the two-qubit system we chose a Bell-state mixture defined in Eq. (1.87). Moreover, since local unitary transformations do not alter the amount of quantum correlations in the system, we apply the rotation $R_z = e^{i\omega_0 t\sigma_z} \otimes e^{i\omega_0 t\sigma_z}$, in order to eliminate the dependency of the density matrix upon the qubit splitting energy ω_0. It follows that the evolved density matrix of the global system has the form:

$$\rho_G(t,\varphi) = \frac{1}{2} \begin{pmatrix} c_1 + c_2 & 0 & 0 & \frac{c_1 - c_2}{e^{2i\nu[\varphi_A(t)+\varphi_B(t)]}} \\ 0 & c_3 + c_4 & \frac{c_3 - c_4}{e^{2i\nu[\varphi_A(t)-\varphi_(t)]}} & 0 \\ 0 & \frac{c_3 - c_4}{e^{-2i\nu[\varphi_A(t)-\varphi_B(t)]}} & c_3 + c_4 & 0 \\ \frac{c_1 - c_2}{e^{-2i\nu[\varphi_A(t)+\varphi_B(t)]}} & 0 & 0 & c_1 + c_2 \end{pmatrix} . \tag{3.6}$$

The two-qubit density operator can be obtained according to Eq. (2.9) as the ensemble average of the global ρ_G over all the possible realizations of the process $B(t)$ (or equivalently $\varphi(t)$):

$$\rho(t) = \mathbb{E}\left[\rho_G(t)\right]. \tag{3.7}$$

Averaging the global density operator Eq. (3.6) means computing the expected value of the quantity $e^{2i\nu\varphi(t)}$. This expectation depends on the nature of the considered stochastic process generating the noise. In the following section we will calculate this average in the cases of Gaussian and non-Gaussian noise and we will analyze the features of the dynamics of quantum correlations in both cases. Two scenarios will be presented: in the case of independent environments, each qubit is coupled to its own stochastic process and in general $B_A(t) \neq B_B(t)$; in the case of a common environment, both qubits feel the effect of the same external field and $B_A(t) = B_B(t)$.

3.1 Dynamics of quantum correlations in the presence of Gaussian noise

In this section, we consider the case where the external classical field $B_{\mathrm{A(B)}}$ affecting the qubits dynamics in Eq. (3.2) is described by means of a zero-mean Gaussian process, characterized by an autocorrelation function $K(t)$. Specifically, we focus on the Ornstein-Uhlenbeck and fractional Brownian motion processes, characterized by autocorrelation functions (2.20) and (2.23) respectively. The relevant quantity we need to compute in order to analyze the qubits dynamics is the characteristic function $\mathbb{E}\left[e^{2i\nu\varphi(t)}\right]$ which, following Eq. (2.17) is given by:

$$\mathbb{E}\left[e^{\pm 2i\nu\varphi_{\mathrm{A(B)}}(t)}\right] = e^{-4\nu^2\beta(t)}. \tag{3.8}$$

Independent environments

If we consider the case of independent environments (IE), the two-qubit density operator

reads:

$$\rho_{\mathtt{IE}}(t) = \frac{1}{2}\begin{pmatrix} c_1+c_2 & 0 & 0 & \frac{c_1-c_2}{e^{4\nu^2\beta(t)}} \\ 0 & c_3+c_4 & \frac{c_3-c_4}{e^{4\nu^2\beta(t)}} & 0 \\ 0 & \frac{c_3-c_4}{e^{4\nu^2\beta(t)}} & c_3+c_4 & 0 \\ \frac{c_1-c_2}{e^{4\nu^2\beta(t)}} & 0 & 0 & c_1+c_2 \end{pmatrix}. \tag{3.9}$$

This is a pure dephasing dynamics. The dephasing coefficients $e^{-4\nu^2\beta(t)}$ affecting the off-diagonal elements of the density operator are monotonic decaying function of time, because of the monotonicity of the β- function in the case of OU and fBm processes (see. Eq.s (2.21) and (2.24)). It is possible to rewrite the density operator in the Pauli matrix basis (1.85) as

$$\rho_{\mathtt{IE}}(t) = \frac{1}{4}\left(\mathbb{I} + e^{-4\nu^2\beta(t)}a_1\sigma_x\otimes\sigma_x + e^{-4\nu^2\beta(t)}a_2\sigma_y\otimes\sigma_y + a_3\sigma_z\otimes\sigma_z\right) \tag{3.10}$$

where a_1, a_2 and a_3 are the component of the initial state ρ_0.

Since the density matrix depends on time only through the function $\beta(t)$, the system will reach the separable steady state $\rho_\infty(t) = \frac{1}{4}\left(\mathbb{I} + a_3\sigma_z\otimes\sigma_z\right)$, for $t\to\infty$. The dynamics of the system can be studied by analyzing the trajectories in the $\{a_x, a_y, a_z\}$ parameter space [125]. The trajectories of the evolved states in the a_i-parameter space are shown in Fig. 3.1 (left). The tetrahedron is the set of valid Bell-diagonal states. The four Bell states sit at the four vertices of the tetrahedron. The blue octahedron, specified by $|a_x| + |a_y| + |a_z| \leq 1$ is the set of separable Bell-diagonal states. There are four entangled regions outside the octahedron, one for each vertex of the tetrahedron. Classical states, diagonal in a product basis, lie on the Cartesian axes.

We notice that, with the exception of initial Bell states, the trajectories of the system actually enter the set of separable states at a finite time, thus showing a sudden death of entanglement.

The negativity as a function of time, for an initial arbitrary Bell-state mixture, is calculated according to Eq. (1.72) and it is given by:

$$\begin{aligned} N_{\mathtt{IE}}(t) = \frac{1}{2}\Big(&\left|c_1+c_2+e^{-4\nu^2\beta(t)}(c_3-c_4)\right| + \left|c_1+c_2-e^{-4\nu^2\beta(t)}(c_3-c_4)\right| + \\ &+ \left|e^{-4\nu^2\beta(t)}(c_1-c_2)+c_3+c_4\right| + \left|-e^{-4\nu^2\beta(t)}(c_1-c_2)+c_3+c_4\right|\Big) - 1. \end{aligned} \tag{3.11}$$

In the asymptotic limit of $t\to\infty$ the entanglement tends toward zero. It does not exists a limiting non-zero value for entanglement.

The discord is calculated using Luo's formula since the evolved state is an X-state. We do not rewrite the expression here, because it is the same as in Eq. (1.86), but for the substitutions: $a_x \to e^{-4\nu^2\beta(t)}a_1$, $a_y \to e^{-4\nu^2\beta(t)}a_2$ and $a_z \to a_3$. In the case of an initial Bell state, for example the $|\Phi^+\rangle$ state, the entanglement and the quantum discord read:

$$N_{\mathtt{IE}}(t) = e^{-4\nu^2\beta(t)} \tag{3.12}$$

$$Q_{\mathtt{IE}}(t) = h\left(e^{-4\nu^2\beta(t)}\right) \tag{3.13}$$

where the function h is defined as:

$$h(x) = \frac{1+x}{2}\log_2(1+x) + \frac{1-x}{2}\log_2(1-x). \tag{3.14}$$

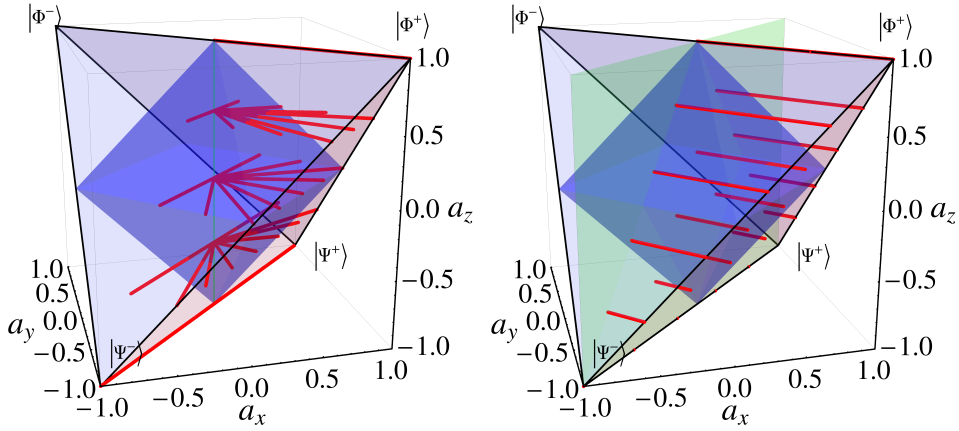

Figure 3.1: Trajectories of the system in the space of parameters $\{a_x, a_y, a_z\}$, for two independent environments (left) and for a common environment (right). The Bell-state mixtures, a subclass of the X-states in Eq. (1.85), form a tetrahedron. The set of separable states is the dark-blue octahedron. The initial states are Bell-state mixtures that lie on the surface of the tetrahedron. For independent environments, the trajectories converge to the green line $a_x = a_y = 0$. For a common environment, the trajectories are directed orthogonally to the plane $a_x = a_y$, shown in green. In both cases, a_z remains constant.

Both the negativity and the discord are monotonically decreasing functions of time that tend to zero as $t \to \infty$.
We already anticipated that in the most general case of an initial mixture of Bell states, the peculiar phenomenon of entanglement sudden death is found. In addition, also the phenomenon of freezing of quantum discord appears. Let us first consider the behavior of entanglement for mixture of Bell states. The ESD can be understood, for our model, by looking at the trajectories in the $\{a_x, a_y, a_z\}$ parameter space, as shown in Fig. 3.1 (left). In fact, they converge to the line $a_x = a_y = 0$ and enter the octahedron of separable states at finite time. This happens for every mixture of Bell states, except for mixtures of $|\Phi^\pm\rangle$ and mixtures of $|\Psi^\pm\rangle$. In this case, the trajectories follows the edge of the tetrahedron and reaches the vertex of the octahedron for $t \to \infty$.

Regarding the behavior of quantum discord, the phenomenon of frozen discord appears for mixtures of Bell states. This can be figured out geometrically by plotting the surfaces of equal discord, as was done by Lang and Caves in Ref. [125] in the parameter space diagram. These surfaces consist of three intersecting tubes running along the axes. The tubes are cut off by the state tetrahedron. As discord decreases, the tubes collapse to the Cartesian axes. Frozen discord appears when the trajectories that lie on the surface of constant discord meet the intersection with another tube. After this intersection, discord decreases monotonically to zero in time as the trajectories reach the Cartesian axes around which the intersecting tube is running.

Fig. 3.2 shows the ESD and the frozen discord for a mixture of two Bell states. The negativity decay to zero at a finite time, while the discord remains constant up to a certain time and then goes to zero monotonically. On the right, the corresponding trajectory of the system is shown together with a surface of constant discord. We see that the trajectory initially lies on the surface of a tube up to the point where two tubes meet. At this point, quantum decoherence starts and discord goes to zero monotonically as the trajectory reaches the a_z axes.

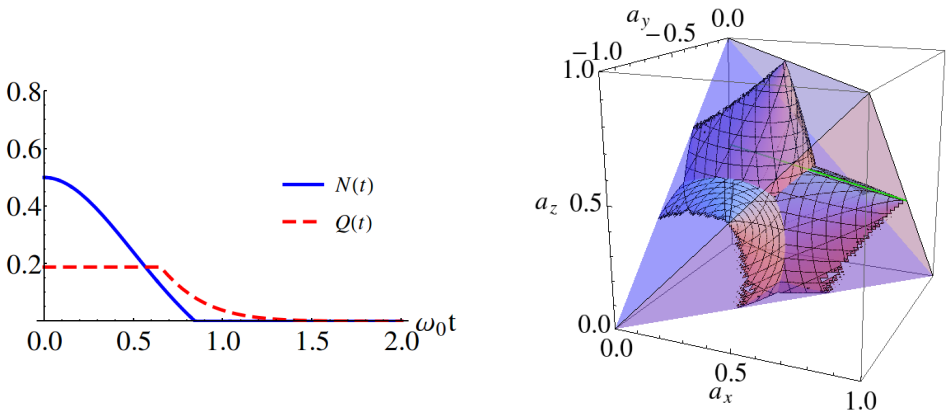

Figure 3.2: Left panel: Evolution of negativity (blue line) and discord (red line) for the initial state $\rho = \frac{3}{4}|\Phi^+\rangle\langle\Phi^+| + \frac{1}{4}|\Psi^+\rangle\langle\Psi^+|$. The classical field is generated by an OU process with $\gamma = 1$ and $\nu = 1$. Both entanglement sudden death and frozen discord appear. Right: Trajectory of the system in the a_i parameter space. The surface corresponding to discord $Q = 0.1877$ is shown: the trajectory initially lies on the surface.

Common environment

In the case of a common environment affecting the dynamics of the system, the two qubits are coupled to the same stochastic process $B_A(t) = B_B(t) = B(t)$ and the density operator has the form:

$$\rho_{\text{CE}}(t) = \frac{1}{2}\begin{pmatrix} c_1 + c_2 & 0 & 0 & \frac{c_1 - c_2}{e^{8\nu^2\beta(t)}} \\ 0 & c_3 + c_4 & c_3 - c_4 & 0 \\ 0 & c_3 - c_4 & c_3 + c_4 & 0 \\ \frac{c_1 - c_2}{e^{8\nu^2\beta(t)}} & 0 & 0 & c_1 + c_2 \end{pmatrix} \tag{3.15}$$

where we use the relation $\mathbb{E}\left[e^{-4i\nu\varphi(t)}\right] = e^{-8\nu^2\beta(t)}$ and this coefficient is still a monotonic decreasing function of time. We can write the density matrix (3.15) in the Pauli matrix basis as:

$$\begin{aligned}\rho(t) =& \frac{1}{4}\left\{\mathbb{I} + \frac{1}{2}\left[e^{-8\nu^2\beta(t)}(a_1 - a_2) + a_1 + a_2\right]\sigma_x \otimes \sigma_x + \right. \\ &\left. + \frac{1}{2}\left[e^{-8\nu^2\beta(t)}(a_2 - a_1) + a_1 + a_2\right]\sigma_y \otimes \sigma_y + a_3\sigma_z \otimes \sigma_z\right\}. \end{aligned} \tag{3.16}$$

In this case, the negativity as a function of time for an initial arbitrary mixture of Bell states, is

$$\begin{aligned} N_{\text{CE}}(t) =& \frac{1}{2}\left[\left|e^{-8\nu^2\beta(t)}(c_1 - c_2) + c_3 + c_4\right| + \left|e^{-8\nu^2\beta(t)}(c_2 - c_1) + c_3 + c_4\right| + \right. && (3.17) \\ &\left. + |1 - 2c_3| + |1 - 2c_4| - 2\right] && (3.18) \end{aligned}$$

The quantum discord has the same expression as that in Eq (1.86), with a_x, a_y and a_z the coefficients in Eq. (3.16). In the case of a Bell state as an initial state, the quantum

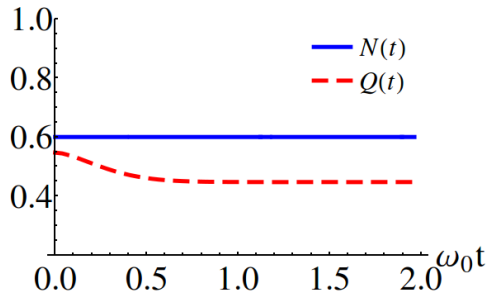

Figure 3.3: Dynamics of negativity (blue line) and discord (red dashed line) for the initial state $\rho = \frac{1}{10}|\Phi^+\rangle\langle\Phi^+| + \frac{8}{10}|\Psi^+\rangle\langle\Psi^+| + \frac{1}{10}|\Psi^-\rangle\langle\Psi^-|$. The negativity is constant over time, while discord stabilizes to a constant value after transintient time. In the plot, the external field is mimicked through a Ornstein-Uhlenbeck process with $\gamma = 1$ and $\nu = 1$.

correlations are given by:

$$N_{\texttt{CE}}(t) = e^{-8\nu^2\beta(t)} \tag{3.19}$$

$$Q_{\texttt{CE}}(t) = h\left(e^{-8\nu^2\beta(t)}\right), \tag{3.20}$$

where h is the function defined in Eq. (3.14). Also in the case of a common environment the quantum correlations between two qubits initially prepared in a Bell state decay monotonically in time.

The trajectories of the system are shown in Fig. 3.1, on the right panel. They run orthogonally to the plane $a_x = a_y$. By looking at the figure, we notice that the system experiences ESD when the initial state has $a_z > 0$, except for mixtures of $|\Phi^\pm\rangle$, for which $N(t) \to 0$ only for $t \to \infty$. For those Bell state mixtures that are entangled and for which $a_z < 0$, the trajectories run parallel to the surface of the octahedron and hence negativity is constant over time. This set also includes the two Bell states $|\Psi^\pm\rangle$ which are stable states of the dephasing dynamics. An example of this behavior is shown in Fig. 3.3. But in general, in the majority of cases, we found that quantum discord is more robust than entanglement.

So far, we showed that the effect of the longitudinal stochastic field is to induce decoherence through a monotonic decay of all quantum correlations. The nature of Gaussian process affects the resulting dynamics only through the time dependence of the β-function, i.e. the decaying velocity, as we can see from Figure 3.4. In particular, depending on the initial state, different behaviors may appear: for initial Bell states, the negativity goes asymptotically to zero, as a smooth function of time; on the contrary, if the initial state is a mixture of Bell states, entanglement displays ESD, reaching zero abruptly. For a fixed initial state, the robustness of quantum correlations depends on the nature of the considered stochastic process: different expressions of the $\beta(t)$ function give different decaying velocities for entanglement.

We now investigate the role of the different considered processes in enhancing the system's ability to retain its coherence. To be quantitative, we define the *entanglement-preserving time* t^* as the time at which the negativity of the system falls below a certain

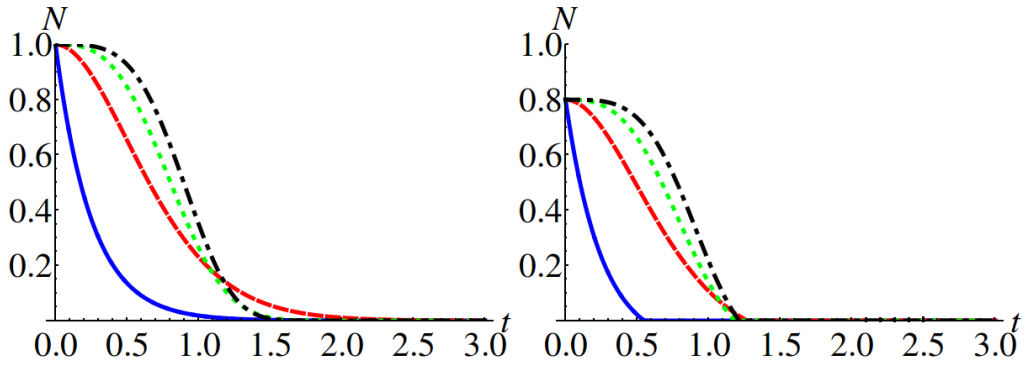

Figure 3.4: Negativity as a function of the interaction time for an initially pure Bell state (left) and for the mixture $\rho = \frac{1}{10}|\Phi^+\rangle\langle\Phi^+| + \frac{9}{10}|\Psi^+\rangle\langle\Psi^+|$ (right) interacting with independent environments driven by different stochastic processes: white noise (solid blue), OU with $\gamma = 1$ (red dashed), Wiener (green dotted), fBm with $H = 0.9$ (dot-dashed black). For pure Bell states, the negativity decreases smoothly to zero, while for mixtures of Bell states ESD appears.

Table 3.1: The entanglement-preserving time t^* for different environments and for an initial pure Bell state. The quantity β^* is given by $\beta^* = -1/4\nu^2 \log(r) \simeq 0.0025$ and $W(z)$ is the Lambert function, i.e. the principal solution of $z = W \exp W$.

Process	t^*
Ornstein-Uhlenbeck	$\frac{1}{\gamma\Gamma}\left[\gamma\beta^* + \Gamma W\left(-e^{-\frac{\gamma\beta^*}{\Gamma}-1}\right) + \Gamma\right]$
White noise	β^*/Γ
	$[(2H+2)\beta^*]^{\frac{1}{2H+2}}$
Wiener	$[3\beta^*]^{1/3}$

threshold, that we fix at the ratio $r = 99\%$ of the initial negativity.
We first consider the case in which the initial state is a Bell state. We already calculated the negativity as a function of time in the case of independent (3.12) and common (3.19) environments. Upon introducing the quantity $\beta^* = -1/(4\nu^2)\log(r) \simeq 0.0025$, we may calculate the entanglement-preserving time by inverting the relation $\beta(t) = \beta^*$. Examples for different processes are shown in Table 3.1, where we wrote the dependencies of t^* on the relevant parameters of the processes, i.e. the inverse of the correlation time γ for the Ornstein-Uhlenbeck process with Γ fixed and the Hurst parameter H for the fractional noise. We also report the results for white noise (i.e. a Gaussian noise with a flat power spectrum, that can be obtained as a limit of the OU process with $\gamma \to \infty$) and the Wiener process (i.e. fBm with $H = \frac{1}{2}$).

The entanglement-preserving time for OU and fB processes is shown in Fig. 3.5 as a function of the characteristic parameters γ and H. For the Ornstein-Uhlenbeck process, in the limit of a quasi-static field, i.e. $\gamma \to 0$, the entanglement-preserving time diverges, $t^* \to \infty$, such that the system retains its coherence indefinitely, while in the Markovian limit, $\gamma \to \infty$, $t^* \to \beta^*/\Gamma$, recovering the behavior typical of the white noise. In the case

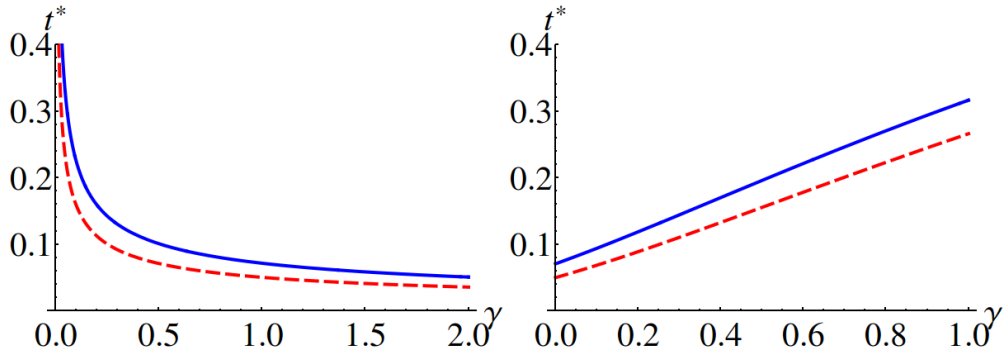

Figure 3.5: The entanglement-preserving time t^* as a function of the characteristic parameter of the external field. We show results for Ornstein-Uhlenbeck with $\Gamma = 1$ (left) and fractional Brownian noise (right) and for the case of independent (solid blue) and common (red dashed) environments.

of fBm, the dependency of t^* on H is well approximated by a linear relation and the higher the diffusion coefficient, the longer the entanglement-preserving time. We also notice that, for vanishing H, t^* is comparable to the OU process with $\gamma = 1$. Indeed, we have that $\beta_{\rm OU}(t) \simeq \frac{1}{2}\gamma t^2$ for small t and $\beta_{\rm fB}(t) \simeq \frac{1}{2}t^2$ for vanishing H. For general mixtures of Bell states, t^* is always smaller than the case of pure Bell states.

In Fig. 3.6 we show t^* as a function of the initial negativity N_0 for a set of randomly generated initial Bell-mixed states interacting with OU and fBm external fields (blue and red points respectively) either independently (left panel) or as a common environment (right panel). As it is apparent from the plots, the larger is the initial entanglement, the longer is the preserving time. This is true both in the case of independent and common environments. In the former case, the entanglement-preserving time is longer than in case of a common bath, for a fixed value of the initial negativity. In both scenarios, the entanglement is more robust in the case of fBm, rather than the OU process, with longer values of the preserving time t^*.

By looking at Fig. 3.6 we see that the values of t^* are not much dispersed. Rather, they concentrate around typical values which strongly depend on the kind of environment and only slightly on the initial negativity itself. Besides, the value of t^* is bounded from below by an increasing function of the initial negativity, the analytical expression of which can be obtained by determining the entanglement-preserving time for mixtures of a Φ^+ and a Ψ^+ Bell state. In this case, for a given ratio r to the initial negativity, t^* satisfies the equation

$$\beta(t^*) = \frac{1}{4A}\log\left[\frac{N_0+1}{N_0(2r-1)+1}\right]. \tag{3.21}$$

where $A = 1$ for independent environments and $A = 2$ for a common environment. From Eq. (3.21) we obtain lower bounds to t^* as a function of N_0, which are shown (solid and dashed black lines) in Fig. 3.6.

As previously discussed, the interaction of the two-qubit system with the external classical field induces a sudden death of entanglement for most of the Bell-state mixtures. In this section we study how the nature of the stochastic Gaussian process affects the *entanglement sudden death time*, $t_{\rm ESD}$, i.e. the time at which the state becomes separable and its negativity goes to zero.

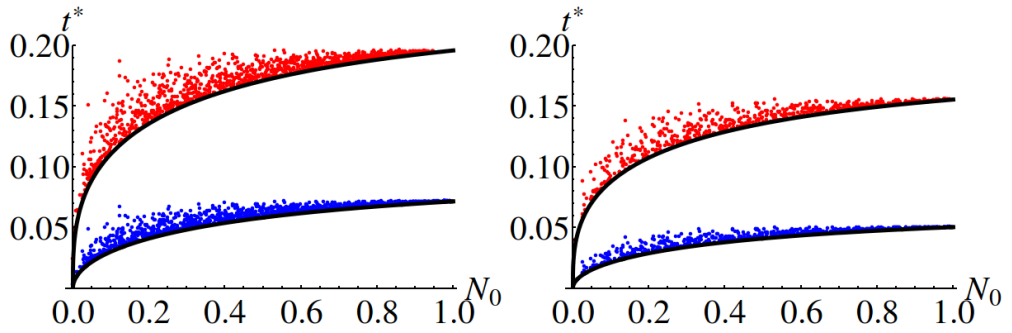

Figure 3.6: The entanglement-preserving time t^* (for a ratio $r = 0.99$ to the initial negativity) as a function of the initial negativity N_0 for randomly chosen initial Bell-state mixtures. We show results for the Ornstein-Uhlenbeck process with $\gamma = 1$ (blue points) and the Wiener process, i.e. fractional Brownian noise with $H = 1/2$ (red points). The solid and dashed black lines are the lower bounds for t^* for the OU and Wiener process respectively, obtained from Eq. 3.21. Left: independent environments. Right: common environment.

In Fig. 3.7 we show t_{ESD} versus the initial negativity N_0 for randomly generated Bell-state mixtures for the OU process and the fBm with $H = \frac{1}{2}$. We can see that t_{ESD} is bounded from below by a monotonically increasing function of negativity, which itself diverges for $N_0 \to 1$, i.e. as the initial state gets closer to a pure Bell state. The analytical expression of this function is obtained by considering initial states belonging to a face of the Bell-state tetrahedron, and thus easily follows from Eq. (3.21) by substituting $r = 0$. We have

$$\beta(t_{\text{ESD}}) = \frac{1}{4A} \log\left(\frac{1+N_0}{1-N_0}\right) \tag{3.22}$$

where $A = 1$ for the independent-environments case and $A = 2$ for the common-environment case. ESD time is thus longer for larger values of the initial entanglement. In the case of independent environments the lower bound is larger than in the case of a common environment, confirming the tendency of entanglement to be more robust in the case of independent noises affecting the two qubits.

3.2 Dynamics of quantum correlations in the presence of non-Gaussian noise

In this section we address the quantum correlations between two non-interacting qubits initially prepared in the Bell state $|\Phi^+\rangle$ whose dynamics is influenced by the stochastic terms $B_i(t)$, $i = A, B$ following a non-Gaussian statistic. In particular, we will focus on two paradigmatic examples of non-Gaussian noise: the random telegraph noise characterized by a switching rate ξ and the $1/f^\alpha$ noise arising from a collection of N RTN sources with switching rates $\{\xi_i\}_{i=1}^N$. Hereafter we will use the dimensionless time and switching rate:

$$\tau = \nu t \qquad \text{and} \qquad \gamma = \xi/\nu, \tag{3.23}$$

re-scaled with the coupling constant ν. The key ingredient in analyzing the dynamics of the two qubit system is to compute the ensemble average of the global state of the system over all the different realizations of the stochastic terms, e.g. the noise phase $\varphi(\tau) =$

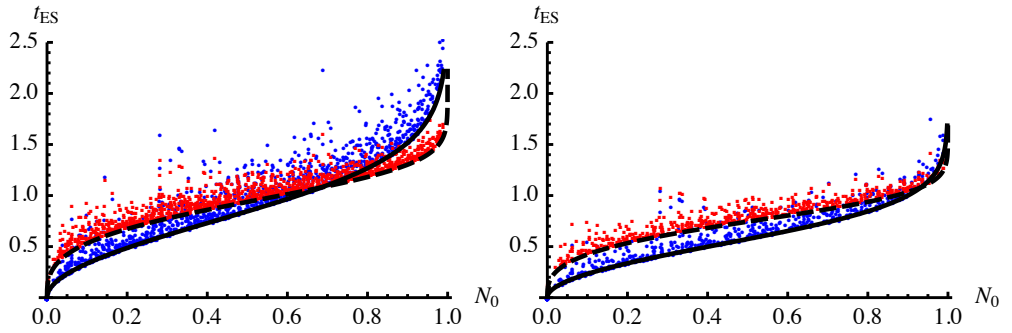

Figure 3.7: The entanglement sudden death time t_{ESD} as a function of the initial negativity N_0 for randomly chosen (initial) Bell-state mixtures, for the Ornstein-Uhlenbeck process with $\gamma = 1$ (blue) and the Wiener process (red). The solid and dashed lines are the lower bounds for t_{ESD} for the OU and Wiener process respectively, obtained from Eq. 3.22. Left: independent environments. Right: common environment.

$\int_0^\tau B(s)ds$. In the following the analyze in detail the dynamics of quantum correlations in the case of two qubits exposed to RTN and $1/f^\alpha$ noise.

3.2.1 Random telegraph noise

The global density matrix ρ_G, describing the state of the two qubits initially prepared in a Bell state, for a specific realization of the stochastic process $B_i(t)$ is given by Eq. (3.6) with coefficients $c_1 = 1$, $c_2 = c_3 = c_4 = 0$. In order to write the expression for the density operator of the two-qubit system, we should perform the average operation over the stochastic noise phase. In the case of RTN, the quantity $\mathbb{E}\left[e^{i\varphi(\tau)}\right]$ is known (see Eq. (2.39)) and it is easily generalized to the case $\mathbb{E}\left[e^{in\varphi(\tau)}\right]$ by applying the substitution $\nu \to n\nu$ where n is some integer:

$$\begin{aligned}\Delta_n(\tau,\gamma) &= \mathbb{E}\left[e^{in\varphi(\tau)}\right] \\ &= \begin{cases} e^{-\gamma\tau}\left[\cosh(\delta\tau) + \frac{\gamma}{\delta}\sinh(\delta\tau)\right] & \delta = \sqrt{\gamma^2 - n^2} \quad \gamma > 2 \\ e^{-\gamma\tau}\left[\cos(\delta\tau) + \frac{\gamma}{\delta}\sin(\delta\tau)\right] & \delta = \sqrt{n^2 - \gamma^2} \quad \gamma < 2 \end{cases}\end{aligned} \tag{3.24}$$

For a fixed value of the switching rate γ, the coefficient (3.24) is a function only of τ, and we can simplify the notation by showing only the dependency on time $\Delta_n(\tau)$. In the case of separate environments $n = 2$ while for a common environment $n = 4$ and the system density operator in the computational basis $\{00, 01, 10, 11\}$ has the expression:

$$\rho_{\text{IE}}(\tau) = \frac{1}{2}\left(|00\rangle\langle 00| + |11\rangle\langle 11|\right) + \frac{1}{2}\Delta_2^2(\tau)(|00\rangle\langle 11| + |11\rangle\langle 00|) \tag{3.25}$$

$$\rho_{\text{CE}}(\tau) = \frac{1}{2}\left(|00\rangle\langle 00| + |11\rangle\langle 11|\right) + \frac{1}{2}\Delta_4(\tau)(|00\rangle\langle 11| + |11\rangle\langle 00|). \tag{3.26}$$

In the limit of long times $\tau \to \infty$ the function Δ_n tends to zero and the states (3.25) and (3.26) reduced to the maximally mixed state $\rho_\infty = \frac{1}{2}\mathbb{I}$. The partial transposed density

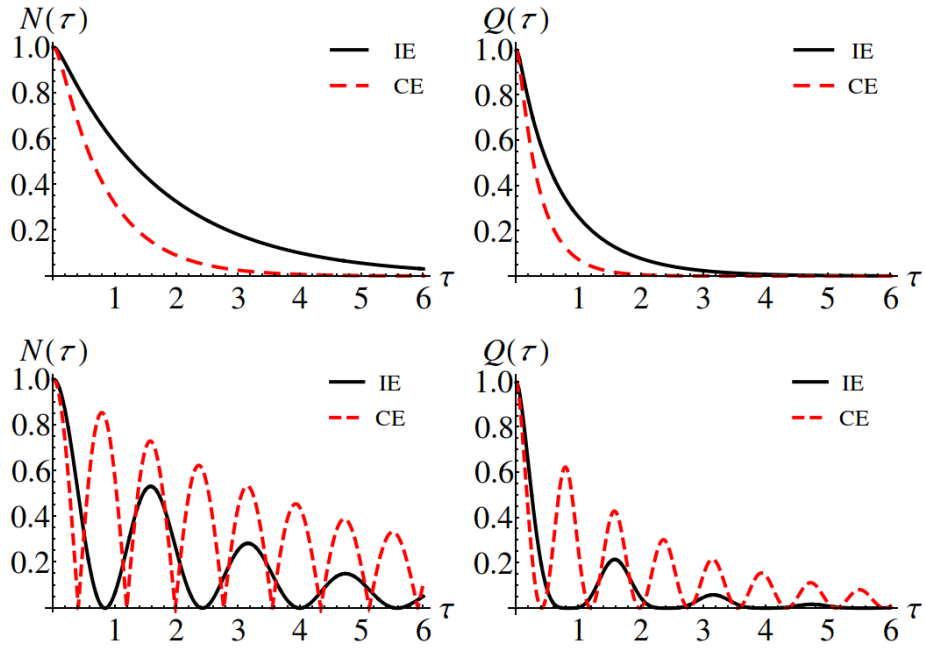

Figure 3.8: Top panels: Time evolution of negativity (left) and discord (right) for two qubits subject to RTN for independent and common environments in the weak coupling regime with $\gamma = 7$. Bottom panels: Time evolution of $N(\tau)$ and $Q(\tau)$ in the strong coupling regime with $\gamma = 0.2$.

matrix has the expression:

$$\rho_{\rm IE}^{\rm PT}(\tau) = \frac{1}{2}\left(|00\rangle\langle 00| + |11\rangle\langle 11|\right) + \frac{1}{2}\Delta_2^2(\tau)(|01\rangle\langle 10| + |10\rangle\langle 01|) \tag{3.27}$$

$$\rho_{\rm CE}^{\rm PT}(\tau) = \frac{1}{2}\left(|00\rangle\langle 00| + |11\rangle\langle 11|\right) + \frac{1}{2}\Delta_4(\tau)(|01\rangle\langle 10| + |10\rangle\langle 01|) \tag{3.28}$$

and the absolute value of its negative eigenvalues gives the negativity:

$$N_{\rm IE}(\tau) = \Delta_2^2(\tau) \qquad N_{\rm CE}(\tau) = |\Delta_4(\tau)|. \tag{3.29}$$

The discord is computed from Eq. (1.86) as:

$$Q_{\rm IE}(\tau) = h\left(\Delta_2^2(\tau)\right) \qquad Q_{\rm CE}(\tau) = h\left(\Delta_4(\tau)\right) \tag{3.30}$$

where $h(x)$ is the function defined in Eq. (3.14). The dynamics of quantum correlations is shown in Fig. 3.8. Note that the choice of a maximally entangled initial state, together with the sheer dephasing nature of the interaction with the environment, makes the quantum discord a function of the negativity only. In these system, in fact, the evolved state is a mixture of Bell states.
In agreement with previous works [116, 126, 127], in the weak regime $\gamma > 2$, quantum correlations decay exponentially with time. On the other hand, in the strong coupling regime $\gamma < 2$ quantum correlations exhibit damped oscillations in time, with alternating ESD and revivals. The peaks of revivals are at times $\tau = k\frac{\pi}{\delta}$ with $k = 0, 1\ldots$ and integer number. This behavior can be explained by noticing that the function $\Delta_n(\tau)$ in

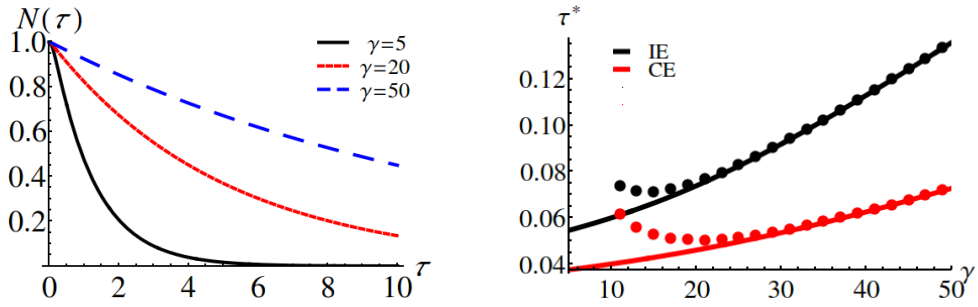

Figure 3.9: Left panel: Negativity between two qubits subject to fast RTN as a function of time for different values of the switching rate. The higher is the switching rate, the less degraded are the quantum correlations. Right panel: Entanglement-preserving time as a function of the switching rate of the RTN in the case of independent and common environments. Solid lines refer to the exact solution found by solving the equation $N(\tau^*) = r$ with $r = 0.99$, while dots are for the approximated expression in Eq.s (3.33) and (3.34).

the strong coupling regime has peaks at times $\tau = k\frac{2\pi}{\delta}$. The negativity has a double number of peaks because of the power of two and absolute values operations in Eq.s (3.29). The smaller the value of the switching rate γ, the higher the height of the peaks, until the limit $\gamma \ll 1$ where the function $\Delta_n(\tau)$ becomes indeed a periodic function with periodicity $T \to \pi$ in the case of independent environments and $T \to \frac{\pi}{2}$ in the case of a common environment.
It should also be noticed that in the weak coupling regime, quantum correlations in a common environment are weaker than in the case of independent environments. The opposite behavior appears in the strong coupling regime, where the effect of a common environment is to better preserve the quantum correlations between the two qubits.

Following the analysis performed for the case of Gaussian processes, we quantify the entanglement-preserving time τ^* also in the case of RTN. We specifically consider only the fast RTN regime, because of the monotonic decay in time of the coherences $\Delta_n(\tau)$. Again, we define the entanglement-preserving time as the time at which the entanglement falls below a certain fraction r of its initial value. In this way we are able to investigate the role of the switching rate in the degradation of the quantum correlations. The left panel in Fig. (3.9) shows the dependency of the negativity for a two-qubit system initially prepared in the $|\Phi^+\rangle$ state, on the switching rate rate, as a function of time. The larger is the value of γ, the less degraded are the quantum correlations. This behavior is due to the fact that large switching rates correspond to weak couplings between the system and the environment and, as a consequence, more time is required for the system to feel the effect of the external noise. The entanglement-preserving time τ^* is obtained by finding the solution to the equation $N_{\mathrm{IE(CE)}}(\tau^*) = r$, since the initial negativity is equal to one. It is not possible to find the analytical solution for this equation for a generic γ, however we compute τ^* numerically. The results are shown in the right panel of Fig. 3.9 for the case of independent and common environments. In agreement with the time evolution of entanglement, we find that τ^* increases with larger values of γ. It means that for faster BFs the quantum correlations are better preserved. We are also able to confirm that the effect of independent environments acting on each qubit helps protecting the system against decoherence better than a common environment acting

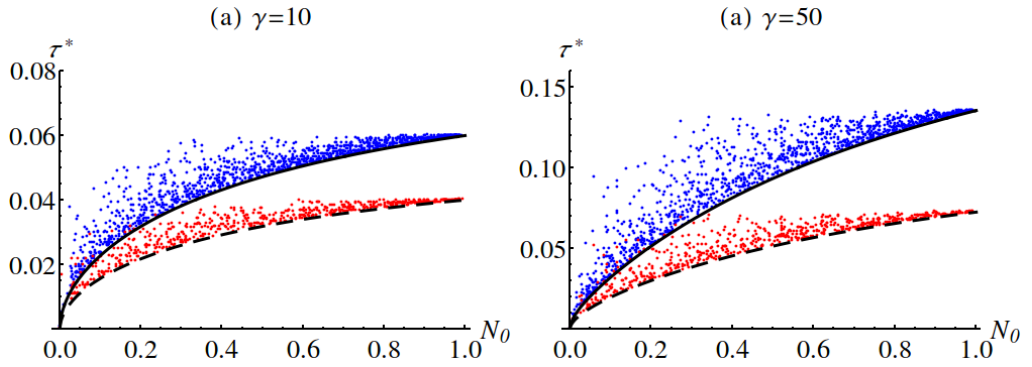

Figure 3.10: (a) Entanglement-preserving time as a function of the initial negativity for a set of randomly generated initial Bell mixtures subject to RTN with $\gamma = 10$. Blue points stand for the case of independents environments acting on the two qubits, while the red points represent the case of a common environment affecting the two-qubit system. (b) Same as panel (a) but with $\gamma = 50$.

on both qubits. Although an analytical expression for τ^* is not found for a generic γ, however in the limit of large switching rates $\gamma \gg 1$, it is possible to write an analytical approximation for the entanglement-preserving time. In fact, in this regime $\delta \simeq \gamma$ so that $\delta - \gamma \simeq 0$ and the and the Δ_n-function may be approximated as:

$$\Delta_n(\tau,\gamma) = \frac{e^{(\delta_n-\gamma)t}}{2}\left(1+\frac{\gamma}{\delta_n}\right) + \frac{e^{-(\delta_n+\gamma)t}}{2}\left(1-\frac{\gamma}{\delta_n}\right) \simeq \frac{e^{(\delta_n-\gamma)t}}{2}\left(1+\frac{\gamma}{\delta_n}\right) \tag{3.31}$$

where $\delta_n = \sqrt{\gamma^2 - n^4}$. The negativity thus reads:

$$N_{\rm IE}(\tau,\gamma) = \frac{e^{2(\delta_2-\gamma)t}}{4}\left(1+\frac{\gamma}{\delta_2}\right)^2 \qquad N_{\rm CE}(\tau,\gamma) = \frac{e^{(\delta_4-\gamma)t}}{2}\left(1+\frac{\gamma}{\delta_4}\right) \tag{3.32}$$

and these expressions can be easily inverted to obtain the entanglement-preserving time:

$$\tau^*_{\rm IE}(\gamma) = \frac{1}{2(\delta_2-\gamma)}\ln\left(\frac{4\,r}{(1+\frac{\gamma}{\delta_2})^2}\right) \tag{3.33}$$

$$\tau^*_{\rm CE}(\gamma) = \frac{1}{\delta_4-\gamma}\ln\left(\frac{2\,r\,\delta_4}{\delta_4+\gamma}\right). \tag{3.34}$$

The points in the left panel of Fig. (3.9) represent the fitting curves calculated using Eq.s (3.33) and (3.34). The agreement between the exact and the approximated solution is very good already for $\gamma \gtrsim 20$, while the true behavior of τ^* is not captured by the approximation for smaller values of the switching rate.
If, instead an initial Bell state, we consider a Bell-mixture, the global evolution is written in Eq. (3.6), and the dynamics of the two-qubit system is described by the density matrix:

$$\rho(\tau,\gamma) = \frac{1}{2}\begin{pmatrix} c_1+c_2 & 0 & 0 & (c_1-c_2)\Delta(\tau,\gamma) \\ 0 & c_3+c_4 & (c_3-c_4)\Delta(\tau,\gamma) & 0 \\ 0 & (c_3-c_4)\Delta(\tau,\gamma) & c_3+c_4 & 0 \\ (c_1-c_2)\Delta(\tau,\gamma) & 0 & 0 & c_1+c_2 \end{pmatrix}. \tag{3.35}$$

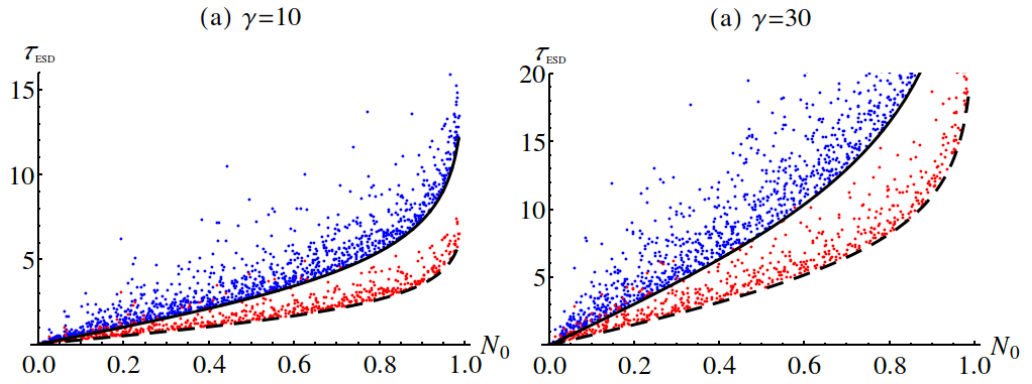

Figure 3.11: Entanglement-sudden-death time as a function of the initial negativity for a set of randomly generated initial Bell mixtures subject to RTN with $\gamma = 10$ (a) and $\gamma = 30$ (b). Blue points stand for the case of independents environments acting on the two qubits, while the red points represent the case of a common environment affecting the two-qubit system.

with $\Delta(\tau,\gamma) = \Delta_2^2(\tau,\gamma)$ for independent environments and $\Delta(\tau,\gamma) = \Delta_4(\tau,\gamma)$ in the case of a common environment. We can notice that Eq. (3.35) has the same expression of the density matrix of a system subject to Gaussian noise in Eq.s (3.9) and (3.15), but for a different dephasing coefficient which, in the case of RTN is a function of Δ_n. It follows that the negativity has the same expression as in the cases presented in the previous Section, but for the substitutions $e^{-4\nu^2\beta(\tau)} \to \Delta_2^2(\tau,\gamma)$ for independent environment and $e^{-8\nu^2\beta(\tau)} \to \Delta_4(\tau,\gamma)$ in the case of a common bath. In Fig. 3.10 we report τ^* as a function of the initial negativity N_0 for a set of randomly generated initial Bell-mixed states subject to fast RTN. As in the case of a Gaussian environment, the larger is the initial negativity, the longer is the entanglement-preserving time. We confirm that the effect of a common environment is to degrade faster the correlations and that larger values of the switching rates preserves better the quantum correlations. . We find again that the minimum entanglement-preserving time for a given value of the initial negativity is given by the mixture of $|\Phi^+\rangle$ and $|\Psi^+\rangle$ states. This minimum value is computed by finding the solutions to the equation $\Delta_n(\tau^*,\gamma) = \left(\frac{1-N_0+2N_0 r}{1+N_0}\right)^{n/4}$.
We also analyze the entanglement-sudden-death time $\tau_{\rm ESD}$ for initial Bell mixtures. In Fig. 3.11 we report the $\tau_{\rm ESD}$ for a set of randomly generated initial states as a function of the initial negativity. The higher is the initial entanglement, the larger is the entanglement-sudden-death time. All the previously discussed behaviors are found: a common environment is more detrimental against quantum correlations than independent baths and the bigger the value of the switching rate, the longer is the time required for the state to become separable. Initial Bell states have an infinite $\tau_{\rm ESD}$, with an exponential decay of entanglement.

3.2.2 $1/f^\alpha$ noise

Consider the case of two qubits interacting with a collection of N fluctuators with fixed switching rates $\{\gamma_i\}_{i=1}^N$, distributed according to the probability distribution $p_\alpha(\gamma)$ in Eq. (2.46). With the expression "fixed switching rates" we want to underline the fact that, before computing the dynamics, it is necessary to assign to each switching rate γ_i a

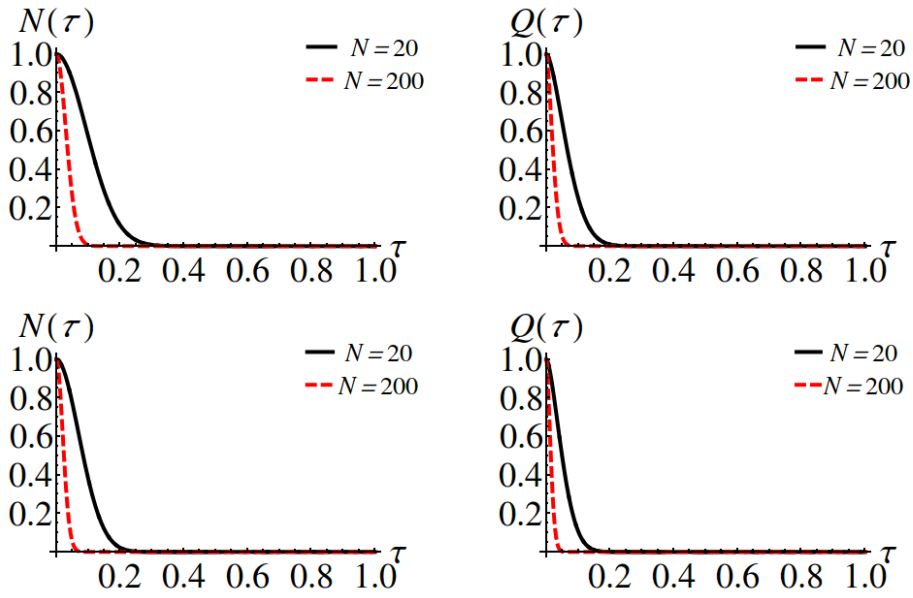

Figure 3.12: Upper panels: Time evolution of negativity and discord for two qubits interacting with two independent environments, consisting in a collection of N bistable fluctuators with spectrum $1/f$ when $[\gamma_1, \gamma_2] = [10^{-4}, 10^4]$. Lower panels: same as before, but with qubits subject to a common environment.

specific value taken from the distribution $p_\alpha(\gamma)$ in a range $[\gamma_1, \gamma_2]$.

The evolution operator in Eq. (3.3) depends upon the global stochastic phase $\varphi(\tau) = \sum_{j=1}^{N} \varphi_j(\tau)$ (we dropped the subscript $A(B)$ to lighten the notation) and the global density matrix is calculated for a fixed realization of the stochastic noise phase $\varphi(\tau)$ as in Eq. (3.6). The two-qubit density matrix at time τ is calculated as the ensemble average of the global density operator over all possible realizations of the global noise phase:

$$\rho(\tau) = \int \rho_G(\tau, \varphi) p_T(\varphi, \tau) d\varphi \tag{3.36}$$

where $p_T(\varphi, \tau) = \prod_j p(\varphi_j, \tau)$ is the global noise phase distribution and $p(\varphi_j, \tau)$ is given by Eq. (2.33) since each bistable fluctuator is a source of RTN. Eq. (3.36) depends upon the characteristic function of the global phase $e^{\pm 2i\varphi(\tau)}$. This quantity can be computed in terms of the RTN coefficient $\Delta_n(\tau, \gamma)$ of Eq. (3.24) as follows:

$$\Lambda(\tau) = \mathbb{E}\left[e^{\pm 2i\varphi(\tau)}\right] = \mathbb{E}\left[e^{\pm \sum_{j=1}^{N} 2i\varphi_j(\tau)}\right] = \prod_{j=1}^{N} \Delta_n(\tau, \gamma_j) \tag{3.37}$$

where the last inequality holds since the RTN phase coefficients are independent and the coefficient $\Delta_n(\tau, \gamma_j)$ corresponds to the j-th fluctuator with switching rate γ_j. We are now able to compute the evolved density matrix for the two-qubit system as:

$$\rho_{\mathrm{IE(CE)}}(\tau) = \frac{1}{2}\left(|00\rangle\langle 00| + |11\rangle\langle 11|\right) + \frac{1}{2}\Lambda_{\mathrm{IE(CE)}}(\tau)\left(|00\rangle\langle 11| + |11\rangle\langle 00|\right) \tag{3.38}$$

where we introduced the time-dependent coefficients:

$$\Lambda_{\text{IE}}(\tau) = \prod_{j=1}^{N} \Delta_2^A(\tau,\gamma_j)\Delta_2^B(t,\gamma_j) \qquad \Lambda_{\text{CE}}(\tau) = \prod_{j=1}^{N} \Delta_4(\tau,\gamma_j). \tag{3.39}$$

Eq. (3.38) has the same mathematical expression as Eq.s (3.25) and (3.26), but for a different time-dependent coefficient. Its partial transpose is thus computed similarly to Eq.s (3.27) and (3.28) and allows us to compute the negativity as:

$$N_{\text{IE(CE)}}(\tau) = |\Lambda_{\text{IE(CE)}}(\tau)|\,, \tag{3.40}$$

and the quantum discord is calculated by using Eq. (1.86):

$$Q_{\text{IE(CE)}}(\tau) = h(\Lambda_{\text{IE(CE)}})\,. \tag{3.41}$$

The negativity is the product of many oscillating coefficients $\Delta_n(\tau,\gamma_i)$, with various periodicities as explained in Sec. 3.2.1, which depend on the value of the selected switching rate. In the case of switching rates taken from a $1/\gamma$ distribution, the product of these terms results in a monotonic decay for both entanglement and discord. This is due to the fact that the γs picked from a $1/\gamma$ distribution tend to have contributions both from the $\gamma > 2$ and the $\gamma < 2$ regimes and the resulting effect is a "destructive interference" that leads to a monotonic behavior.

In Fig. 3.12 we report the behavior of such quantities in the case of 20 and 100 fluctuators. As the number of fluctuators is increased the quantum correlations decay faster. We consider 20 sources of RTN as the minimum number of fluctuator needed to obtain both a reliable profile of the frequency spectrum and a representative sample of the $p_\alpha(\gamma)$ distribution. Although it is possible to obtain a pink noise spectrum even with a smaller number of fluctuators, this case is a too strong approximation and it does not describe a sample of $1/\gamma$-distributed switching rates.
A very different behavior arises when the γ's are selected from a $1/\gamma^2$ distribution (see Fig. 3.13). Phenomena of sudden death and revivals appear for both entanglement and quantum discord. As the number of fluctuators is increased, the heights of the peaks decrease. The peaks have a periodicity of $\pi/2$ and $\pi/4$ for different and common environments respectively. This is explained by considering that the selected switching rates γ_i have small and very close values, since they are picked from a $1/\gamma^2$ distribution. We already know from Sec. 3.40 that for small values of γ the function $\Delta_n(\tau)$ tends to become a periodic function with periodicity π and $\pi/2$ for independent and common environments respectively and this periodicity will be halved for the functions $\Delta_n^2(\tau)$ and $|\Delta_n(\tau)|$. The product of functions with almost the same periodicity gives a periodic behavior with narrow peaks.

In Fig. 3.14 we report the negativity and the discord as a function of time τ and the noise parameter α, for a specific sample of the $\{\gamma_j\}$ and for $N = 100$ fluctuators in the case of independent environments. We confirm that the same qualitative behavior is found for entanglement and discord, due to the fact that quantum discord is a function of the negativity. For small values of α the quantum correlations decay in an exponential way, while at increasing values of α revival peaks, with $\pi/2$ periodicity, begin to appear. The height of the peaks raises with α and reaches its maximum for the $1/f^2$ noise .The qualitative trend is clearly identified, while it is not possible to make precise claims about the heights of the peaks or about a threshold value. In fact, the quantitative results

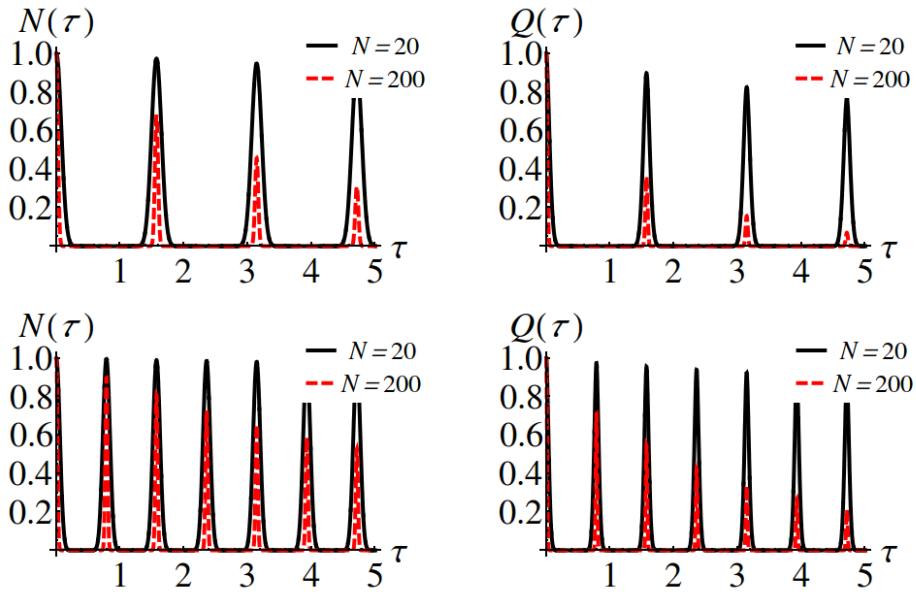

Figure 3.13: Upper panels: Time evolution of negativity and discord for two qubits interacting with two independent environments, consisting in a collection of N bistable fluctuators with spectrum $1/f^2$ when $[\gamma_1, \gamma_2] = [10^{-4}, 10^4]$. Lower panels: same as before, but with qubits subject to a common environment.

depends upon the range of selected switching rates, upon the number of fluctuators, and upon the $\{\gamma_j\}$ sample.

Fig.s 3.12, 3.13 and 3.14 were obtained by numerical simulation of the dynamics of the N bistable fluctuators. Indeed, the quantum correlations described by Eq.s (3.40) and (3.41) are computed numerically after the selection of the switching rates $\{\gamma_i\}_{i=1}^N$. The values N of the γ's are generated through a Monte Carlo method. Starting from the probability distribution $p_\alpha(\gamma)$ of the switching rates and introducing a random number $0 < r < 1$ we can select the proper switching rates $\{\gamma_i\}$ as:

$$\alpha = 1 \qquad r = \int_{\gamma_1}^{\gamma_i} p_1(\gamma) d\gamma = \frac{1}{\ln(\gamma_2/\gamma_1)} \ln\left(\frac{\gamma_i}{\gamma_1}\right) \tag{3.42}$$

$$\rightarrow \gamma_i = \gamma_1 \left(\frac{\gamma_2}{\gamma_1}\right)^r \tag{3.43}$$

$$\alpha \neq 1 \qquad r = \int_{\gamma_1}^{\gamma_i} p_\alpha(\gamma) d\gamma = \frac{\gamma_2^{\alpha-1}}{\gamma_2^{\alpha-1} - \gamma_1^{\alpha-1}} \frac{\gamma_i^{\alpha-1} - \gamma_1^{\alpha-1}}{\gamma_i^{\alpha-1}}$$

$$\longrightarrow \gamma_i = \frac{\gamma_1 \gamma_2}{\left[\gamma_2^{\alpha-1} - r\left(\gamma_2^{\alpha-1} - \gamma_1^{\alpha-1}\right)\right]^{1/(\alpha-1)}} \tag{3.44}$$

In order to get a better insight into the dependency of quantum correlations upon the selected sample $\{\gamma_i\}$, in Fig. 3.15 we compare the time evolution of the entanglement

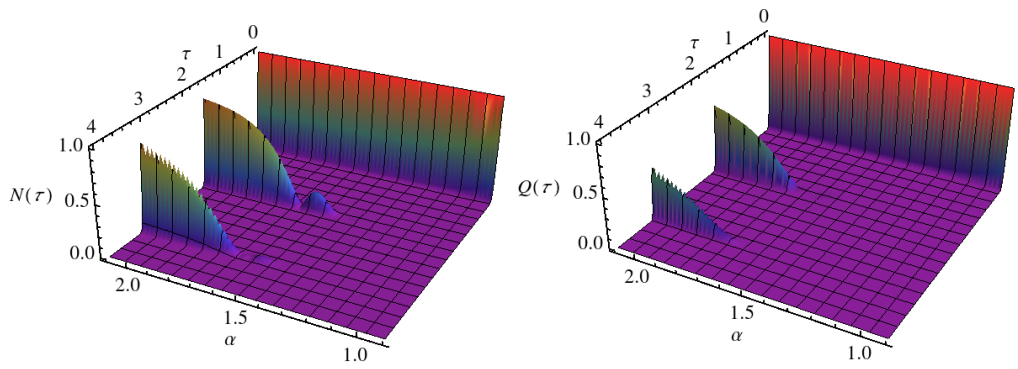

Figure 3.14: Negativity (left) and quantum discord (right) as a function of the dimensionless time τ and the noise parameter α, between two qubits interacting with independent collections of $N = 100$ bistable fluctuators.

between two qubit in independent environments for the case of $N = 20, 50, 100$ fluctuators, and for two values of the parameter α, i.e.: $\alpha = 1$ (solid-black line) and $\alpha = 2$ (dashed-red line). 30 curves are drawn for each value of α, corresponding to 30 different samples of the switching rates $\{\gamma_j\}$. Different choices of the range $[\gamma_1, \gamma_2]$ are confronted (see figure caption). Increasing the number of fluctuators make the results less sensitive to the specific selection of the switching rates. Consider, as example, the top panels in Fig. 3.15 and let us focus on the $1/f$ noise. For a small number of fluctuator ($N = 20$), different samples $\{\gamma_i\}$ give rise to different qualitative behavior: rather than the monotonic decaying, some samples of the γs show a little revival at $\tau = \pi/\delta$. As the number of bistable fluctuators is increased, only the monotonic behavior appears.

For high frequencies both $1/f$ and $1/f^2$ noise spectra induce an exponential decay of correlations, while at low frequencies revival peaks appears, whose heights decrease increasing the number of fluctuators. Indeed a number of peaks with periodicity $\pi/2$ and exponentially decreasing heights are present. In Fig. 3.15, to make the picture more readable, only the first peak is shown.

We showed that the qualitative behavior of the quantum correlations in the case of two qubits subject to $1/f^\alpha$ noise, depends upon the selected sample of switching rates $\{\gamma_i\}$ and upon the range of the distribution $[\gamma_1, \gamma_2]$. However, we are interested in analyzing the general dynamics of quantum correlations by eliminating at least the dependency upon the sample, i.e. in studying an average behavior, which does not depend on the specific choice of the γ_i's but only on the probability distribution $p_\alpha(\gamma)$. Moreover, we want to be able to consider situations in which the $1/f^\alpha$ noise raises from a collection of few fluctuators, up to the limit where a single fluctuator is interacting with the quantum system.
In order to study the general behavior of quantum correlations, independently on the selected switching rates, we introduce an alternative microscopic model for $1/f^\alpha$ in which the noise arises from a collection of random bistable fluctuators. This model is presented in the next section.

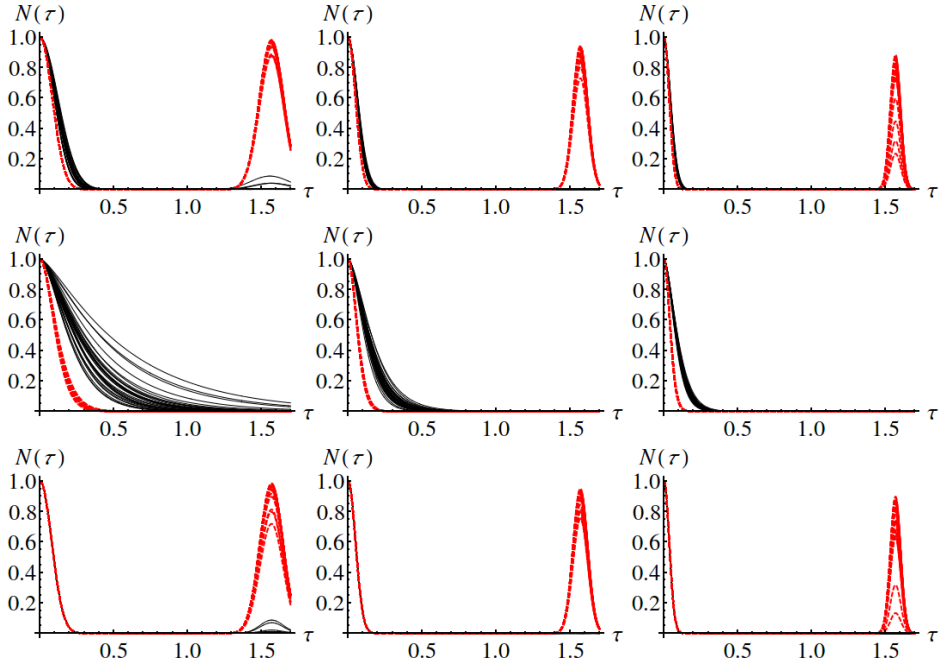

Figure 3.15: Time evolution of the negativity for three different numbers of bistable fluctuators $N = 20$ (left column), 50 (central column) and 100 (right column) for two specific values of the noise parameter α: $\alpha = 1$ (black lines) and $\alpha = 2$ (red lines). 30 curves are shown for each value of α corresponding to 30 different samples of the γ_j's. Different choices of the range $[\gamma_1, \gamma_2]$ are presented. Specifically $[10^{-4}, 10^4]$ (top panels), $[1, 10^4]$ (central panels) and $[10^{-4}, 1]$ (right panel).

3.2.3 $1/f^\alpha$ noise generated by random bistable fluctuators

We call *random bistable fluctuator* (RBF) a quantity which flips between two values with a random switching rate. This means that the switching rate γ is not known a priori, but the fluctuator is described by a statistical mixture whose elements are taken from the ensemble $\{\gamma, p_\alpha(\gamma)\}$ and $\gamma \in [\gamma_1, \gamma_2]$.
$1/f^\alpha$ noise can be ascribed to a single random bistable fluctuator or to a collection of them. In order to validate this model from a mathematical point of view, we recall Eq. (2.47) which provides a way to reproduce the $1/f^\alpha$ noise:

$$S_{1/f^\alpha}(\omega) = \int_{\gamma_1}^{\gamma_2} S_{\mathrm{RTN}}(\omega, \gamma) p_\alpha(\gamma) d\gamma. \tag{3.45}$$

This integral can be interpreted as the spectrum of a single fluctuator whose switching rate is randomly chosen from a distribution $p_\alpha(\gamma)$. In fact, the autocorrelations function of a random bistable fluctuator $B(t)$ may be written as:

$$\begin{aligned} C_{\mathrm{RBF}}(\tau) &= \mathbb{E}\left[B(\tau)B(0)\right] \\ &= \iint B(\tau)B(0)p(B)dB\, p_\alpha(\gamma)d\gamma = \int C_{\mathrm{RTN}}(\tau, \gamma)\, p_\alpha(\gamma)d\gamma \end{aligned} \tag{3.46}$$

where C_{RTN} is the autocorrelation function of the random telegraph noise Eq. (2.30) with an explicit dependence on the switching rate. The power spectrum is calculated from

Eq. (2.8) and can be written as:

$$S_{\mathrm{RBF}}(\omega)=\int_{-\infty}^{\infty}e^{-i\omega\tau}C_{\mathrm{RBF}}(\tau)d\tau=\int p_\alpha(\gamma)d\gamma\int_{-\infty}^{\infty}e^{-i\omega\tau}C_{\mathrm{RTN}}(\tau,\gamma)d\tau \tag{3.47}$$

which gives exactly Eq. (3.45) upon assuming that the probability distribution $p_\alpha(\gamma)$ is non-zero only in the range of values $[\gamma_1,\gamma_2]$. If we have a collection of N random bistable fluctuators , the spectrum would be

$$S_{\mathrm{RBF}}(\omega)=\sum_{j=1}^{N}S_{1/f^\alpha}(\omega)\propto\frac{N}{\omega^\alpha}. \tag{3.48}$$

Within this model of noise, the stochasticity of the environment does not only arise from the process $B_{\mathrm{A(B)}}(\tau)$ in the Hamiltonian (3.2), but also from the randomness in the switching rates. The global state of the system (3.6) corresponds to a specific realization of the global stochastic phase $\varphi_{\mathrm{A(B)}}(\tau)=\sum_{j=1}^{N}\varphi_{j\,\mathrm{A(B)}}(\tau)$ and a specific choice of the switching rates $\{\gamma_j\}$. Two ensemble averages are required in order to describe the density matrix of the two-qubit system: the first average in over all the possible realizations of the noise phase, and the results is exactly the same as Eq. (3.36) obtained from a collection of bistable fluctuators:

$$\rho(\tau,\{\gamma_i\})=\int\rho_G(\tau,\{\gamma_i\},\varphi)p_T(\varphi,\tau)d\varphi \tag{3.49}$$

where we wrote explicitly the dependency of the global density matrix on the choice of the switching rates and the noise phase. The second average is over the possible choices for the switching rates:

$$\rho_{\mathrm{IE}}(\tau)=\int_{\gamma_1}^{\gamma_2}\int_{\gamma_1}^{\gamma_2}\rho_{\mathrm{IE}}(\tau,\{\gamma\})p_\alpha(\{\gamma_A\})p_\alpha(\{\gamma_B\})d\{\gamma_A\}d\{\gamma_B\} \tag{3.50}$$

$$\rho_{\mathrm{CE}}(\tau)=\int_{\gamma_1}^{\gamma_2}\rho_{\mathrm{CE}}(\tau,\{\gamma\})p_\alpha(\{\gamma\})d\{\gamma_j\} \tag{3.51}$$

where we used the notation $p_\alpha(\{\gamma\})=\prod_{j=1}^{N}p_\alpha(\gamma_j)$ and $d\{\gamma\}=\prod_j d\gamma_j$.

If we consider as initial state the Bell state $|\Phi^+\rangle$, then the first ensemble average Eq. (3.49) gives the same result as in the case of a collection of bistable fluctuators Eq. (3.38). The second average gives the solution for the two-qubit density operator:

$$\rho_{\mathrm{IE(CE)}}(\tau)=\frac{1}{2}\left(|00\rangle\langle 00|+|11\rangle\langle 11|\right)+\frac{1}{2}\Gamma_{\mathrm{IE(CE)}}(\tau)(|00\rangle\langle 11|+|11\rangle\langle 00|) \tag{3.52}$$

where we introduced the time dependent coefficient

$$\begin{aligned}\Gamma_{\mathrm{IE}}(\tau)&=\int_{\gamma_1}^{\gamma_2}\int_{\gamma_1}^{\gamma_2}\Lambda_{\mathrm{IE}}(\tau,\{\gamma\})p_\alpha(\{\gamma_A\})p_\alpha(\{\gamma_B\})d\{\gamma_A\}d\{\gamma_B\}\\&=\left[\int_{\gamma_1}^{\gamma_2}\Delta_2(\tau,\gamma)p_\alpha(\gamma)d\gamma\right]^{2N}\end{aligned} \tag{3.53}$$

$$\Gamma_{\mathrm{CE}}(\tau)=\int_{\gamma_1}^{\gamma_2}\Lambda_{\mathrm{CE}}(\tau,\{\gamma\})p_\alpha(\{\gamma\})d\{\gamma\}=\left[\int_{\gamma_1}^{\gamma_2}\Delta_4(\tau,\gamma)p_\alpha(\gamma)d\gamma\right]^{N} \tag{3.54}$$

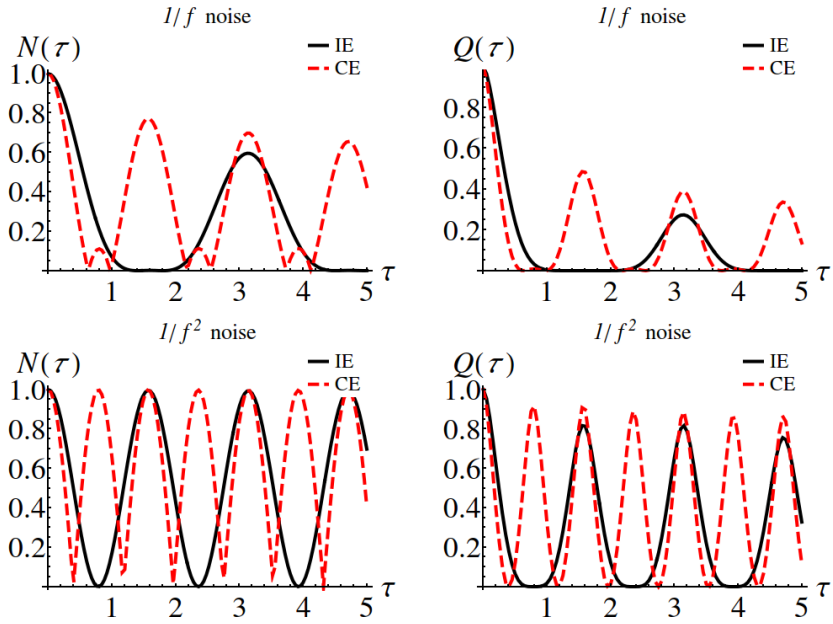

Figure 3.16: Upper panels: Time evolution of the negativity $N(\tau)$ (left) and the quantum discord $Q(\tau)$ (right) for two qubits interacting with a single random bistable fluctuator with $1/f$ spectrum for different (solid black line) and common (dashed red line) environments when $[\gamma_1, \gamma_2] = [10^{-4}, 10^4]$. Bottom panels: Time evolution of negativity (left) and discord (right) for two qubits interacting with a single random fluctuator with $1/f^2$ spectrum for different (solid black line) and common (dashed red line) environments when $[\gamma_1, \gamma_2] = [10^{-4}, 10^4]$.

The partial transposed matrix of Eq. (3.52) is trivial to compute and through its negative eigenvalues we are able to write the expression for the negativity, and through Eq. (1.86) the expression for the quantum discord:

$$N_{\mathrm{IE(CE)}}(\tau) = |\Gamma_{\mathrm{IE(CE)}}(\tau)| \tag{3.55}$$

$$D_{\mathrm{IE(CE)}}(\tau) = h\big[\Gamma_{\mathrm{IE(CE)}}(\tau)\big] \tag{3.56}$$

where $h(x)$ is the function defined in Eq. (3.14). The dynamics of the qubit and thus of the quantum correlations is governed by the function $\Gamma_{\mathrm{IE(CE)}}(\tau)$. This time-dependent coefficient may be easily evaluated numerically, either by numerical integration or by equivalent series representation (see Sec. 3.2.3), as reported at the end of this chapter.

As explained at the beginning of this section, Eq. (3.45) can be interpreted as the spectrum arising from a single random bistable fluctuator. This means that one RBF is sufficient to mimic $1/f^\alpha$ noise. In the following we analyze the case of a single random bistable fluctuator interacting with the two-qubit system in both configurations of independent and common environments.

The dynamics of $N(\tau)$ and $D(\tau)$ is shown in Fig 3.16, for the cases of pink and brown noise. The range of integration is $[10^{-4}, 10^4]$. The expressions for the negativity and the discord are written in Eq.s (3.55) and (3.56) for $N = 1$ with the integral $\Gamma_{\mathrm{IE(CE)}}$ to be computed numerically. Quantum correlations decay with damped oscillations. In the case of

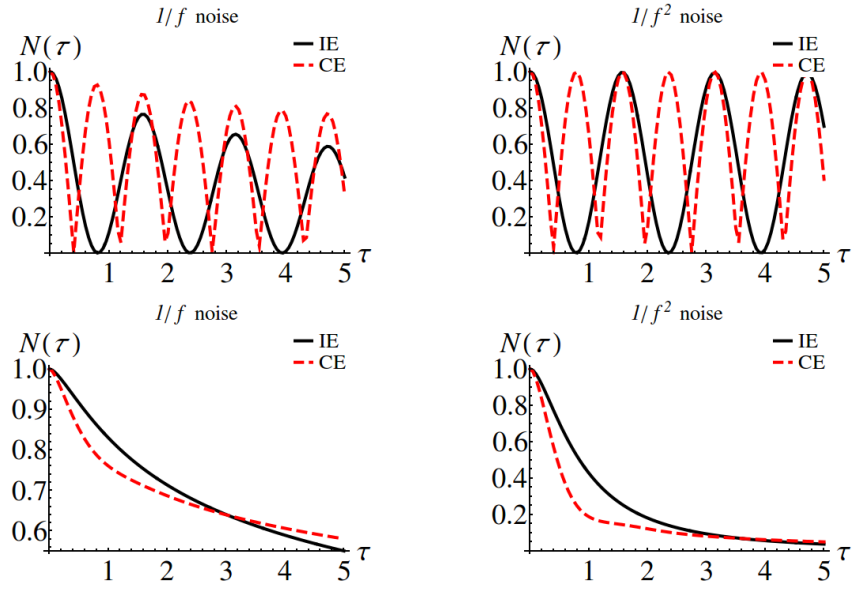

Figure 3.17: Dynamics of entanglement for two qubits interacting with a single random bistable fluctuator with $1/f$ and $1/f^2$ spectrum for different ranges of integrations: (Upper panels) $[\gamma_1, \gamma_2] = [10^{-4}, 2]$ and (Lower panels) $[\gamma_1, \gamma_2] = [2, 10^4]$.

qubits subject to independent noises with $1/f$ spectrum, the oscillations have a periodicity of π. This periodicity can be explained by analyzing the analytical expressions of the quantum correlations. In particular, we recall that in the integrals (3.53) and (3.54), the $\Delta_2(\tau, \gamma)$ functions exhibit damped oscillations for $\gamma < 2$ with periodicity $2\pi/\delta$, and for $\gamma > 2$ monotonically decay. Their weighted superposition leads to an interference effect that can be summarized as follows: the oscillating components result in the formation of alternatively positive and negative peaks spaced by $\pi/2$. On the other hand, the monotonic decaying components combine to cancel the negative peaks and to preserve the positive ones. Finally we are left with an oscillating function with periodicity of π. The same concept applies in the case of a common environment, but now the $\Delta_4(\tau, \gamma)$'s sum up in an oscillating function with periodicity of $\pi/2$.

The $1/f^2$ noise leads to oscillating functions of time with periodicity $\pi/2$ and $\pi/4$ for different and common environments respectively. Again this periodicity is related to the fact that with the $\frac{1}{\gamma^2}$ distribution, the selected values of γ accumulate near the lower value of the frequency range, thus leading to a beat phenomenon with constructive interference with the above mentioned periodicity.
If different ranges of integration are considered, different time-behavior for the quantum correlations can arise. In particular, if we engineer the environment to have only low-frequency components $\gamma \ll 1$, the quantum correlations evolve in time with damped oscillations. On the other hand, if one could select only fast components $\gamma \gg 1$, both entanglement and discord decay monotonically in time. Fig. (3.17) shows these features for the entanglement in the case of $\alpha = 1$ and $\alpha = 2$.

In the most general case, in which there are N random bistable fluctuators, we are able to recover the behavior in Fig. 3.12 and 3.13 for the same number N of oscillators.

Quantum correlations decay exponentially in the case of $1/f$ noise and with damped oscillations in the case of $1/f^2$ noise. The scenario with N RBF can be useful to obtain the average behavior of a collection of bistable fluctuators. Indeed, it describes the ensemble average over all possible realizations of the sample $\{\gamma_j\}_{j=1}^{N}$.

Our results about the $1/f^\alpha$ noise clearly show that the mere knowledge of the spectrum is not sufficient to determine the dynamical evolution of the quantum correlations. Indeed, the number of decoherence channels also play a key role. Different physical models for the environment can lead to the same spectrum. But, if the two-qubit system interact with only one decoherence channel, revivals may appear more easily because the system is affected only by one source of classical noise and information can flow back. If many sources of decoherence are present, then the information may be completely lost depending on the channel characteristics, that is, the distribution of the switching rates. This interpretation of revivals as information backflow is just a conjecture here. In the next chapter, I will prove the association between the presence of revivals and the backflow of information by calculating the BLP measure of non-Markovinity for two qubits interacting with different numbers of RBF N.

Series representation for $\Gamma_{\mathrm{IE(CE)}}(\tau)$

The dynamics of the two-qubit system depends upon the quantities $\Gamma_{\mathrm{IE(CE)}}(\tau)$ introduced in Eq. (3.53) and (3.54). In order to evaluate these quantities, we must be able to compute the integral:

$$\Gamma(\tau,\alpha)=\int_{\gamma_1}^{\gamma_2}\Delta_n(\tau,\gamma)p_\alpha(\gamma)d\gamma \tag{3.57}$$

where Δ_n and p_α are given in Eq.s (3.24) and (2.46) respectively. Let us focus on the case $n=2$ for the Δ_n-function. The evaluation of Eq. (3.57) can be done by numerical evaluation of the integral. Another possible way, may be through its series representation, as shown in the following.

Eq. (3.57) may be rewritten as

$$\Gamma(\tau,\alpha)=N_\alpha(\gamma_1,\gamma_2)\int_{\gamma_1}^{\gamma_2}d\gamma\, e^{-\gamma\tau}\gamma^{-\alpha}\times\left[\cosh\delta\tau+\gamma\tau\frac{\sinh\delta\tau}{\delta\tau}\right] \tag{3.58}$$

where we substituted $t\to\tau=\nu t$ and $\gamma\to\gamma=\gamma/\nu$, and the normalization N_α reads as follows

$$N_\alpha(\gamma_1,\gamma_2)=\begin{cases}\frac{1}{\ln\gamma_2-\ln\gamma_1} & \alpha=1\\ (\alpha-1)\left[\frac{(\gamma_1\gamma_2)^{\alpha-1}}{\gamma_2^{\alpha-1}-\gamma_1^{\alpha-1}}\right] & \alpha\neq 1\end{cases}. \tag{3.59}$$

Using the new variable $y=\gamma\tau$ we may write the integral (3.58) as the sum of two contributions:

$$\Gamma(\tau,\alpha)=N_\alpha(\gamma_1,\gamma_2)\Big[F(\gamma_2\tau,\alpha,\tau)-F(\gamma_1\tau,\alpha,\tau)\Big], \tag{3.60}$$

where

$$F(y,\alpha,\tau)=\tau^{\alpha-1}\Big[F_1(y,\alpha,\tau)+F_2(y,\alpha,\tau)\Big],$$

and

$$F_1(y,\alpha,\tau) = \int dy\, e^{-y}\, y^{-\alpha}\, \cosh\sqrt{y^2-4\tau^2}\,, \tag{3.61}$$

$$F_2(y,\alpha,\tau) = \int dy\, e^{-y}\, y^{-\alpha+1}\, \frac{\sinh\sqrt{y^2-4\tau^2}}{\sqrt{y^2-4\tau^2}}\,. \tag{3.62}$$

Upon expanding the hyperbolic functions and using the relation

$$\int dy\, e^{-y}\, y^{-\alpha}\, (y^2-4\tau^2)^k = \sum_{p=0}^{k} (-)^{1+k+p}\, (2\tau)^{2(k-p)} \times \left(\begin{array}{c} k \\ p \end{array}\right) \Gamma(2p+1-\alpha, y)\,, \tag{3.63}$$

where $\Gamma(a,x)$ is the (incomplete) Euler Gamma function, the two functions F_k may be rewritten as

$$F_1(y,\alpha,\tau) = \sum_{k=0}^{\infty}\sum_{p=0}^{k} (-)^{1+k+p}\, \frac{\tau^{2(k-p)}}{(2k)!} \times \left(\begin{array}{c} k \\ p \end{array}\right) \Gamma(2p+1-\alpha, y)\,, \tag{3.64}$$

$$F_2(y,\alpha,\tau) = \sum_{k=0}^{\infty}\sum_{p=0}^{k} (-)^{1+k+p}\, \frac{\tau^{2(k-p)}}{(2k+1)!} \times \left(\begin{array}{c} k \\ p \end{array}\right) \Gamma(2p+2-\alpha, y)\,. \tag{3.65}$$

We now introduce the new index $s = k - p$ and rearrange series as

$$\sum_{k=0}^{\infty}\sum_{p=0}^{k} \ldots = \sum_{p=0}^{\infty}\sum_{k=p}^{\infty} \ldots = \sum_{p=0}^{\infty}\sum_{s=0}^{\infty} \ldots\,,$$

thus arriving at

$$\begin{aligned} F_1(y,\alpha,\tau) &= \sum_{p=0}^{\infty}\sum_{s=0}^{\infty} \frac{(-)^{1+s}}{[2(p+s)]!} \left(\begin{array}{c} p+s \\ s \end{array}\right) (2\tau)^s\, \Gamma(2p+1-\alpha, y) \\ &= -\sum_{p=0}^{\infty} \frac{1}{(2p)!}\, \Phi_{p+\frac{1}{2}}(-\tau^2)\, \Gamma(2p+1-\alpha, y)\,, \end{aligned} \tag{3.66}$$

where $\Phi_n(x)$ denotes the confluent hypergeometric function ${}_0F_1(n,x)$. Analogously, we arrive at

$$F_2(y,\alpha,\tau) = -\sum_{p=0}^{\infty} \frac{1}{(2p+1)!}\, \Phi_{p+\frac{3}{2}}(-\tau^2)\, \Gamma(2p+2-\alpha, y)\,. \tag{3.67}$$

Upon substituting Eqs. (3.66) and (3.67) in Eq. (3.60) we obtain a series representation for the quantity $\Gamma(\tau,\alpha)$. As a matter of fact, truncating the series at the first term, i.e. $p = 0$ in Eqs. (3.66) and (3.67), already provides an excellent approximation for $\alpha \gtrsim 3/2$ and any value of τ. In formula

$$\begin{aligned} \Gamma(\tau,\alpha) \simeq & \frac{1}{2} N_\alpha(\gamma_1,\gamma_2)\tau^{\alpha-2} \big[2\tau\cos 2\tau\, \Gamma^*(1-\alpha,\gamma_1\tau,\gamma_2\tau) \\ & + \sin 2\tau\, \Gamma^*(2-\alpha,\gamma_1\tau,\gamma_2\tau)\big], \end{aligned} \tag{3.68}$$

where $\Gamma^*(a,x,y) = \Gamma(a,x) - \Gamma(a,y)$. On the other hand, for $\alpha \lesssim 3/2$ the number of terms needed for a reliable approximation rapidly grows.

3.3 Summary

- We analyzed the dynamics of quantum correlations of two qubits subject either to Gaussian or to non-Gaussian noise in the two different scenarios of independent and common environments.
- In the case of Gaussian noise affecting the system, the dynamics depends upon the time dependence of the β-function. Quantum correlations decay monotonically in the case of qubits initially prepared in a Bell state both for the case of independent and common Gaussian environments. If the initial state is in a Bell-mixture, entanglement displays sudden death, while quantum discord may have a different behavior depending on the initial state and the independent/common environment scenario considered.
- Entanglement preserving time and sudden death time as a function of the Gaussian noise parameters, depends upon the specific process considered.
- Random telegraph noise gives rise to two different regimes for the dynamics of quantum correlations. In the weak coupling regime, quantum correlations decay monotonically in time, while in the strong coupling regime they decay with damped oscillations. Entanglement-preserving times and sudden-death times depend upon the value of the switching rate, in the case of qubits subject to fast RTN: the larger is γ, the longer are the decoherence times. The effect of a common environment is to destroy correlations faster with respect to the case of independent environments.
- The effect of $1/f^{\alpha}$ noise arising from a collection of bistable fluctuators on the dynamics of quantum correlations depends on the value of α. In particular, for small values of the parameter, they decay monotonically. On the other hand, for low-frequency noise, that is higher values of α, the quantum correlations decay with oscillations. Decoherence becomes stronger as the number of fluctuators increases.
- When the environment is described using random bistable fluctuators giving rise to a $1/f^{\alpha}$ noise, a strong dependence on the number of random fluctuators for the dynamics of entanglement and discord is found. In particular, for a single fluctuator, revivals appear for all considered values of α. However increasing the number of fluctuators leads to a behavior in agreement with the case of a collection of bistable fluctuators with fixed switching rates.

CHAPTER 4

Non-Markovianity of Gaussian and non-Gaussian noisy channels

In this chapter we analyze the non-Markovian character of a noisy channel by applying the BLP and BCM measures of non-Markovianity, as introduced in Sec. 1.3, to a single- and two-qubit system subject to classical noise. The dynamical map of the quantum system interacting with these kinds of environment is pure dephasing. The aim of this chapter is to analyze the non-Markovian features of the dephasing channel and to verify if there exist any relationship between the monotonic or non-monotonic decaying of quantum correlations and the non-Markovian nature of the dynamical map. In particular, we want to verify the conjecture that the presence of revivals of quantum correlations is a sign for an underlying non-Markovian nature of the considered quantum channel, at least for the systems we consider in this thesis.

In order to address the non-Markovianity of a dephasing channel arising from the interaction of a quantum system with a classical field, we start with the simple case of a single qubit interacting with classical environment. The single qubit case can be treated analytically and, as we will show in the following, the results in terms of non-Markovianity are the same for the single- and a two-qubit dephasing map we are investigating.
Consider a single qubit interacting with a classical field, whose Hamiltonian is described by Eq. (3.2):

$$H(t) = \omega_0 \sigma_z + \nu\, B(t) \sigma_z \tag{4.1}$$

where $B(t)$ is the stochastic process generating the noise. Let us consider a generic qubit-state described by the state vector

$$|\psi_0\rangle = \alpha|0\rangle + \beta|1\rangle, \tag{4.2}$$

where α and β are complex numbers satisfying the condition $|\alpha|^2 + |\beta|^2 = 1$. The system-environment interaction of Eq. (4.1) describes a non-dissipative dephasing channel, and it is suitable to portray situations where the typical frequencies of the environment are smaller than the natural frequency of the qubit.
Different expressions for $B(t)$ may be employed, corresponding to different kinds of classical noise. In the next sections, we briefly review the dynamics of the generic qubit state (4.2) and then we will employ these results to explicitly evaluate the non-Markovianity of the corresponding channels in the cases of both Gaussian and non-Gaussian noise. Given an initial state $\rho_0 = |\psi_0\rangle\langle\psi_0|$ at initial time $t_0 = 0$, the global system evolves according to the evolution operator in Eq. (3.3) and the global density

matrix $\rho_G(t) = U(t)\rho_0 U^\dagger(t)$. If, in addition, we multiply it by a rotation matrix $e^{i\omega_0 t\sigma_z}$, its expression is given by:

$$\rho_G(t) = \begin{pmatrix} |\alpha|^2 & e^{-2i\nu\varphi(t)}\alpha\beta^* \\ e^{2i\nu\varphi(t)}\alpha^*\beta & |\beta|^2 \end{pmatrix} \tag{4.3}$$

where $\varphi(t)$ is again the noise phase $\varphi(t) = \int_0^t B(s)ds$. The qubit density matrix is calculated as the ensemble average of the global density operator $\rho(t) = \mathbb{E}[\rho_G(t)]$. The expectation of the quantity $\mathbb{E}\left[e^{2i\nu\varphi(t)}\right]$ depends on the nature of the stochastic process considered $B(t)$, as shown in the previous chapter. In the following sections, different kinds of noise will be taken into account and compared.

4.1 Non-Markovianity of Gaussian noisy channels

We show in Sec. (3.1) that the dynamics of quantum correlations is monotonically decreasing in the case of Gaussian noise (we are only referring to states which have both entanglement and quantum discord, i.e. are non-separable). The characteristic function of the noise phase is given by Eq. (3.8). For a fixed value of the coupling constant ν, it depends only on the β-function and it coincides with the dephasing coefficient of the density operator $\rho(t) = \mathbb{E}[\rho_G(t)]$.
We start by considering the BLP measure of non-Markovianity. We already know from Eq. (1.96), that in the case of a dephasing channel, the analytical expression for the optimal trace distance is known and it coincides with the absolute value of the dephasing coefficient. It immediately follows that, for Gaussian processes, the optimal trace distance reads:

$$D(t) = e^{-4\nu^2\beta(t)}. \tag{4.4}$$

Since the function $\beta(t)$ is a monotone function for all the Gaussian processes we introduced in Sec. 2.1.1, the derivative of the optimal trace distance is always negative and the BLP measure of non-Markovianity (1.95) is identically zero for all times.

We expect to find the same Markovian character in the case in which the quantum system is composed by two non-interacting qubits. To this purpose, consider a two-qubit system interacting subject to classical Gaussian noise. We analyze both the case where the two qubits are coupled to separate and independent environments, and the case in which they interact with the same environment. An analytical proof of the Markovianity of the quantum map for a generic two-qubit system seems intractable since a two qubit density operator is described by 9 independent parameters. We can however show that the trace distance decreases monotonically for an X-state.
First, we analyze the different-environment case. We consider two initial arbitrary X-states

$$\rho_1(0) = \frac{1}{4}\left(\mathbb{I} + \sum_{j=x,y,z} a_j\sigma_j \otimes \sigma_j\right), \qquad \rho_2(0) = \frac{1}{4}\left(\mathbb{I} + \sum_{j=x,y,z} b_j\sigma_j \otimes \sigma_j\right) \tag{4.5}$$

whose time evolution is given by Eq. (3.10):

$$\rho_1(t) = \frac{1}{4}\left(\mathbb{I} + e^{-4\nu^2\beta(t)}a_x\sigma_x \otimes \sigma_x + e^{-4\nu^2\beta(t)}a_y\sigma_y \otimes \sigma_y + a_z\sigma_z \otimes \sigma_z\right) \tag{4.6}$$

and an analogue expression for $\rho_2(t)$ where the coefficients a_j are substituted by the coefficients b_j. The trace distance is computed following Eq. (1.90) and it is given by:

$$\begin{aligned} D(t,\rho_1,\rho_2) = &\frac{1}{8}\Big[\Big|e^{-4\nu^2\beta(t)}(a_x+a_y-b_x-b_y)+(a_z-b_z)\Big| + \\ &\Big|e^{-4\nu^2\beta(t)}(a_x+a_y-b_x-b_y)+(-a_z+b_z)\Big| + \\ &\Big|e^{-4\nu^2\beta(t)}(a_x-a_y-b_x+b_y)+(a_z-b_z)\Big| + \\ &\Big|e^{-4\nu^2\beta(t)}(a_x-a_y-b_x+b_y)+(-a_z-b_z)\Big|\Big]. \end{aligned} \tag{4.7}$$

There is no need to find the optimal pair, since the trace distance is a non-increasing function of time for every choice of the initial pair. In a similar way we can find the expression of the trace distance between two qubits interacting with a common environment and again we find that it is a non-increasing function of time.

Gaussian noise leads to Markovian dynamical maps. This means that there is no regrowth in distinguishability between any two quantum states. The BCM measure of non-Markovianity confirms this result.

4.2 Non-Markovianity of non-Gaussian noisy channels

Consider a single qubit subject to a classical non-Gaussian noise. Its evolved density matrix is obtained from Eq. (4.3) once we specify the stochastic process generating the noise, i.e. the expectation $\mathbb{E}\left[e^{2i\nu\varphi(t)}\right]$.
In the following we study the non-Markovian character of a qubit subject to random telegraph noise and colored noise with $1/f^\alpha$ spectrum.

4.2.1 Random telegraph noise

The evolved density matrix in the case of a qubit subject to random telegraph noise with switching rate ξ is easily computed averaging the global density matrix (4.3) and using Eq. (3.24) to calculate the dephasing coefficient:

$$\rho_G(\tau) = \begin{pmatrix} |\alpha|^2 & \Delta_2(\tau,\gamma)\alpha\beta^* \\ \Delta_2(\tau,\gamma)\alpha^*\beta & |\beta|^2 \end{pmatrix}. \tag{4.8}$$

Hereafter we use dimensionless time $\tau \equiv \nu t$ and switching rate $\gamma \equiv \xi/\nu$. The first step to compute the BLP and BCM non-Markovianity measures is the evaluation of the optimal trace distance and the quantum capacity, respectively. From Eqs. (1.96) and (1.101), we can write:

$$D(t)(\tau,\gamma) = |\Delta_2(\tau,\gamma)|, \tag{4.9}$$

$$C_Q(\tau,\gamma) = 1 - S_E\left(\frac{1-\Delta_2(\tau,\gamma)}{2}\right). \tag{4.10}$$

Two different regimes naturally arise: for $\gamma < 2$ both the trace distance and the quantum capacity display damped oscillations, i.e. the dynamics is non-Markovian, whereas for $\gamma \geq 2$ they decay monotonically, i.e. the dynamics is Markovian. In fact, the non-Markovianity measures N_{BLP} and N_{BCM} correspond to the integrals, over their range of

positivity, of the quantities

$$\sigma_{\rm BLP} = \frac{d}{d\tau} D(\tau,\gamma) = -\gamma\,|\Delta_2(\tau,\gamma)| + \text{sgn}\left[\Delta_2(\tau,\gamma)\right](\gamma\cosh\delta\tau + \delta\sinh\delta\tau)\,e^{-\gamma\tau} \tag{4.11}$$

$$\sigma_{\rm BCM} = \frac{d}{d\tau} C_Q(\tau,\gamma) = -\frac{4}{\ln 2} e^{-\gamma\tau}\,\frac{\sinh\delta\tau}{\delta}\,\text{arctanh}\left[\Delta_2(\tau,\gamma)\right]\,, \tag{4.12}$$

respectively. If $\gamma > 2$ Eq. (4.11) can be simplified since $\Delta_2(\tau,\gamma) > 0\ \forall\, t$. It has expression:

$$\begin{aligned}\sigma_{\rm BLP} &= -\gamma e^{-\gamma\tau}\left[\cosh(\delta\tau) + \frac{\gamma}{\delta}\sinh(\delta\tau)\right] + (\gamma\cosh\delta\tau + \delta\sinh\delta\tau)\,e^{-\gamma\tau} \\ &= -4\,e^{-\gamma\tau}\,\frac{\sinh\delta\tau}{\delta} \qquad \text{if } \gamma \geq 2\end{aligned} \tag{4.13}$$

while $\sigma_{\rm BCM}$ keeps the same expression. As it is apparent from the expressions, for $\gamma \geq 2$, both the σ's are negative definite such that both the measures $N_{\rm BLP}$ and $N_{\rm BCM}$ vanish. On the other hand, both the σ's show an oscillatory behavior as a function of time, which includes positive values, for any values of $\gamma < 2$.

We are interested in finding the extrema of the functions $D(\tau,\gamma)$ and $C_Q(\gamma,\tau)$ in order to define the regions where they are increasing function of time and thus computing the non-Markovianity measures (1.95) and (1.100). The maxima $\tau_k^{\rm max}$ and minima $\tau_k^{\rm min}$ of D and C_Q are at the same points for the two functions. As we discussed in Sec. 3.40, the $\Delta_n(\gamma,\tau)$ function has the maxima located at $\tau = k\pi/\delta$. The minima of the function $D(t)$ can be computed easily in the strong coupling regime $\gamma < 2$ by looking for the time-points in which Eq. (4.9) goes to zero:

$$\begin{aligned}\cos(\delta t) + \frac{\gamma}{\delta}\sin(\delta t) = 0 \quad &\rightarrow \quad \tan(\delta t) = -\frac{\delta}{\gamma} \\ t &= \frac{\arctan\left(\frac{-\delta}{\gamma}\right) + k\pi}{\delta}\end{aligned} \tag{4.14}$$

where $\delta = \sqrt{4-\gamma^2}$. Note that the minima are the points where the two functions D and C_Q vanish. It follows that we can write the extremal points for the two functions as:

$$\tau_k^{\rm max} = k\pi/\sqrt{4-\gamma^2} \tag{4.15}$$

$$\tau_k^{\rm min} = \tau_k^{\rm max} + \tau^* = \tau_k^{\rm max} + (4-\gamma^2)^{-\frac{1}{2}}\arctan\left[\frac{-(4-\gamma^2)^{\frac{1}{2}}}{\gamma}\right]. \tag{4.16}$$

We now have all the ingredients to compute the non-Markovianity of the dephasing channel through the BLP and BCM measures:

$$N_{\rm BLP} = \sum_{k=1}^{\infty} D(\gamma,\tau_k^{\rm max}) = \frac{1}{\exp\left(\frac{\pi\gamma}{\sqrt{4-\gamma^2}}\right) - 1} \tag{4.17}$$

$$N_{\rm BCM} = \sum_{k=1}^{\infty} C_Q(\gamma,\tau_k^{\rm max}) \tag{4.18}$$

In the left panel of Fig. 4.1 we show the optimal trace distance dynamics in the non-Markovian regime $\gamma < 2$ for three specific values of γ. We notice that the smaller is

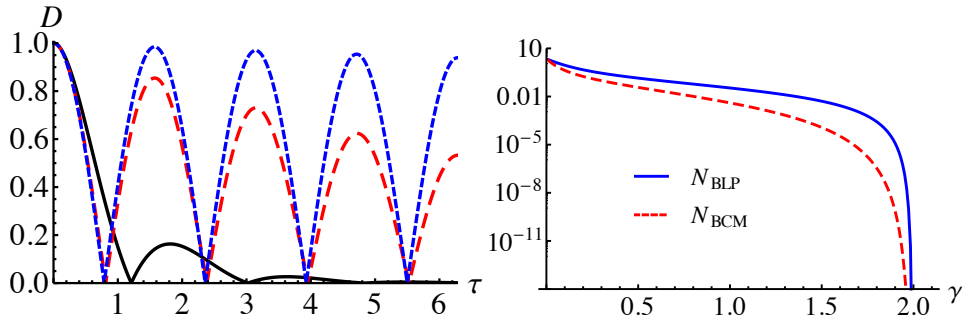

Figure 4.1: Non-Markovianity of RTN channels. The left panel shows the trace distance as a function of time for three different values of the switching rate: $\gamma = 1$ (solid black line), $\gamma = 0.1$ (dashed red line) and $\gamma = 0.01$ (dotted blue line). The right panel is a log-plot of both BLP and BCM non-Markovianity measures as a function of γ.

γ, the higher are the revivals of the trace distance, and thus the more enhanced is the non-Markovian character of the dynamics. A similar behavior occurs for the quantum capacity. We do not show it here, because the qualitative behavior is exactly the same as the trace distance's. But because of the important operational meaning of the quantum capacity, it is worth a comment. For low values of γ the quantum capacity has revivals. This means that there are specific channel lengths for which it is possible to reliably transmit information through the channel. Moreover, if the switching rate is very small, the channel capacity almost recovers its initial value. On the other end, there are channel length for which $C_Q(\tau, \gamma)$ is zero, thus no information can be sent through the channel. If it is possible to properly engineer the environment to select the channel length, information can be sent through the quantum channel without any loss.
We can see from the right panel of Fig. 4.1 that both N_{BLP} and N_{BCM} increase for decreasing values of γ. From a physical point of view this reflects the fact that small values of γ correspond to non-negligible and long-living environmental correlations, as described by the RTN autocorrelation function in Eq. (2.30), and therefore to more pronounced memory effects. The left panel of Fig. 4.1 also shows that N_{BCM} decays faster than N_{BLP} as a function of γ. On the other hand, as mentioned above, the threshold between the Markovian and non-Markovian regime is the same for both measures and corresponds to $\gamma = 2$, for which both measures vanish. More precisely, for $\gamma \geq 2$ both the measures are identically zero since the time derivatives of both the trace distance and the quantum capacity are negative definite, meaning that information permanently leaks away from the system.

4.2.2 Colored $1/f^{\alpha}$ noise

In this section we describe the environment as a collection of N random bistable fluctuators, as described in Sec. 3.2.3, giving rise to a $1/f^{\alpha}$ noise. The dynamics of a single-qubit system subject to $1/f^{\alpha}$ noise can be analyze through the density matrix

$$\rho(t) = \begin{pmatrix} |\alpha|^2 & \Gamma(\tau, \alpha, N)\alpha\beta^* \\ \Gamma(\tau, \alpha, N)\alpha^*\beta & |\beta|^2 \end{pmatrix} \tag{4.19}$$

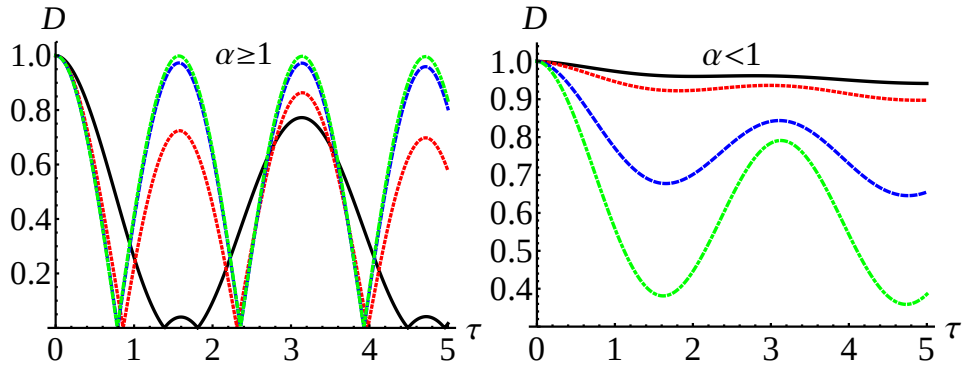

Figure 4.2: Non-Markovianity of colored channels. The left panel shows the trace distance for a qubit subject to $1/f^{\alpha}$ noise generated by a single random fluctuator for different values of $\alpha \geq 1$: $\alpha = 1$ (solid black line), $\alpha = 1.3$ (dotted red line), $\alpha = 1.5$ (dashed blue line) and $\alpha = 2$ (dotdashed green line). The right panel shows the same quantity for values of $\alpha < 1$: $\alpha = 0.5$ (solid black line), $\alpha = 0.6$ (dotted red line), $\alpha = 0.8$ (dashed blue line) and $\alpha = 0.9$ (dotdashed green line).

where

$$\Gamma(\tau, \alpha, N) = \left[\int_{\gamma_1}^{\gamma_2} \Delta_2(t, \gamma) p_{\alpha}(\gamma) d\gamma\right]^N \tag{4.20}$$

is the dephasing coefficient depending upon the noise parameter α and the number N of bistable fluctuators. The expression for $\Gamma(\tau, \alpha, N)$ was obtain in an analogue way to the coefficient $\Gamma_{\text{IE}}(t)$ in Eq. (3.53). Remember that with this microscopic model for the noise already $N = 1$ random bistable fluctuator is sufficient to gnerate a $1/f^{\alpha}$ noise spectrum. We already mentioned that N_{BLP} and N_{BCM} have the same qualitative behavior since they depend only on the dephasing factor. For this reason, we focus initially only on the behavior of trace distance. For colored noise with spectrum $1/f^{\alpha}$, the optimal trace distance is calculate according to Eq. (1.96):

$$D(\tau, \alpha, N) = |\Gamma(\tau, \alpha, N)|. \tag{4.21}$$

This quantity cannot be evaluated analytically since the integral in Eq. (4.20) is not analytically solvable. We computed it numerically upon assuming that the range of integration is $[\gamma_1, \gamma_2] = [10^{-4}, 10^4]$.

The optimal trace distance for a generic number of fluctuators may be written in terms of the same quantity for a single fluctuator as follows

$$D(\tau, \alpha, N) = D(\tau, \alpha)^N, \tag{4.22}$$

where $D(\tau, \alpha) = |\Gamma(\tau, \alpha)|$. We thus first analyze the non-Markovianity of a colored environment generated by a single random fluctuator. For a fixed value of α and $N = 1$ the trace distance is always a non-monotonic function of time, as illustrated in Fig. 4.2. Therefore, contrarily to the case of RTN, the dynamics is always non-Markovian for a single fluctuator. However, one can still identify two regimes depending on the value of α. For, $\alpha \geq 1$ the optimal trace distance is characterized by pronounced oscillations in time between zero and a maximum value, which depends upon the value of α. The larger is α, the larger are the local maxima. For $\alpha = 1$ higher and lower maxima alternate periodically at times $\tau = \pi/2$. As α increases, the height of the alternating peaks

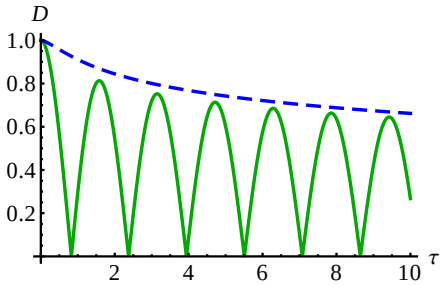

Figure 4.3: Non-Markovianity of colored channels. The plot shows the trace distance as a function of time for $\alpha = 1$. The two curves refer two different ranges of integration in Eq. (4.20): $[10^{-4}, 2]$ (green solid line) and $[2, 10^4]$(blue dashed line).

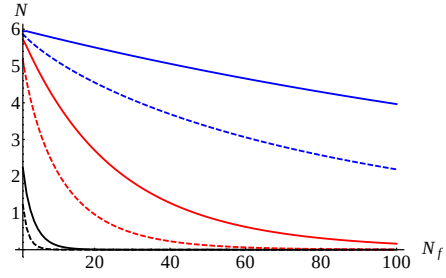

Figure 4.4: Non-Markovianity of colored channels. The plot shows the non-Markovianity measures as a function of the number of fluctuators. The plot shows $N_{\rm BLP}$ (solid lines) and $N_{\rm BCM}$ (dashed lines) as a function of the number of fluctuators for different values of α. The three pairs of lines (from top to bottom) refer to $\alpha = 1.0$ (black), $\alpha = 1.5$ (red) and $\alpha = 2$ (blue).

increases until it becomes uniform, as shown in Fig. 4.2 (left). For $\alpha < 1$, D is still non-monotonic, but the oscillations are less noticeable and the optimal trace distance never vanishes. This case is illustrated in Fig. 4.2 (right). Generally, as α decreases, the amplitude of the oscillations in the trace distance decreases, both in the $\alpha < 1$ and in the $\alpha \geq 1$ region of parameter space. Non-Markovianity is thus stronger for systems interacting with environments with a dominant low frequency component in the frequency spectrum. By changing the range of integration in Eq. (4.20), we can analyze the contribution of small and large switching rates on non-Markovianity. In particular, in Fig. 4.3 we compare the behavior of the trace distance for two mutually exclusive ranges of integration, namely for $\gamma \in [10^{-4}, 2]$ and $\gamma \in [2, 10^4]$. In the first case we integrate only over small values of the switching rates, and the trace distance exhibits revivals, revealing the presence of information back flow. In the second case the integration is performed over big values of γ and, as a result, $D(t, \alpha, 1)$ decays monotonically. This behavior is consistent with the results obtained for the RTN channel: memory effects are dominant for low switching rates, i.e. longer correlation times. Thus non-Markovianity is a distinctive trait of low-frequency noise spectrum.

We now consider the case of a larger number of fluctuators $N \gg 1$. From Eq. (4.22), and remembering that $0 \leq D \leq 1$, one sees immediately that the overall effect of having a large number of fluctuators is to decrease the value of the optimal trace distance. As a consequence, oscillations in the trace distance are damped and may disappear, depending also on the value of α, leading to a monotonic decay. This behavior is illustrated in Fig. 4.4, where $N_{\rm BLP}$ and $N_{\rm BCM}$ are plotted as a function of the numbers of fluctuators and for three different exemplary values of α. The figure clearly shows that for smaller values of α, i.e. in the $\alpha < 1$ regime, a small number of fluctuators is sufficient to completely wash out memory effects. For increasingly larger values of α, non-Markovianity persists also for $N_f \approx 100$. Generally, increasing the number of fluctuators brings the system towards a Markovian dynamics. Summarizing, non-Markovianity is typical of environments with a small number of fluctuators and a noise spectrum dominated by low-frequencies.

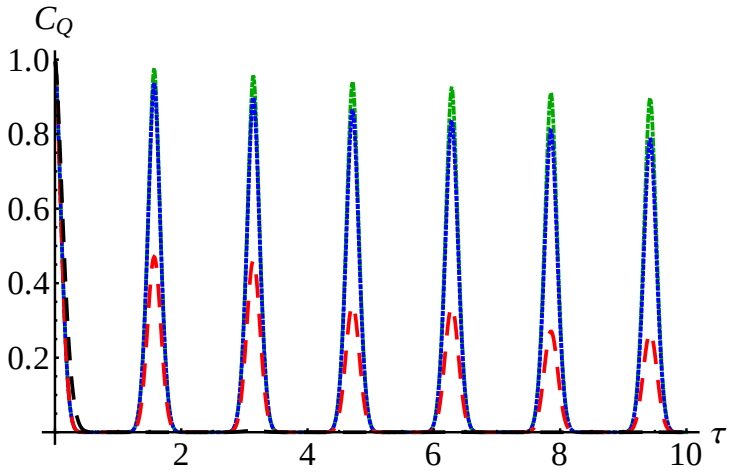

Figure 4.5: Non-Markovianity of colored channels. The plot shows the quantum capacity for a qubit subject to $1/f^{\alpha}$ noise generated by 10 random bistable fluctuators for different values of α: $\alpha = 1$ (dashed black line), $\alpha = 1.5$ (dashed red line), $\alpha = 2$ (dotted blue line) and $\alpha = 2.5$ (dotdashed green line).

Let us now analyze the behavior of the quantum channel capacity. In Fig. 4.5 we consider as an example the case of ten random fluctuators and different values of α. As expected, $C_Q(\tau, \alpha, N)$ is an increasing function of α. It has revivals at times multiples of $\pi/2$. As the number of fluctuators is increased the peaks become narrower and smaller, and the $C_Q(\tau, \alpha, N)$ is zero almost everywhere. The quantum capacity is thus very sensitive to the channel length or, equivalently, to the time during which the qubit is subjected to noise. In more detail: only certain lengths of the channel, corresponding to non-zero values of $C_Q(\tau, \alpha, N)$, allow for reliable transmission of quantum information. This characteristic lengths depend on the specific parameters of the noise. Besides, the range of non-zero values of $C_Q(\tau, \alpha, N)$, decreases as N increases, making robust quantum communication a more challenging task. From our results, we conclude that non-Markovian quantum channels may be advantageous compared to Markovian ones, because they may lead to an increase in the quantum capacity, allowing for a reliable transfer and distribution of information. A proper environment manipulation based on the exploitation memory effects may be used to induce revivals of the quantum correlations of a system and the channel capacity. As mentioned above, these conclusions hold upon assuming that the channel is reset after each use, i.e. focusing on memory effects during the propagation and neglecting memory effects among subsequent uses of the channel. Of course, memory effects among uses should be eventually addressed in view of realistic implementations. Our results should be considered a first step toward a complete analysis of this class of channels, including both types of memory effects.

4.2.3 Two-qubits non-Markovianity

We conclude this section by addressing the non-Markovianity of RTN and colored environments acting independently on two dephasing qubits. The dynamics is governed by

the Hamiltonian

$$H(t) = H_A(t) \otimes \mathbb{I}_B + \mathbb{I}_A \otimes H_B(t) \tag{4.23}$$

where $H_{\mathrm{A(B)}}(t)$ is the single qubit Hamiltonian in Eq. (4.1). If we focus on the BLP measure, numerical maximization should be performed in order to find the maximizing initial pair of states, due to the large number of parameters in the Hilbert space. The numerical approach consists in generating random pairs of initial states, in order to sample the state space. For every initial pair, we calculate the evolved density matrix, following the prescriptions in Sec. 3.2. Given the eigenvalues λ_i of the evolved density matrix, the trace distance is the sum $D(t) = \sum_i |\lambda_i|$. We then study the numerical derivative of the trace distance and sum up those regions where the $\sigma = \frac{dD}{dt} > 0$. The initial pair which give the largest value for N_{BLP} is the numeric optimal initial pair.
In both the case of RTN and colored noise, the maximizing pair corresponds to the two orthogonal factorized states $|++\rangle$ and $|--\rangle$.
We have numerically confirmed that the optimal trace distance in this case also takes the form: $D(t) = |\Delta_2(\tau, \gamma)|$ and $D(t) = |\Gamma(\tau, \alpha, N)|$ for RTN and $1/f^\alpha$ noise respectively.. The BCM non-Markovianity measure is straightforward to calculate because the quantum capacity is additive for degradable channels as the one here considered, namely $C_{2q}(\Phi(t)) = 2C_Q(\Phi(t))$, where the subscript $2q$ stands for two qubits. It follows that the non-Markovian dynamics of two qubits subjected to independent RTN or colored noise is simply related to the single-qubit non-Markovianity, and therefore it is the same.

Our results show that non-Markovianity features are actually connected to the revivals of quantum correlation. In fact, if we compare Eq. (3.29) and Eq. (3.55) for the negativity in the case of RTN and colored noise respectively, with the results (4.9) and (4.21) for the optimal trace distance, it is immediate to see that revivals in the entanglement coincide with revivals of the optimal trace distance, i.e. non-Markovianity. On the other hand, a monotonic decay of quantum correlations implies a Markovian quantum dynamical map for the quantum system.

4.3 Summary

- We studied the non-Markovian character of the dynamical map of a qubit subject to classical noise. Non-Markovianity was evaluated by means of BLP and BCM measure, based on the trace distance and the quantum capacity respectively.
- Gaussian noise always leads to a Markovian dynamics.
- Depending on the value of the switching rate, random telegraph noise induces two regimes: fast RTN corresponds to a Markovian dynamics, while slow RTN makes the dynamics of the quantum system non-Markovian.
- When the environment is modeled as a single random bistable fluctuator, the dynamics of the system is always non-Markovian, independently on the value of α. As the number of random fluctuators is increased, low frequency environments preserve the non-Markovianity, while smaller values of α induces a Markovian dynamical map.

CHAPTER 5

Quantum probes for the spectral properties of a classical environment

So far, we have analyzed the effects of a classical environment on the quantum properties of a simple quantum system such as a single- or two-qubit system. We described classical noise by means of a stochastic term in the system Hamiltonian. We now want to study a complementary situation. The question we ask ourselves is if and how we can characterize the stochastic process generating the noise affecting the system using minimal resources. To this aim, we address the characterization of a random classical field by quantum probes. With the term quantum probes we mean a microscopic system, say a qubit encoded into a particle, subject to classical noise, that we can use to estimate the parameters of the noise itself. The idea is to exploit quantum measurements performed at a fixed interaction time on the qubit to extract information about the classical environment. This is possible because the decoherent dynamics of the probe is induced by interaction with the environment and it strongly depends on the properties of the latter, such as its spectrum. If the probe can be easily controlled and manipulated, then it may be possible to extract information about a complex environment in an efficient way. In this chapter, we focus on the characterization of the noise by estimating the parameters of its autocorrelation function (or the spectrum). The scheme we follow requires to find the optimal state preparation of the probe, the optimal interaction time and the efficient measurement to be performed on the open quantum system, in order to extract the maximum information possible about the external noise.
As in the previous chapter, here we focus on dephasing dynamics, assuming that relaxation effects are negligible. We consider a single-qubit system interacting with classical noise arising from a stochastic process with a Gaussian or non-Gaussian statistics. Again, the system Hamiltonian has the form:

$$H(t) = \omega_0 \sigma_z + B(t)\sigma_z \tag{5.1}$$

where $B(t)$ is a stochastic process, whose autocorrelation function depends upon an unknown parameter λ. Starting from a generic initial pure state belonging to the family of states:

$$|\psi_0\rangle = \cos\left(\frac{\theta}{2}\right)|0\rangle + \sin\left(\frac{\theta}{2}\right)|1\rangle, \tag{5.2}$$

we are able to write the evolved density matrix of the two-qubit system, as done in Chapter 4, as

$$\rho(t) = \frac{1}{2}\begin{pmatrix} 1+\cos\theta & e^{-2i\omega_0 t} f(\lambda)\sin\theta \\ e^{2i\omega_0 t} f(\lambda)\sin\theta & 1-\cos\theta \end{pmatrix}, \tag{5.3}$$

and the expectation $f(\lambda) = \mathbb{E}\left[e^{-2i\varphi(t,\lambda)}\right]$ depends upon the considered stochastic process $B(t)$ and we explicitly wrote its dependency upon the noise parameter λ we want to estimate. By using the tools of quantum estimation theory we are able to analyze the performances of an efficient estimator for the noise parameters. In fact, the goal of an estimation procedure is not only to determine the value of an unknown parameter, but also to infer this value with the largest possible precision, as imposed by the Cramèr-Rao inequality. Our main aim is to optimize the parameter estimation procedure by using quantum probes. In other words, we determine the initial qubit state preparation and the interaction time that maximize the quantum Fisher information. We show that the ultimate precision may be achieved by a population measurement in the rotating frame of the qubit. Finally we establish under which conditions it is possible to estimate efficiently the spectral properties of the environmental noise.
In order to calculate the QFI as in Eq. (1.108), we need the eigenvalues $\rho_\pm$ and eigenvectors $|\rho_\pm\rangle$ of the density operator. The eigenvalues are given by:

$$\rho_\pm(\lambda) = \frac{1}{2}\left(1 \pm \sqrt{\cos^2\theta + f^2(\lambda)\sin^2\theta}\right) \tag{5.4}$$

where we substituted the symbol $\rho_{1,2}$ with $\rho_\pm$ to denote eigenvalues. The eigenvectors depend upon the angle θ, the expectation $f(\lambda)$, the interaction time τ and the qubit frequency ω_0. We do not write them here since they have a very long expression. Instead we write the analytical expression of the coefficients $|\langle\rho_m|\partial_\lambda\rho_n\rangle|^2$ with $m, n = \pm$:

$$|\langle\rho_\pm|\partial_\lambda\rho_\pm\rangle|^2 = \frac{\cos^2\theta\,\sin^2\theta\,\left[\partial_\lambda f(\lambda)\right]^2}{4\left(\cos^2\theta + f(\lambda)^2\sin^2\theta\right)^2} \tag{5.5}$$

The quantum Fischer information (1.108) is calculated analytically:

$$\begin{aligned} G(\lambda) &= \left[\frac{\sin^2\theta\, f^2(\lambda)}{\left(f^2(\lambda)-1\right)\left(\cos^2\theta + f^2(\lambda)\sin^2\theta\right)} + \frac{\sin^2\theta\cos^2\theta}{\cos^2\theta + f^2(\lambda)\sin^2\theta}\right]\left[\partial_\lambda f(\lambda)\right]^2 \\ &= \frac{\left[\partial_\lambda f(\lambda)\right]^2\,\sin^2\theta}{1-f^2(\lambda)} \end{aligned} \tag{5.6}$$

Eq. (5.6) is maximized for $\theta = \frac{\pi}{2}$. It follows that the optimal initial state is the superposition $|\psi_0\rangle = \frac{1}{\sqrt{2}}(|0\rangle + |1\rangle) = |+\rangle$.
To complete our analysis, we now prove that the optimal measurement achieving the QFI is a realistic one, since it corresponds to the projectors onto the eigenstates of the system. For the optimal initial $|+\rangle$, the eigenvalues and eigenvectors of the density operators have the expression:

$$\rho_\pm(\lambda) = \frac{1}{2}\left[1 \pm f(\lambda)\right] \tag{5.7}$$

$$|\rho_\pm\rangle = \frac{1}{\sqrt{2}}\left[\pm e^{-2i\omega_0 t}|0\rangle + |1\rangle\right]. \tag{5.8}$$

Since the eigenvalues do not depend upon the parameter λ, the second term in the QFI (1.108) vanishes and the QFI coincides with the FI of the distributions (5.7), computed from Eq. (1.104):

$$F(\lambda) = \frac{[\partial_\lambda\rho_+(\lambda)]^2}{\rho_+(\lambda)} + \frac{[\partial_\lambda\rho_-(\lambda)]^2}{\rho_-(\lambda)} = G(\lambda), \tag{5.9}$$

The optimal measurement is thus obtained from the projectors onto the eigenstates of the density matrix $\Pi_\pm = |\rho_\pm\rangle\langle\rho_\pm|$:

$$\Pi_\pm = \frac{1}{2}\begin{pmatrix} 1 & \pm e^{-2i\omega_o t} \\ \pm e^{2i\omega_o t} & 1 \end{pmatrix} \tag{5.10}$$

$$= e^{-i\omega_0 t\sigma_z}|\pm\rangle\langle\pm|e^{i\omega_0 t\sigma_z}. \tag{5.11}$$

In other words, the optimal measurement corresponds to σ_x in the qubit reference frame which rotates with frequency ω_0.

5.1 Characterization of classical Gaussian processes

In this section we focus on three particular Gaussian processes. Specifically, we assume that the stochastic field in Eq. (5.1) is driven either by an Ornstein-Uhlenbeck or by a Gaussian or a power-law process. The corresponding autocorrelation functions are given in Eq.s (2.20), (2.25) and (2.26) respectively. From these autocorrelation functions, it is possible to calculated the β-functions (2.21), (2.27) and (2.28), which can be re-written in terms of the dimensionless quantities $g = \gamma/\Gamma$ and $\tau = \Gamma t$ as:

$$\beta_{OU}(g,\tau) = \frac{1}{g}\left(g\tau + e^{-g\tau} - 1\right) \tag{5.12}$$

$$\beta_G(g,\tau) = \frac{1}{g}\left[g\tau\,\mathrm{Erf}(g\tau) + \frac{e^{-(g\tau)^2} - 1}{\sqrt{\pi}}\right] \tag{5.13}$$

$$\beta_{PL}(g,\tau) = \frac{1}{g}\left[\frac{(1+g\tau)^{2-\alpha} + g\tau(\alpha-2) - 1}{(\alpha-2)}\right]. \tag{5.14}$$

The qubit evolved density operator is described by the matrix reported in Eq. (5.3) with the substitution $f(\lambda) = \mathbb{E}\left[e^{-2i\varphi(t,\lambda)}\right] = e^{-2\beta(g,\tau)}$. The characterization of the classical noise amounts to estimate the overall noise parameter g by performing measurements on the quantum probe after the interaction with the environment, as described by the density matrices in Eq. (5.3). In order to make this procedure as effective as possible, i.e. to extract the maximum amount of information on the noise by inspecting the state of the probe, we have to suitably optimize the interaction time, the measurement to be performed at the output and finally, the data processing after collecting an experimental sample.
In particular we want to study the quantum Fisher information and the quantum signal-to-noise ratio for the estimation of the noise parameter g of the considered processes and assess the performances of the ML estimator by a set of simulated experiments.

The quantum Fisher information gives the ultimate quantum bound to the precision of an inference procedure. The analytic expression for the QFI is given by Eq. (5.6) and, in the case of a Gaussian process affecting the dynamics of the qubit initially prepared in the optimal state, it takes the form:

$$G(g,\tau) = \frac{4}{e^{4\,\beta(g,\tau)} - 1}\left[\partial_g\,\beta(g,\tau)\right]^2. \tag{5.15}$$

Given the β-functions in Eqs. (5.12)-(5.14), the QSNR is calculated from Eq. (1.109) and

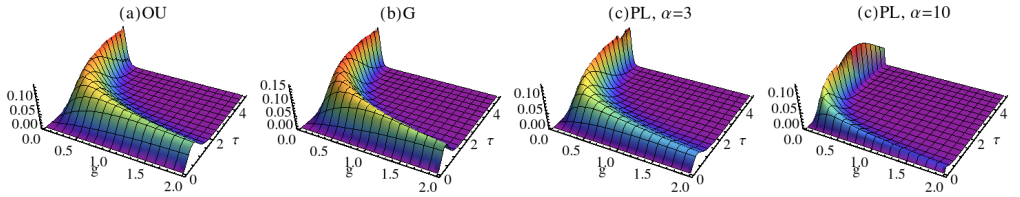

Figure 5.1: The quantum signal-to-noise ratio $R(g)$ as a function of g and the interaction time τ for different stochastic processes: (a) OU, (b) G, and PL with (c) $\alpha = 3$ and (d) $\alpha = 10$.

it is given by:

$$R_{OU}(g,\tau) = \frac{4\,e^{-2g\tau}}{g^2}\left[\frac{(1-e^{g\tau}+g\tau)^2}{e^{4\left(\tau+\frac{e^{-g\tau}-1}{g}\right)}-1}\right] \tag{5.16}$$

$$R_{G}(g,\tau) = \frac{4}{\pi g^2}\left[\frac{\left(e^{-g^2\tau^2}-1\right)^2}{e^{4\left(\frac{e^{-g^2\tau^2}-1}{\sqrt{\pi}g}+\tau\,\mathrm{Erf}(g\tau)\right)}-1}\right] \tag{5.17}$$

$$R_{PL}(g,\tau) = \frac{4}{g^2}\left[\frac{(1+\alpha g\tau+(\alpha-1)(g\tau)^2-(1+g\tau)^{\alpha})^2}{\left(e^{4\left(\tau+\frac{(1+g\tau)^{2-\alpha}-1}{g(\alpha-2)}\right)}-1\right)(\alpha-2)^2(1+g\tau)^{2\alpha}}\right] \tag{5.18}$$

The QSNRs of Eqs. (5.16)-(5.18) are shown in Fig. 5.1. As it is apparent from the plots, the qualitative behavior is the same for all processes. At any fixed value of g there is a maximum in the QSNR, achieved for an optimal value of the interaction time $\tau_M(g)$. The value of this maximum $R_M = R(\tau_M)$ decreases with g. It follows that smaller values of g may be better estimated than larger ones. The optimal time $\tau_M(g)$ decreases with increasing values of the parameter. This means that the smaller is g, the longer is the interaction time that is required to effectively *imprint* the effects of the external environment on the probe. The dependency of τ_M on the parameter g is shown in the upper left of Fig. 5.2, for the three considered processes. For small values of g we can approximate the curves with the function $\tau_M \simeq a/\sqrt{g}$ (with $a \simeq 0.89$ for OU and similar values for the other processes) while for $g \gg 1$ we may write $\tau_M \simeq b/g$, with $b \simeq 2.5$ for OU. The corresponding values of the QSNR, i.e. R_M are shown in the right panel of the same figure. R_M is almost constant for small g and then start to decrease. We have $R_M \simeq a - b\sqrt{g}$ for $g \ll 1$, where $a \simeq 0.161$ and $b = 0.096$ for OU, and $R_M \simeq b/g$ for $g \gg 1$, with $b \simeq 0.33$ for OU. It follows that g may be effectively estimated when it is small, since the QSNR is large. In this regime, the estimation procedure is also robust, since the optimal interaction time and the resulting value of the QSNR depend only weakly on the value of g. On the other hand, for larger g the estimation procedure is unavoidably less effective.

Efficient estimator for a Gaussian process

In this Section we present the results of simulated experiments, performed to assess the performances of the maximum likelihood estimator and to characterize its asymptotic regime. In particular, we have numerically simulated repeated measurements of the observable described by the projectors $\Pi_{\pm}$ in Eq. (5.11), and then estimated the value of the parameter g in the case of OU process using the MLE.

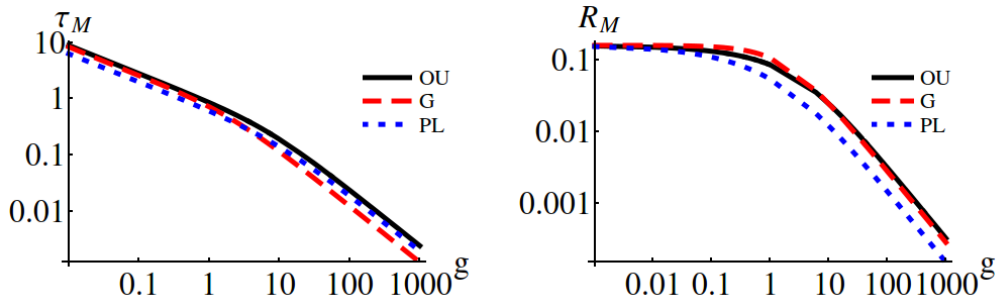

Figure 5.2: The left panel shows the optimal interaction time $\tau_M(g)$, which maximizes the QSNR, for the three different processes: OU (solid black), G (dashed red) and PL (dotted blue). In the PL case, we set $\alpha = 3$. The right panel shows the corresponding (maximized) values of the QSNR R_M, using the same color code.

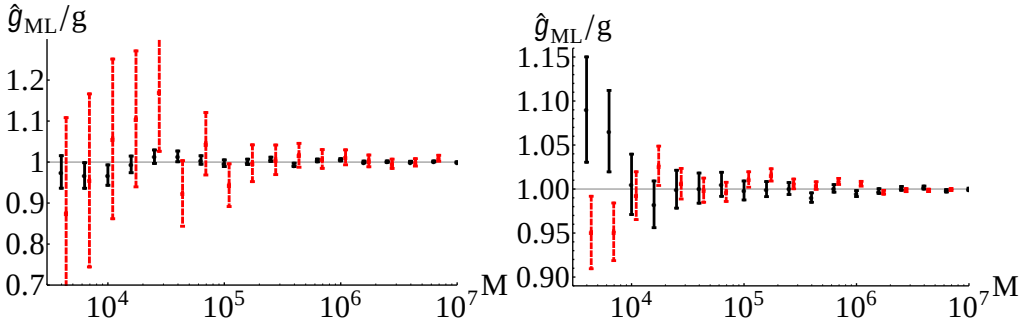

Figure 5.3: Estimated ratio g_{ML}/g between the ML estimated value of g and the true value, together with the corresponding error bars as a function of the number of repeated measurements M as obtained from simulations. In the left panel the results for $g = 0.01$ (solid black) and $g = 100$ (red dashed) are compared. Smaller values of the parameter are better estimated. In the right panel the considered values are $g = 0.1$ (solid black) and $g = 1$ (red dashed). Note that the simulated data in both panels are computed for the same values of M and then the red points are slightly shifted along the x-axes for the sake of clarity.

Imagine to have performed M repeated measurements of $\Pi_\pm$ at the optimal time τ_M. Each run returns ± 1, according the probability distributions (5.7). Let us call N the number of outcomes with value $+1$. The frequentist interpretation of probability leads us to write the relation

$$\rho_+(g,\tau) = \frac{N}{M}\,, \tag{5.19}$$

implicitly assuming that the number of measurement is large $M \gg 1$.

In order to simplify the notation, we hereafter call $p(g,\tau) \equiv \rho_+(g,\tau)$. By inverting Eq. (5.19), we can write the inversion estimator $\hat{g}$ of g: $\hat{g}(N,M) = p^{-1}\left(\frac{N}{M},\tau_M\right)$. Before analyzing the performances of this estimator we show that it coincides with the ML estimator. In fact, from Eqs. (1.110) and (1.111) we have:

$$\mathcal{L}(g,\tau) = p(g,\tau)^N \left[1-p(g,\tau)\right]^{M-N} \tag{5.20}$$

$$\partial_g \mathcal{L}(g,\tau) = -\left[1-p(g,\tau)\right]^{M-N-1} p(g,\tau)^{N-1} [M\,p(g,\tau) - N]\partial_g p(g,\tau). \tag{5.21}$$

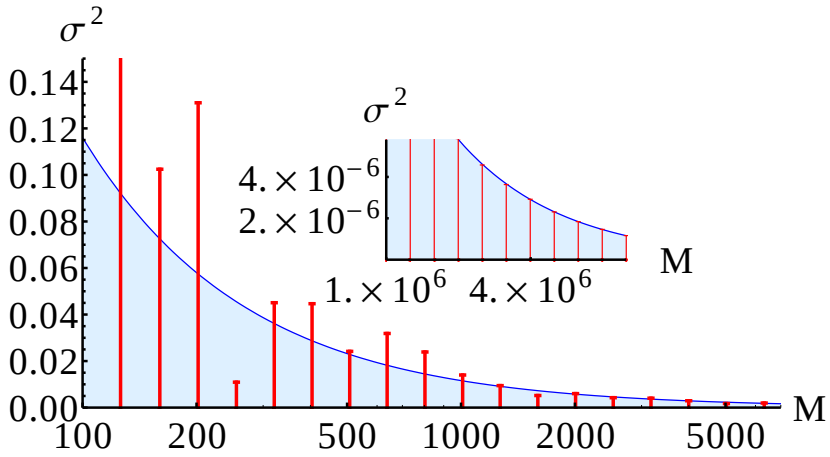

Figure 5.4: Dependency of the variance (red lines) of the ML estimator as a function of the number of measurements for the case $g = 1$. The blue shaded area represents the QCR bound. Variances below the quantum bound mean that the estimator has a bias. Inset: The same as in the main frame but for a large number of measurements: the bias is no longer present.

Eq. (5.21) has a maximum for $p(g,\tau) = \frac{N}{M}$ which, by inversion, gives the inversion estimator

$$\hat{g}_{ML}(N,M) = p^{-1}\left(\frac{N}{M},\tau_M\right). \tag{5.22}$$

Since we want to find the most precise estimation of the parameter which is allowed by quantum mechanics, we compute Eq. (5.22) at the optimal time τ_M which maximizes the quantum Fisher information. The ML estimator is a function of the number of repeated measurements M and the number N of outcomes with value $+1$. By numerical simulations, we mimic the results of experiments. This is done by generating a set of random numbers whose values are between 0 and 1. Then, we evaluate N by counting the number of elements of the set whose value is smaller than $p(\hat{g}_{ML},\tau_M)$. We repeat the procedure for different numbers of repeated measurements. The variance of the ML estimator (5.22) is computed using the error propagation theory. Upon assuming that the measure outcomes follow a binomial distribution, the estimator variance $\sigma^2$is given by:

$$\sigma^2(\hat{g}_{ML}) = \left|\frac{\partial \hat{g}_{ML}(N,M)}{\partial N}\right|^2 N\left(1-\frac{N}{M}\right). \tag{5.23}$$

In Fig. 5.3 we shows the ratio between the estimated value $\hat{g}_{ML}$ and the true value as a function of the number of repeated measurements for different values of the true parameter g. The estimated value oscillates around the true one, with standard deviations σ decreasing as a function of M. In fact, as the number of measurements becomes larger, the ratio $\hat{g}_{ML}/g$ gets closer to unity. The error associated to each point is smaller with increasing number of measurements. The sets of data in Fig. 5.3 refer to $g = 0.01$ (black solid line) and $g = 100$ (red dashed line) in the left panel and $g = 0.1$ (black solid line) and $g = 1$ (red dashed line) in the right one. The left panel in Fig. 5.3 highlights the fact that for the data associated to small g, the ratio converges more rapidly to unity and with smaller error with respect to the case $g = 100$. This is in agreement with the results of the previous subsection, where we found that R_M is larger for smaller values of the

parameter, meaning that the parameter is better estimable in the regime $g \ll 1$. The right panel of Fig. (5.3) confirm the behavior found in Fig. 5.2: in the region $g < 1$ it is possible to easily estimate the parameter almost independently on the value of g.

As already mentioned, the variance σ^2 decreases with increasing M. This is expected from the QCR bound in Eq. (1.107) because the QFI is a fixed quantity for fixed g, so the minimum error scales as $\frac{1}{M}$.

In Fig. 5.4 we illustrate the behavior of the variance σ^2 as a function of the measurement number in the case $g = 1$. The red lines represent the variance and the shaded area outlines the QCR bound. The reader may note that in certain cases the variance is below the quantum bound. This means that the estimator is lightly biased. But as the number of measurements in increased the bias tends to zero and the estimator becomes efficient (it saturates the QCR bound, as shown in the inset) as expected for ML estimator. The same qualitative behavior is found for other values of the parameter g. From our analysis, we see that the asymptotic regime for ML estimator appears for a number of repeated measurements of about $10^4 - 10^5$. We have also analyzed the convergence of a Bayesian estimator and found that the required M to have the asymptotic behavior is larger. It follows that, to achieve the characterization of the spectral properties of a Gaussian noise, a ML procedure leads to a faster estimation of the unknown parameters. The estimation scheme presented here would be suitable also to infer the amplitude of white noise, characterized by an autocorrelation function proportional to the Dirac delta. In this case, the optimal state preparation and measurement are the same as those obtained for the considered Gaussian noises. However, the quantum signal-to-noise ratio is a monotonically descreasing function of time, leaving no room for any optimization procedure.

5.2 Characterization of classical non-Gaussian processes

Let us assume now that the stochastic term in the Hamiltonian (5.1) has a non-Gaussian statistic. Specifically, in this section we will focus on the random telegraph noise and the $1/f^\alpha$ noise. Following the approach used in the case of Gaussian noise, we maximize the quantum Fisher information over the interaction time τ in order to estimate the noise parameters: the switching rate γ in the case of RTN and the exponent α in the case of colored noise.

5.2.1 Random telegraph noise

In the case of RTN, the dephasing factor in Eq. (5.3) coincides with $f(\lambda) = \Delta_2(\tau, \gamma)$ in the Eq. (3.24) and, for the optimal state $|+\rangle$, the QFI may be written as:

$$G(\gamma, \tau) = \frac{\left[\partial_\gamma \Delta_2(\tau, \gamma)\right]^2}{1 - \Delta_2^2(\tau, \gamma)}. \tag{5.24}$$

The two different regimes of slow and fast RTN give rise to different behaviors for the QFI, which are illustrated in Fig. 5.5. For slow RTN, G is shown in the left panel of Fig. 5.5: the QFI is characterized by an oscillating behavior and, in particular, for $\gamma \ll 2$ the peaks are located at multiples of $\tau = \frac{\pi}{2}$. In the fast RTN case (see the right panel of Fig. 5.5), G has only one peak and its maximum value decreases with γ.

In order to optimize the inference procedure we look for the interaction time that maximizes the QFI $G(\tau, \gamma)$ (and, in turn, the QSNR R) at each fixed value of the switching

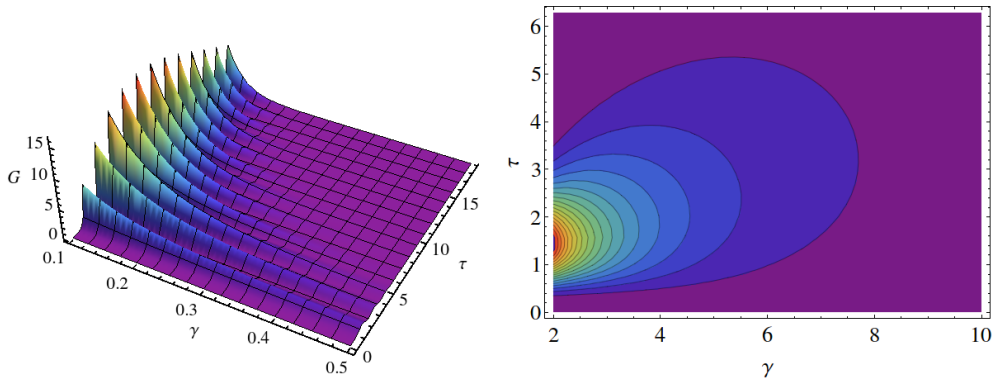

Figure 5.5: The left panel shows the QFI $G(\tau, \gamma)$ as a function of the interaction time τ and the switching rate γ for slow RTN. The lower panel shows a contour plot of of $G(\tau, \gamma)$ for fast RTN.

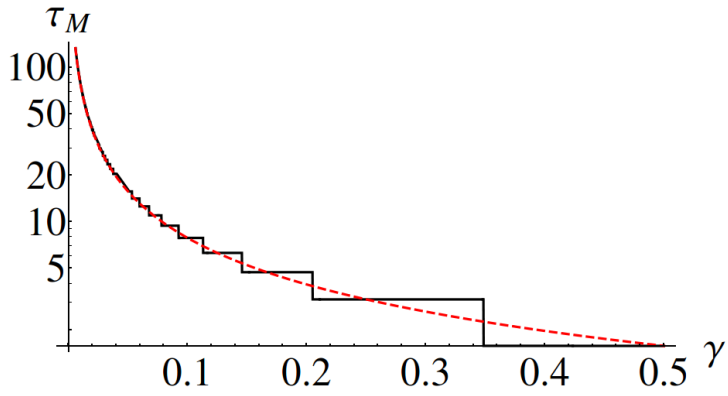

Figure 5.6: The optimal interaction time τ_M, maximizing the quantum Fisher information $G(\tau, \gamma)$ for slow RTN, as a function of the switching rate γ (black line). The dashed red curve denotes the function $\pi/4\gamma$.

rate γ. The maximization of the QFI has been performed numerically, leading to the following approximation

$$\tau_M(\gamma) \simeq \begin{cases} \text{nint}\left[\frac{1}{2\gamma}\right]\frac{\pi}{2} & \gamma < 2 \\ \\ \frac{2}{5}\gamma & \gamma > 2 \end{cases} . \tag{5.25}$$

The approximation is very good for γ in range $[10^{-3}, 10^3]$ except for $\gamma \simeq 2$ where the peaks are not exactly located at multiples of $\tau = \frac{\pi}{2}$ and Eq. (5.25) is valid only to a first approximation. In order to further illustrate the behavior of the QFI in the slow RTN regime, in Fig. 5.6 we show the optimal interaction time τ_M as a function of the switching rate. The steplike behavior of τ_M is due to the oscillating behavior of the QFI. On the other hand, in the fast RTN regime, the maximum moves continuously as a function of γ.

As seen from Eq. (5.25), optimal times increase with decreasing γ in the slow RTN regime and with increasing γ in the fast RTN regime. When small switching rates are

considered, long times are necessary to see the effect of the environment on the probe, in agreement with the non-Markovian character of the corresponding evolution map (see Sec. 4.2.1). In the case of $\gamma \gg 2$, the qubit and the external fluctuators act as if they were decoupled, so long observation times are required to see the influence of the external noise on the dynamics of the qubit. In both cases, the maximum values $G(\tau_M, \gamma)$ of the QFI are inversely proportional to γ^2. In particular, a numerical fit in range $[10^{-3}, 10^3]$ leads to

$$G(\gamma) \approx \frac{a}{\gamma^2}, \tag{5.26}$$

where a is of the order of 0.1. The quantum signal-to-noise ratio $R = \gamma^2 G(\gamma) \simeq a$ is thus constant, meaning that quantum probes allow one for a uniform estimation of the switching rate in the whole range of values we have considered.

5.2.2 Colored $1/f^\alpha$ noise

In the case of a collection of random bistable fluctuators, the relevant parameter to be estimated is the "color" of the noise, i.e. the exponent α. In this case, the decoherence coefficient is given by:

$$\begin{aligned} f(\tau, \alpha, N) &= \mathbb{E}\left[e^{-2i\varphi(\tau,\lambda)}\right] = \Gamma(\tau, \alpha, N) \\ &= \left[\int_{\gamma_1}^{\gamma_2} \Delta_2(t, \gamma) p_\alpha(\gamma) d\gamma\right]^N = \left[\Gamma(\tau, \alpha)\right]^N \end{aligned} \tag{5.27}$$

and the quantum Fisher information is computed according to Eq. (5.6) as:

$$G(\tau, \alpha, N) = N^2 \, \frac{\Gamma(\tau, \alpha)^{2N-2}}{1 - \Gamma(\tau, \alpha)^{2N}} \left[\partial_\alpha \Gamma(\tau, \alpha)\right]^2 . \tag{5.28}$$

For colored environments realized by a single random fluctuator the above formula reduces to

$$G(\tau, \alpha) = \frac{\left[\partial_\alpha \Gamma(\tau, \alpha)\right]^2}{1 - \Gamma(\tau, \alpha)^2} . \tag{5.29}$$

The QFI depends on the interaction time τ, the exponent α and the number of fluctuators N. Different values for α and N may lead to considerably different temporal behaviors for the QFI. This is illustrated in Fig. 5.7, where we show the QSNR $R(\tau, \alpha, N) = \alpha^2 G(\tau, \alpha, N)$ as a function of α and τ for two different numbers of fluctuators. When a single fluctuator is considered, the QSNR has a maximum located at $\alpha = 1$, which corresponds to the best estimable value for the parameter. The situation is totally reversed in the case of a bigger number of RBFs, for example $N = 10$, where values of α close to one correspond to a very low QSNR.

In order to further illustrate this behavior, in Fig. 5.8 we show the QSNR, already maximized over the interaction time, as a function of the exponent α for (three) fixed numbers of fluctuators. For a single fluctuator the QSNR exhibits a single maximum located at $\alpha = 1$, i.e. pink noise is more precisely estimable than other kind of noise. On the other hand, when the number of fluctuators is increased, two maxima appear and their location move away from $\alpha = 1$ for increasing N, with the largest maximum drifting towards $\alpha = 2$.

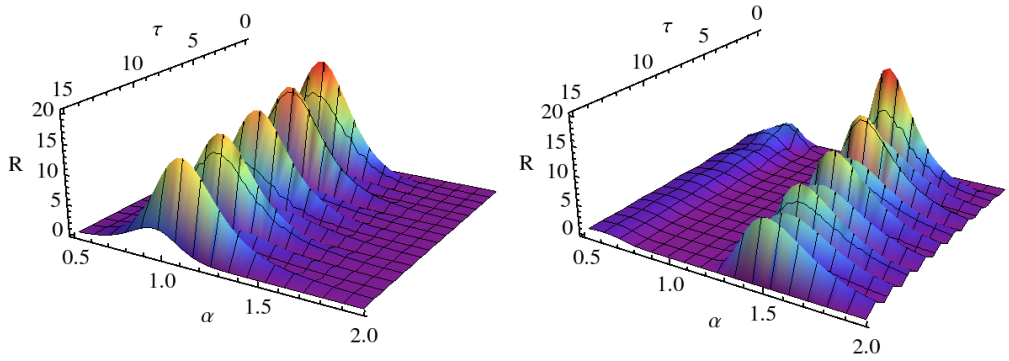

Figure 5.7: Spectral characterization of colored noise: The left panel shows the QSNR $R(\tau, \alpha, N)$ as a function of the interaction time and the exponent α for a single fluctuator $N = 1$. The right panel shows the same quantity for $N = 10$.

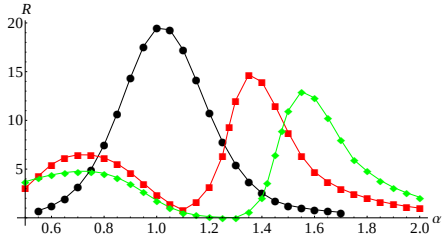

Figure 5.8: Spectral characterization of colored noise: The plot shows the QSNR $R(\tau_M, \alpha, N)$ as a function of α for different numbers of fluctuators: $N = 1$ (black circles), $N = 10$ (red squares) and $N = 50$ (green rhombuses). Lines are guides for the eyes.

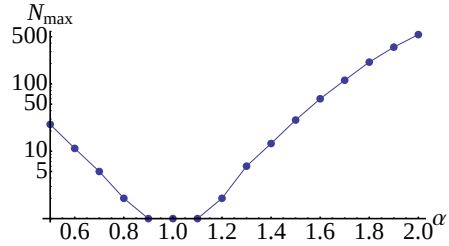

Figure 5.9: Spectral characterization of colored noise: The plots shows the number of fluctuators $N_{\max}$ that maximizes the QFI as a function of the exponent α. The line is a guide for the eyes.

To complete our analysis we also investigate with some more details the dependence of the QFI on the structure of the environment, i.e. on the number of fluctuators describing the environment. In Fig. 5.9 we show the number of fluctuators $N_{\max}$ maximizing the QFI as a function of α. We first notice that there is indeed a dependence, and that $N_{\max}$ may be considerably different for, say, pink or brown noise. As it is apparent from Fig. 5.9 $N_{\max}$ decreases with increasing α until it reaches the value $N_{\max} = 1$ for values of α close to 1. Then it increases with α, up to $N_{\max} = 540$ for $\alpha = 2$. As a final remark, we also notice that when the number of fluctuators is taken equal to $N_{\max}$, then the optimal interaction time maximizing the QFI is $\tau_M \simeq \pi/2$ independently on α.

Efficient estimator for a non-Gaussian process

In order to illustrate the inference procedure that leads to an efficient estimator for the spectral parameter of a non-Gaussian process, we consider here the case of fast RTN. We simulate an experiment in which we perform M independent optimal measurements and use the collected outputs to built an estimator and assess its performances. The probability to obtain as a result of the measurement the state $|+\rangle$ is given by Eq. (5.7),

i.e. $p(\gamma,\tau) = \frac{1}{2}[1+\Delta_2(\gamma,\tau)]$. We simulate the outcomes of M repeated measurements according to this probability distribution and we call N the number of outcomes with value $+1$. As in the previous case, this is done by generating a set of M random number in the interval $[0,1]$ and counting the number N of elements of the set which are smaller than $p(\gamma_T,\tau)$ with γ_T the true value of the parameter.
The use of a maximum likelihood estimator to estimate the value of γ in this case is not recommended, because the relation $p(\gamma_{ML},\tau) = \frac{N}{M}$ cannot be analytically inverted. In this case we are able to numerically find the estimate for γ, but we are not able to calculate the variance of the estimator according to Eq. (5.23). If we use a data-blocking technique, i.e. we divide the the M outputs in blocks for each of which we compute the ML estimator, the variance obtained as the spread of one block to another is very large, even for a very large number of measurements ($\sim 10^7$).
A better strategy is to address a Bayesian estimation procedure. The conditional probability to obtain N outputs with value $+1$ when the true value of the parameter is γ is the likelihood function:

$$p(N|\gamma) = p(\gamma,\tau)^N[1-p(\gamma,\tau)]^{M-N}. \tag{5.30}$$

The *a posteriori* conditional probability distribution is calculated from Eq. (1.113). The *a priori* probability can be guessed based on the information available before any measurement. In our case, however, we do not have any prior information about the parameter, so we assume for $p(\gamma)$ an uniform distribution in an interval $[\gamma_1,\gamma_2]$ and zero elsewhere. With this assumption, the conditional probability distribution $p(\gamma|N)$ takes the form:

$$p(\gamma|N) = \frac{1}{N_p}\,p(N|\gamma) \tag{5.31}$$

with $N_p = \int_{\gamma_1}^{\gamma_2} p(N|\gamma)d\gamma$ to have a normalized probability distribution.
The estimated switching rate and its associated variance are numerically calculated according to Eq.s (1.114) and (1.115) at the optimal time $\tau = \tau_M$:

$$\hat{\gamma}_B = \int_{\gamma_1}^{\gamma_2} \gamma\, p(\gamma|N)d\gamma \tag{5.32}$$

$$\mathrm{Var}[\hat{\gamma}_B] = \int_{\gamma_1}^{\gamma_2} [\gamma-\hat{\gamma}_B]^2\, p(\gamma|N)d\gamma \tag{5.33}$$

and the range of integration has been fixed. In Fig. 5.10 (left), we show the estimated ratio $\hat{\gamma}_B/\gamma_T$ as a function of the number of repeated measurements M for two different values of the true switching rate, specifically $\gamma_T = 5$ (black) and $\gamma_T = 200$ (red). The estimated error $\sigma = \sqrt{\mathrm{Var}_B[\hat{\gamma}_B]}/\gamma_T$, i.e. the signal-to-noise ratio R, is also displayed. Our results clearly show that the estimated values converge on the true value with smaller error as the number of measurements is increased, i.e. the ratios tend to unity for both analyzed cases. Moreover, the errors bar (normalized with γ_T) associated with the two estimates have the same length, confirming that the signal-to-noise ratio calculated from Eq. (5.26) is independent upon the true value of the parameter and the estimation procedure is robust against changes in the value of γ_T. The asymptotic regime of the Bayesian estimator, in which it becomes efficient, is reached after already for $\sim 10^4$ measurements. In the right panel of Fig. 5.10, we report the behavior of the variance as a function of the repeated measurements for the case $\gamma_T = 20$. The shaded area represents the region where the quantum Cramèr-Rao bound is violated. The cases where the variance

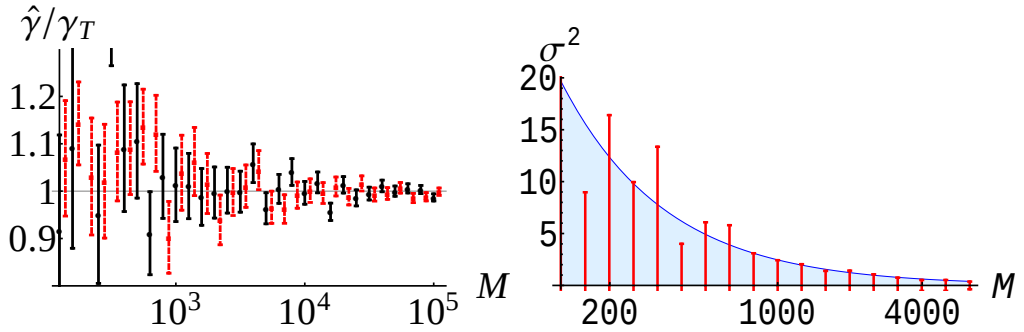

Figure 5.10: Left panel: Estimated ratio $\hat{\gamma}_B/\gamma_T$ between the Bayesian estimated value of the switching rate of the random telegraph noise and its true value, together with the corresponding error bars as a function of the repeated measurements M. Two different values for γ_T are considered: $\gamma_T = 5$ (black points and lines) and $\gamma_T = 200$ (red points and lines). Right panel: Dependency of the variance (red lines) of the Bayesian estimator on the number of repeated measurements M in the case $\gamma_T = 20$. The blue dashed area represents the violation of the Cramèr-Rao bound.

is smaller than limit imposed by quantum mechanics corresponds to biased estimators. This may happen for a small number of measurements. As M is increased, the Cramèr-Rao is saturated and the Bayesian estimator becomes efficient. These results show that it is possible to efficiently characterize a classical noise following a non-Gaussian statistics by performing repeated measurements only at one optimal instant of time.

5.3 Summary

- Simple quantum systems, such as a qubit, may be used as quantum probes to characterize complex environments. In fact, the dynamics of an open quantum system is affected by the environments which is interacting with. By measuring the state of a quantum probe, it is possible to gain information about the environment.
- In order to maximize the extraction of information about the environment, it is necessary to optimize the preparation of the probe, the interaction time and the measurement to be performed on the quantum system.
- The figure of merit we address in order to evaluate the efficiency of the estimation procedure is the quantum Fisher information (or equivalently the quantum signal-to-noise ratio). In the case of a Gaussian process, the QFI exhibits a peak at the optimal interaction time. For the analyzed processes, small values of the noise parameters may be estimated with very high precision. We showed that a maximum likelihood estimator allows one to efficiently estimate the spectral properties of an Ornstein-Uhlenbeck process with the minimum variance allowed by quantum mechanics.
- The efficient estimation of the switching rate of the non-Gaussian random telegraph noise is robust against changes in the value of γ, meaning that the signal-to-noise ration is uniform with respect the value of γ. The optimal interaction time decreases with increasing γ in the slow RTN regime, while it increases with growing γ for fast RTN.

- The estimation of the color of the noise α in the case of colored $1/f^{\alpha}$ noise strongly depends on the microscopic structure of the environment, i.e. the number N of fluctuators used to model it. For $N = 1$ the estimation at the optimal time is more precise for $\alpha = 1$, while for $N > 1$ the quantum Fisher information exhibits two maxima drifting away from $\alpha = 1$ as N is increased. We also find the optimal microscopic structure, i.e. the optimal number of fluctuators, that maximizes the signal-to-noise ratio.
- As an example of inference procedure for a non-Gaussian process, we analyzed the performances of a Bayesian estimator of the switching rate of the fast RTN. The estimator becomes unbiased and efficient as the number of measurements is increased and the asymptotic regime is reached already after few thousand measurements.

Conclusions

In this thesis I presented and discussed the results of the research I carried out during my PhD, which has been devoted to the analysis of the decoherence in qubit systems subject to classical noise and the characterization of a classical stochastic processes using quantum probes.

The unavoidable interaction between a quantum system and its environment usually destroys the coherence and the quantumness in the system. However, a coherent dynamics and the survivals of quantum correlations are necessary conditions for the quantum information processing. A detailed description of the mechanism of decoherence is thus of great relevance for the development of quantum technologies and the precise characterization of the noise acting on a quantum system is the main tool in designing protocols robust against the detrimental effects of decoherence.
The usual approach to study the decoherence due to the interaction between a quantum system and the environment is to describe the latter as a quantum bath. But there exist situations where this description may be challenging or inappropriate. In these cases, modeling the environment with classical random fields, without invoking a quantum environment at all, is a necessary approach. For certain types of dynamics, for example phase damping, the decoherence induced by a quantum bath may be equivalently described in terms of stochastic fluctuating classical fields.

In this thesis, I addressed the decoherence induced on a quantum system by a classical noise. The aim was twofold. The first was to study the mechanism of decoherence through the analysis of the dynamics of quantum correlations, both entanglement and quantum discord, and the non-Markovian character of the dynamical map of the system. The second was to address the characterization of the spectral properties of a complex classical environment using a simple qubit system as quantum probe.

In particular, I investigated the role of classical noise on the dynamics of quantum correlations in a quantum system composed by two non-interacting qubits initially prepared in a maximally entangled state or in a Bell-state mixture. The environment was modeled through stochastic processes following either a Gaussian or a non-Gaussian statistics. I computed the time evolved density matrix of the two qubits by performing the ensemble average over the stochastic process, both in the case of independent and common environments. In the case of Gaussian noise, I focused on two diffusion processes generating the noise: Ornstein-Uhlenbeck, characterized by a decoherence parameter, and the fractional Brownian motion, characterized by the Hurst parameter. I

have characterized the trajectories of the system inside the set of mixtures of Bell-states and shown the occurrence of sudden death of entanglement for certain sets of initial quantum states. I introduced the entanglement-preserving time t^* and the entanglement sudden death time t_{ESD} in order to analyze the effects of the nature of the noise on the decoherence. I found that t^* is larger for fractional Brownian motion than Ornstein-Uhlenbeck process and that a larger initial entanglement corresponds to a longer preserving time. Moreover, I found that the entanglement-preserving time is bounded from below by an increasing function of the initial entanglement. Regarding the effect of independent baths on the dynamics of correlations, independent environments degrade them more weakly than a common one. Overall, I showed that engineering the environment has only a slightly influence over the occurrence of entanglement sudden death, while it represents a valuable resource to increase the entanglement-preserving time.
In the case of qubits subject to a non-Gaussian environment, I focused on two examples of noise: the random telegraph noise and the colored $1/f^\alpha$ noise arising from a collection of bistable fluctuators with switching rates selected from a specific distribution $p_\alpha(\gamma)$. In the case of a two-qubit system affected by random telegraph noise, we confirm that two regimes arises: quantum correlations decay monotonically for values of the switching rate over a certain threshold, while they display revival of correlations for small values of the switching rate. Moreover, a common environment preserves better the quantum correlations in the case of slow RTN; the opposite behavior is found for qubits subjects to fast RTN, where the effect of a common noise results in a faster decay of entanglement and discord with respect to the case of independent environments.
In the case of a two-qubit system acted on by a $1/f^\alpha$ noise, the dynamics of quantum correlations depends upon the color of the noise α and the number of fluctuators used to model the environment. Depending on the characteristic of the spectrum, i.e. the exponent α, quantum correlations display either a monotonic or a damped oscillating behavior. For example, for pink noise, i.e. $\alpha = 1$, quantum correlations decay monotonically, while for brown noise, i.e. $\alpha = 2$, sudden death and revivals occur. Quantum correlations are written as a product of oscillating and exponential functions. Since the switching rates of the fluctuators are selected from a distribution proportional to $1/\gamma^\alpha$, for pink noise they lead to destructive interference, while brown noise enhances constructive interference. The action of independent or common environment has different effects on the robustness of quantum correlations. The qualitative trend is identified, whereas the quantification of the result depends explicitly upon the number of fluctuators and the specific sample of the switching rates $\{\gamma_j\}$. In order to eliminate the dependency of the dynamics of quantum correlations on the chosen sample, I introduced a new microscopic model for the environment generating a $1/f^\alpha$ noise, based on random bistable fluctuators.
When the two-qubit system interacts with a single bistable fluctuator, an oscillating behavior of quantum correlations has been found, independently on the value of α. The effect of a common environment is of better preserving the correlations and to double the number of revivals compared to the case of independent baths. If $\alpha = 1$, the peaks of entanglement and discord decay faster than in the presence of brown noise, i.e. $\alpha = 2$. In fact, for pink noise the switching rates are more uniformly distributed over the range $[\gamma_1, \gamma_2]$ than in the case of $1/f^2$ noise, thus leading to massive destructive "interference". The results presented clearly show that the behavior of quantum correlations is influenced not only by the spectrum of the environment but also by the number of fluctuators used to describe the microscopic structure of the environment. With a single decoherence channel revivals of correlations appear. When the number of fluctuators is increased, correlations decay monotonically. In order to relate this behavior with the

flow of information in the system, I addressed the non-Markovianity of a quantum system made of one or two qubits interacting with a classical random field. I considered two measures of non-Markovianity, based on the trace distance and the quantum capacity respectively, and I showed that their behavior is qualitatively similar. The fact that the two measures agree confirms, at least for dephasing channels, that the trace distance may be considered a measure of the flow of information from the system to the environment.
I found the analytical expressions of the optimal trace distance and the quantum capacity and, by analyzing their time derivatives, I was able to identify the Markovian or non-Markovian character of the dynamical map as a function of the noise parameters. For Gaussian environments, the dynamical map is always Markovian. This arise from the monotonic decaying of the trace distance or the quantum channel capacity. When the environment has non-Gaussian fluctuations, environments with a spectrum dominated by low-frequency contributions are generally non-Markovian. In the case of random telegraph noise the non-Markovianity measures display a threshold in the switching rates below with the dynamics is non-Markovian. Colored noise with $1/f^\alpha$ spectrum induces a non-Markovian dynamical map in the case of a single random bistable fluctuator realizing the environment, independently on the value of α. For a larger number of fluctuators, non-Markovianity is typical of environments with a large values of the exponent α. Moreover, non-Markovianity decreases when the number of random bistable fluctuators modeling the environment increases.

As a final point in my analysis, I have addressed estimation of a classical noise parameter using a qubit system as a quantum probe. By maximizing the quantum signal-to-noise ratio, I have found the optimal setting, i.e. optimal state preparation and optimal interaction time, to perform optimal measurements and maximize the extraction of information. The ultimate bound to precision may be achieved by measuring the "polarization" of the qubit, i.e. the observable σ_x in the rotating frame of the qubit.
In the case of Gaussian noise, the estimable parameter was the decoherence parameter. I showed that for any fixed value of the estimable parameter, the QSNR has a maximum, corresponding to an optimal value of the interaction time. This maximum is larger for smaller values of the parameter, which may be estimated more precisely. The Cramèr-Rao bound is reached by employing a maximum likelihood estimator, which achieves the asymptotic regimes and the optimal performances after few thousand measurements.
In the case of non-Gaussian noise, I have focus my attention on the estimation of the switching rate for random telegraph noise and the color of noise through the exponent α for $1/f^\alpha$ noise. For random telegraph noise, the quantum Fisher information is inversely proportional to the square of the switching rate, meaning that the quantum signal-to-noise ratio is constant. It follows that the switching rate may be estimated with uniform precision in its whole range of variation and is thus the inference procedure is robust against variations of the parameter value. The corresponding value of the optimal interaction time decreases with increasing switching rates for slow RTN, while it grows linearly with the switching rate in the fast RTN regime. I analyzed the performances of a Bayesian estimator and compared its variance with the quantum Cramèr-Rao bound. I showed that the asymptotic region is reached after only few thousand measurements.
For colored noise generated by random bistable fluctuators, the optimal characterization of the noise strongly depends on the structure of the environment and two different scenarios emerge. If the environment is modeled by a single random bistable fluctuator, estimation is more precise for $\alpha = 1$. On the other hand, when the environment is described as a collection of several random fluctuators, the quantum Fisher information

has two local maxima, whose positions drift towards the boundaries of the α-interval as the number of fluctuator is increased. I also found that for any fixed value of α there is a specific number of fluctuators maximizing the quantum Fisher information.

The characterization and control of quantum correlations are fundamental for the development of quantum technologies. Not only quantum correlations constitute a resource to process the quantum information, but a deep understanding of their nature will provide better insight into the nature of quantum states themselves.
The dynamics of open quantum systems and especially the possibility of controlling it lies at heart of quantum information processing. The microscopic structure of the environment, in addition to the noise spectrum, is relevant for the decoherence mechanisms in quantum systems and may be a valid starting point for the engineering of colored environments.

Together with quantum correlations, non-Markovianity represents a resources for quantum information processing. Indeed, non-Markovian features are connected to the revivals of quantum correlations. Whenever the dynamics is non-Markovian, revivals of entanglement and discord are present, while they decay monotonically for a Markovian dephasing map. The results presented in this thesis confirm that non-Markovianity cannot be considered as a mere label to identify different kinds of dynamical evolutions. Rather, it may be exploited for a better control of quantum channels and to better preserve the quantum correlations useful for the quantum communication protocols and the quantum information processing.

The external noise plays thus a central role in the dynamics of a quantum system. Under suitable reservoir engineering, noise could be used as tool to enhance the quantum properties of a system. The features of a complex environment may be reliably determined by monitoring and controlling a small quantum probe. At present, I cannot provide a quantitative statement about the performances of quantum probes compared to classical ones since the modeling of the latter would be rather challenging. On the other hand, the presented results show that quantum probes, besides having the advantage of introducing small perturbations into the system, require only measurement performed at a single optimal interaction time, thus avoiding the need of observing the system for a long time in order to collect a time series.

Having showed that the structural characteristics of the environment sensitively affect the dynamics of a quantum system opens the doors to the world of environment engineering aimed to improve the persistence of quantum properties or, for example, to optimize transmission and transport protocols.

Bibliography

[1] H. Ollivier and W. H. Zurek, Phys. Rev. Lett. **88**, 017901 (2001).

[2] L. Henderson and V. Vedral, J. Phys. A **34**, 6899 (2001).

[3] J. Maziero, L. C. Céleri, R. M. Serra, and V. Vedral, Phys. Rev. A **80**, 044102 (2009).

[4] T. Werlang, S. Souza, F. F. Fanchini, and C. J. Villas Boas, Phys. Rev. A **80**, 024103 (2009).

[5] J. Helm and W. T. Strunz, Phys. Rev. A **80**, 042108 (2009).

[6] D. Crow and R. Joynt, Phys. Rev. A **89**, 042123 (2014).

[7] W. M. Witzel, K. Young, and S. Das Sarma, arXiv:1307.2597v1 .

[8] T. Fink and H. Bluhm, arXiv:1402.0235v1 .

[9] B. Bylicka, C. D., and M. S., Sci. Rep. **4**, 5720 (2014).

[10] S. Lorenzo, F. Plastina, and M. Paternostro, Phys. Rev. A **88**, 020102 (2013).

[11] S. Luo, S. Fu, and H. Song, Phys. Rev. A **86**, 044101 (2012).

[12] E.-M. Laine, J. Piilo, and H.-P. Breuer, Phys. Rev. A **81**, 062115 (2010).

[13] A. Rivas, S. F. Huelga, and M. B. Plenio, Phys. Rev. Lett. **105**, 050403 (2010).

[14] X.-M. Lu, X. Wang, and C. P. Sun, Phys. Rev. A **82**, 042103 (2010).

[15] M. M. Wolf, J. Eisert, T. S. Cubitt, and J. I. Cirac, Phys. Rev. Lett. **101**, 150402 (2008).

[16] V. Bassano, A. Smirne, J. Laine, E.-M. Piilo, and H.-P. Breuer, New J.Phys. **13**, 093004 (2011).

[17] V. Bassano, J. Phys. B **45**, 154007 (2012).

[18] A. W. Chin, S. F. Huelga, and M. B. Plenio, Phys. Rev. Lett. **109**, 233601 (2012).

[19] R. Vasile, S. Olivares, M. A. Paris, and S. Maniscalco, Phys. Rev. A **83**, 042321 (2011).

[20] E.-M. Laine, H.-P. Breuer, and J. Piilo, Sci. Rep. **4**, 4620 (2014).

[21] S. F. Huelga, A. Rivas, and M. B. Plenio, Phys. Rev. Lett. **108**, 160402 (2012).

[22] M. Thorwart, J. Eckel, J. H. Reina, P. Nalbach, and S. Weiss, Chem. Phys. Lett. **478**, 234 (2009).

[23] P. Szańkowski, M. Trippenbach, and Y. B. Band, Phys. Rev. E **87**, 052112 (2013).

[24] A. I. Nesterov and G. P. Berman, Phys. Rev. A **85**, 052125 (2012).

[25] Y. M. Galperin, B. L. Altshuler, J. Bergli, and D. V. Shantsev, Phys. Rev. Lett. **96**, 097009 (2006).

[26] J. Helm, W. T. Strunz, S. Rietzler, and L. E. Würflinger, Phys. Rev. A **83**, 042103 (2011).

[27] D. B. Percival, Metrologia **40**, S289 (2003).

[28] J. Barunik and L. Kristoufek, Physica A **389**, 3844 (2010).

[29] C. M. Kendziorski, J. B. Bassingthwaighte, and P. J. Tonellato, Physica A **273**, 439 (1999).

[30] M. Wilde, *Quantum information theory* (Cambridge University Press, Cambridge, 2013).

[31] J. D. Malley and J. Hornstein, Stat. Sci. **8**, 433 (1993).

[32] S. Braunstein and C. Caves, Phys. Rev. Lett. **72**, 3439 (1994).

[33] M. G. A. Paris, Int. J. Quantum Inf. **7**, 125 (2009).

[34] G. De Chiara and G. M. Palma, Phys. Rev. Lett. **91**, 090404 (2003).

[35] A. Fiasconaro and B. Spagnolo, Phys. Rev. E **80**, 041110 (2009).

[36] B. B. Mandelbrot and J. W. Van Ness, SIAM Rev. **10**, 422 (1968).

[37] K. S. Ralls *et al.*, Phys. Rev. Lett. **52**, 228 (1984).

[38] C. T. Rogers and R. A. Buhrman, Phys. Rev. Lett. **53**, 1272 (1984).

[39] C. E. Parman, N. E. Israeloff, and J. Kakalios, Phys. Rev. B **44**, 8391 (1991).

[40] M. G. Peters, J. I. Dijkhuis, and L. W. Molenkamp, J. Appl. Phys. **86**, 1523 (1999).

[41] T. Duty, D. Gunnarsson, K. Bladh, and P. Delsing, Phys. Rev. B **69**, 140503 (2004).

[42] E. Paladino, L. Faoro, G. Falci, and R. Fazio, Phys. Rev. Lett. **88**, 228304 (2002).

[43] L. Faoro, J. Bergli, B. L. Altshuler, and Y. M. Galperin, Phys. Rev. Lett. **95**, 046805 (2005).

[44] B. Abel and F. Marquardt, Phys. Rev. B **78**, 201302 (2008).

[45] P. Dutta and P. M. Horn, Rev. Mod. Phys. **53**, 497 (1981).

[46] M. B. Weissman, Rev. Mod. Phys. **60**, 537 (1988).

[47] S. M. Kogan, *Electronic Noise and Fluctuations in Solids* (Cambridge University Press, Cambridge, England, 1996).

[48] E. Paladino, Y. M. Galperin, G. Falci, and B. L. Altshuler, Rev. Mod. Phys. **86**, 361 (2014).

[49] M. A. Nielsen and I. L. Chuang, *Quantum Computation and Quantum Information* (Cambridge University Press, New York, 2011).

[50] K. Kraus, *States, Effects and Operations* (Springer-Verlag, Berlin, 1983).

[51] C. E. Shannon, Bell Syst. Tech. J. **27**, 378 (1948).

[52] B. Schumacher, Phys. Rev. A **51**, 2738 (1995).

[53] E. Knill and R. Laflamme, Phys. Rev. Lett. **81**, 5672 (1998).

[54] S. Lloyd, Phys. Rev. A **61**, 010301 (1999).

[55] C. H. Bennett *et al.*, Phys. Rev. A **59**, 1070 (1999).

[56] E. Bihama, G. Brassardb, D. Kenigsberga, and T. Mora, Theor. Comp. Sci. **320**, 15 (2004).

[57] B. Groisman, S. Popescu, and A. Winter, Phys. Rev. A **72**, 032317 (2005).

[58] S. Luo, Phys. Rev. A **77**, 022301 (2008).

[59] K. Modi, T. Paterek, W. Son, V. Vedral, and M. Williamson, Phys. Rev. Lett. **104**, 080501 (2010).

[60] A. Datta, A. Shaji, and C. M. Caves, Phys. Rev. Lett. **100**, 050502 (2008).

[61] V. Madhok and A. Datta, Int. J. Mod. Phys. B **27**, 1345041 (2013).

[62] B. Dakić *et al.*, Nat. Phys. **8**, 666 (2012).

[63] A. K. Ekert, Phys. Rev. Lett. **67**, 661 (1991).

[64] C. H. Bennett and S. J. Wiesner, Phys. Rev. Lett. **69**, 2881 (1992).

[65] C. H. Bennett, G. Brassard, and N. D. Mermin, Phys. Rev. Lett. **68**, 557 (1992).

[66] R. Raussendorf and H. J. Briegel, Phys. Rev. Lett. **86**, 5188 (2001).

[67] J. S. Bell, Physiscs **1**, 195 (1964).

[68] N. D. Mermin, Phys. Rev. Lett. **65**, 1838 (1990).

[69] A. Zeilinger, Rev. Mod. Phys. **71**, S288 (1999).

[70] B. M. Terhal, Phys. Lett. A **271**, 319 (2000).

[71] S. Popescu, A. J. Short, and A. Winter, Nat. Phys. **2**, 754 (2006).

[72] R. Horodecki, P. Horodecki, M. Horodecki, and K. Horodecki, Rev. Mod. Phys. **81**, 865 (2009).

[73] M. B. Plenio and S. Virmani, Quantum. Inform. Compu. **7**, 001 (2007).

[74] O. Gühne and G. Tóth, Phys. Rep. **474**, 1 (2009).

[75] T. Yu and H. Eberly, Science **323**, 598 (2009).

[76] A. Peres, Phys. Rev. Lett. **77**, 1413 (1996).

[77] M. Horodecki, P. Horodecki, and R. Horodecki, Phys. Lett. A **223**, 1 (1996).

[78] P. Horodecki, Phys. Lett. A **232**, 333 (1997).

[79] S. Hill and W. K. Wootters, Phys. Rev. Lett. **78**, 5022 (1997).

[80] P. Rungta, V. Buzek, C. M. Caves, M. Hillery, and G. J. Milburn, Phys. Rev. A **64**, 042315 (2001).

[81] C. H. Bennett, D. P. DiVincezo, and J. A. Smolin, Phys. Rev. A **54**, 3824 (1996).

[82] W. K. Wootters, Phys. Rev. Lett. **80**, 2245 (1998).

[83] V. Vedral and M. B. Plenio, Phys. Rev. A **57**, 1619 (1998).

[84] G. Vidal and R. F. Werner, Phys. Rev. A **65**, 032314 (2002).

[85] V. Vedral, Phys. Rev. Lett. **90**, 050401 (2003).

[86] M. Piani, P. Horodecki, and R. Horodecki, Phys. Rev. Lett. **100**.

[87] S. Luo, Phys. Rev. A **77**, 042303 (2008).

[88] D. Girolami and G. Adesso, Phys. Rev. A **83**, 052108 (2011).

[89] L. Mazzola, J. Piilo, and S. Maniscalco, Phys. Rev. Lett. **104**, 200401 (2010).

[90] H.-P. Breuer, E.-M. Laine, and J. Piilo, Phys. Rev. Lett. **103**, 210401 (2009).

[91] R. Vasile, S. Maniscalco, M. G. A. Paris, H.-P. Breuer, and J. Piilo, Phys. Rev. A **84**, 052118 (2011).

[92] A. Gilchrist, N. K. Langford, and M. A. Nielsen, Phys. Rev. A **71**, 062310 (2005).

[93] S. Wißmann, A. Karlsson, E.-M. Laine, J. Piilo, and H.-P. Breuer, Phys. Rev. A **86**, 062108 (2012).

[94] Z. Y. Xu, W. L. Yang, and M. Feng, Phys. Rev. A **81**, 044105 (2010).

[95] Z. He, J. Zou, L. Li, and B. Shao, Phys. Rev. A **83**, 012108 (2011).

[96] J.-G. Li, J. Zou, and B. Shao, Phys. Rev. A **81**, 062124 (2010).

[97] I. Devetak and P. W. Shor, Commun. Math. Phys. **256**, 287 (2005).

[98] B. Schumacher and M. A. Nielsen, Phys. Rev. A **54**, 2629 (1996).

[99] B. Schumacher, Phys. Rev. A **54**, 2614 (1996).

[100] A. D'Arrigo, G. Benenti, and G. Falci, New J. Phys. **9**, 310 (2007).

[101] M. B. Plenio and S. Virmani, Phys. Rev. Lett. **99**, 120504 (2007).

[102] F. Caruso, V. Giovannetti, C. Lupo, and S. Mancini, ArXiv:1207.5435 .

[103] C. W. Helstrom, *Quantum Detection and Estimation Theory* (Academic Press, New York, 1976).

[104] A. S. Holevo, *Statistical structure of Quantum Theory* (Lect. Not. Phys. **61**, Springer, Berlin, 2001).

[105] E. L. Lehmann and G. Casella, *Theory of Point Estimation* (Springer-Verlag, New York, 1998).

[106] E. Parzen, *Stochastic Processes* (Holden-Day Inc., Amsterdam, 1964).

[107] N. G. van Kampen, *Stochastic processes in physics and chemistry* (North-Holland, Amsterdam, 1992).

[108] C. W. Gardiner, *Handbook of Stochastic Methods* (Springer, Berlin, 1983).

[109] N. Wiener, Acta Math. **55**, 117 (1930).

[110] A. Khintchine, Math. Ann. **109**, 604 (1934).

[111] G. E. Uhlenbeck and L. S. Ornstein, Phys. Rev. **36**, 823 (1930).

[112] H. E. Hurst, Trans. Amer. Soc. Civ. Eng. **116**, 770 (1951).

[113] P. Flandrin, IEEE Trans. Inform. Theory **35**, 197 (1989).

[114] J. Bergli, Y. M. Galeprin, and B. L. Altshuler, New J. Phys. **11**, 025002 (2009).

[115] J. Bergli, Y. M. Galperin, and B. L. Altshuler, Phys. Rev. B **74**, 024509 (2006).

[116] D. Zhou, A. Lang, and R. Joynt, Quantum Inf. Proc. **9**, 727 (2010).

[117] J. B. Johnson, Phys. Rev. **26**, 71 (1925).

[118] K. Kakuyanagi *et al.*, Phys. Rev. Lett. **bf 98**, 047004 (2007).

[119] F. Yoshihara, K. Harrabi, A. O. Niskanen, Y. Nakamura, and J. S. Tsai, Phys. Rev. Lett. **97**, 167001 (2006).

[120]

[121] E. Paladino, A. D'Arrigo, A. Mastellone, and G. Falci, New J. Phys. **13**, 093037 (2011).

[122] B. Bellomo *et al.*, Phys. Rev. A **81**, 062309 (2010).

[123] G. Burkard, Phys. Rev. B .

[124] M. Niemann, H. Kantz, and E. Barkai, Phys. Rev. Lett. **110**, 140603.

[125] M. D. Lang and C. M. Caves, Phys. Rev. Lett. **105**, 150501 (2010).

[126] R. Lo Franco, A. D'Arrigo, G. Falci, G. Compagno, and E. Paladino, Phys. Scr. **T147**, 014019 (2012).

[127] A. D'Arrigo, R. Lo Franco, G. Benenti, E. Paladino, and G. Falci, Phys. Scr. **T153**, 014014 (2013).